Characterization of Polystyrene-*b*-poly(acrylic acid) Copolymer Micelles by Nuclear Magnetic Resonance Spectroscopy

by

Sachiko Chijiwa

A thesis submitted to the Faculty of Graduate Studies and Research in partial fulfillment of the requirements for the degree of

Master of Science

Department of Chemistry
McGill University
Montreal, Quebec
Canada, H3A 2K6

July 2001

0-612-75293-3

Abstract

This dissertation describes the characterization of polystyrene-*b*-poly(acrylic acid) (PS-*b*-PAA) copolymer micelles by nuclear magnetic resonance spectroscopy (NMR). The segmental chain dynamics of the polystyrene-*b*-poly(acrylic acid) copolymer during the micellization process was investigated by solution-state proton NMR measurements. The spin-lattice and spin-spin relaxation parameters revealed the increased motional restriction of the PS blocks of the PS-*b*-PAA copolymer as aggregation was induced. The mobility of the PAA segments also decreased during the micellization process. However, the PAA blocks experienced greater motional freedom than the PS component forming the aggregate core.

^{129}Xenon NMR spectroscopy was used to determine the glass transition temperature of the PS core of the polystyrene-*b*-poly(acrylic acid) copolymer aggregates in dioxane/water mixtures. The temperature dependence of the NMR line shapes and resonance shifts of xenon in the PS and solvent phases of the PS-*b*-PAA copolymer micelles was analyzed. Discontinuities in the slope of the chemical shift-temperature curves for xenon sorbed in the PS component revealed phase transitions in the copolymer micelles. The PS core of the phase separated PS_{100}-*b*-PAA_{25} copolymer aggregates underwent the glass transition in the temperature region of 40 °C to 45 °C. The glass transition temperature of the PS core of PS_{218}-*b*-PAA_{20} copolymer aggregates suspended in solution was in the 33 °C to 35 °C temperature region.

Resume

Cette dissertation décrit la caractérisation de micelles de copolymère de polystyrène-*b*-poly(acide acrylique) (PS-*b*-PAA) par spectroscopie de la résonance magnétique nucléaire (RMN). La dynamique des chaines de copolymère de polystyrène-*b*-poly(acide acrylique) (PS-*b*-PAA) au cours du processus de micellisation a été étudiée par RMN du proton en solution. Les paramêtres de relaxation spin-réseau et spin-spin montrent une restriction accrue du mouvement des blocs PS du copolymère PS-*b*-PAA alors que l'aggrégation est induite. La mobilité des segments PAA décroît aussi pendant le processus de micellisation. Cependant, les blocs PAA connaissant une plus grande liberté de mouvement que la partie PS formant le coeur de l'aggrégat.

La spectroscopie du ^{129}Xénon a été utilisée pour determiner la temperature de transition vitreuse du coeur PS des aggrégats de copolymère de polystyrène-*b*-poly(acide acrylique) dans des mélanges dioxane/eau. La variation de la température en fonction de la forme des pics RMN et des déplacements de la résonance du Xénon dans les phases de PS et de solvent a été analysée dans les micelles de copolymère PS-*b*-PAA. Les discontinuités de la pente des courbes déplacements chimiques-température pour le Xénon adsorbé dans la partie PS révèlent les transitions de phase dans les micelles de copolymère. Le coeur PS des aggrégats de copolymère PS_{218}-*b*-PAA_{25} en phase séparée subissent une transition de phase vitreuse dans une région de température comprise entre 40°C et 45°C. La température de transition de phase vitreuse du coeur de PS des aggrégats de copolymère PS_{218}-*b*-PAA_{20} en suspension se trouve dans l'intervalle de température 33°C et 35°C.

Foreword

This dissertation is comprised of four chapters. Chapter 1 provides a general introduction to the aggregation phenomena of PS-*b*-PAA copolymers. In addition, brief introductions to the principal characterization techniques used in this study are included. The second chapter discusses the investigation of the segmental chain dynamics of the PS-*b*-PAA copolymer during the aggregation process by solution-state proton NMR measurements. In Chapter 3, the characterization of PS-*b*-PAA copolymer aggregates in dioxane/water mixtures by ^{129}Xenon NMR spectroscopy is discussed. The variable temperature NMR measurements of the xenon probe in the PS core of the PS-*b*-PAA micelles are analyzed to elucidate the glass transition temperature of the aggregate core. The final chapter consists of the conclusions of the investigation and suggestions for future work.

Contributions

Dr. Yisong Yu synthesized the PS homopolymer and PS-*b*-PAA copolymers used in the investigations discussed in Chapter 2 and Chapter 3. Carl Bartels programmed the source code used to calculate the correlation times described in Chapter 2. Christian Krueger synthesized the PS beads analyzed in Chapter 3. Antisar Hlil performed the DSC measurements of the PS homopolymer described in Chapter 3. Apart from the advice and direction from Dr. Linda Reven and Dr. Adi Eisenberg, and the contributions mentioned above, the work in this dissertation was performed by the author.

Acknowledgements

I am grateful to both Dr. Adi Eisenberg and Dr. Linda Reven for allowing me to pursue a jointly supervised research project. My desire to incorporate aspects of polymer chemistry and NMR spectroscopy in my thesis has required them to extend their knowledge beyond their main areas of expertise and I am indebted to them both for their extra efforts.

I would like to thank Dr. Adi Eisenberg for his supervision and expertise over the past few years. It has been a unique opportunity to learn from someone with such a vast knowledge of the polymer field. Through his guidance, not only have I acquired skills as a chemist, I have also gained personal qualities which will serve me well in the future.

I am deeply indebted to Dr. Linda Reven for her continuous support and direction during my graduate studies. Her passion for her research and her attention towards her students has inspired me, and I feel very fortunate to have been part of her research group during my graduate studies.

I have also benefited from the support of numerous people in the Department of Chemistry.

- Dr. Fred Morin and Dr. Paul Xia for their assistance in the NMR aspects of this study
- Antisar Hlil for the DSC analysis of the PS homopolymer samples
- Dr. Yisong Yu for the synthesis of the PS homopolymer and PS-*b*-PAA copolymer samples
- Jeannie Mui for her assistance in the TEM laboratory
- Fred Kluck for his technical assistance associated with the ^{129}Xe gas loading apparatus
- Rick Rossi for his assistance in terms of the electronic aspects of the research project
- George Kopp for his glass blowing expertise during the preparation of the ^{129}Xe NMR samples
- Carl Bartels for his valuable discussions and for programming the source code used to calculate the correlation times

- Christrian Krueger for the synthesis of the PS bead samples
- Renee Charron, Chantal Marotte, Sandra Aerssen, Carol Brown, Paulette Henault and Fay Nurse for their assistance during my graduate studies.
- Felaniaina Rakotondradany for translating the abstract into French

I feel fortunate to have interacted with my colleagues from the Eisenberg and Reven groups, and with numerous people within the Department of Chemistry.
Amira, Anne, Andrew, Carl, Christine, Claudia, Feli, Hongwei, Izabel, Kim, Kui, Laibin, Lifeng, Michael, Mohua, Neil, Owen, Patrick, Renata, Shane, Susan, Victor, Yisong, Zhaotie
Thank you for the support and light moments

Finally, I would like to thank my family. Mom, Dad, Chieko, Akiko, and Takashi

Table of Contents

List of Tables

List of Figures

I remember staring up into the darkness from my bed with my ears focused on the stirring downstairs. I could hear the back door open and close, the sound of your key as it turned the lock clockwise with a resounding click, and your footsteps as they grew fainter. I would make a pact to stay awake to hear your return, but as always, even before I realized I was falling asleep, I would awake the next morning to the sound of the kettle boiling water and your voices in the kitchen. With the sun seeping through my curtains, I would close my eyes and relax back into bed as a small weight was lifted from my chest.

Dedicated to my parents

Chapter 1

General Introduction

The overall objective of this thesis is to investigate the dynamics of polystyrene-*b*-poly(acrylic acid) (PS-*b*-PAA) micelles at the molecular level. Nuclear magnetic resonance spectroscopy (NMR) techniques are used to study this system as NMR can resolve chemically different sites through their resonance shifts. Proton (^{1}H) NMR is used to monitor the mobility of the polystyrene chains during the micellization of PS-b-PAA in deuterated dioxane/deuterium oxide solvent mixtures. In addition to ^{1}H NMR solution-state experiments, ^{129}xenon (^{129}Xe) NMR is used to probe the PS-*b*-PAA micellar environment and determine the glass transition temperature (T_g) of the micelle core.

In 1995, the direct observation of multiple morphologies, arising from the self-assembly of asymmetric amphiphilic diblock copolymers in selective solvents, has driven intense study of these systems. These structures, known as "crew-cut" aggregates, consist of a large insoluble core, which is surrounded by a thin corona. Our group has documented a vast library of structures including spheres, rods, vesicles, as well as more complex architectures.[1,2] Furthermore, we have identified thermodynamic and kinetic parameters involved in morphogenesis.[3,4] These systems are versatile as the morphologies can be tailored by adjusting micellization parameters.[5] This flexibility has encouraged extensive study of these systems in various applications such as drug delivery.[6] Research in these areas has steadily progressed; however, the characterization of "crew-cut" aggregates at the molecular level has not been pursued in depth.

This introduction contains four sections. The first section describes the relevant fundamental aspects of polymer chemistry. The second section discusses aggregation phenomena of diblock copolymers with an emphasis on the PS-*b*-PAA system. This section is followed by a description of transmission electron microscopy and nuclear magnetic resonance spectroscopy. The fourth section contains the scope of the thesis and brief summaries of each chapter.

1.1 Introduction to Polymers

Polymers play an integral role in daily life. They are found in great abundance from both natural and synthetic sources. Natural materials such as wood and DNA are composed of polymers, as are synthetic plastics and gels. The term polymer refers to a diverse class of large molecules composed of repeating units connected by covalent bonds.[7]

Polymers are not characterized by a single molecular weight since random processes control their synthesis. Therefore, a polymer is composed of chains of varying length and the molecular weight is a statistical average. This value can be expressed in various ways. The number average molecular weight, M_n, is the sum of all the molecular weights of the molecules present divided by their total number.[8]

$$M_n = \frac{\sum M_i N_i}{\sum N_i} \qquad 1$$

In equation 1, M_i is the molecular weight of the molecule i, and N_i is the number of moles of molecule i. In addition to a number average, the molecular weight of a polymer can be a weight average. In this case, each molecule contributes to the average value according to the ratio of its weight to that of the total.[8] The molecular weight average, M_w is expressed as:

$$M_w = \frac{\sum M_i^2 N_i}{\sum M_i N_i} \qquad 2$$

The weight average molecular weight is sensitive to the higher molecular weight chains, while in contrast the number average molecular weight is sensitive to the lower weight species. The ratio between M_w and M_n, known as the polydispersity, is a measure of the width of the molecular weight distribution. If the polymer chains are of equal length, the number average molecular weight is equal to the weight average molecular weight. In this case, the polymer is said to be monodisperse. In all synthetic polymers, this ratio is greater than one.[8]

The simplest polymer structure is the linear polymer where the units are connected in a sequence. The polymer structure can increase in complexity as displayed by branched polymers. Polymer branching can be in the form of both long and short chains. This diversity results in numerous branched polymer structures ranging from linear, branched, star-shaped, network, comb and ladder.[9]

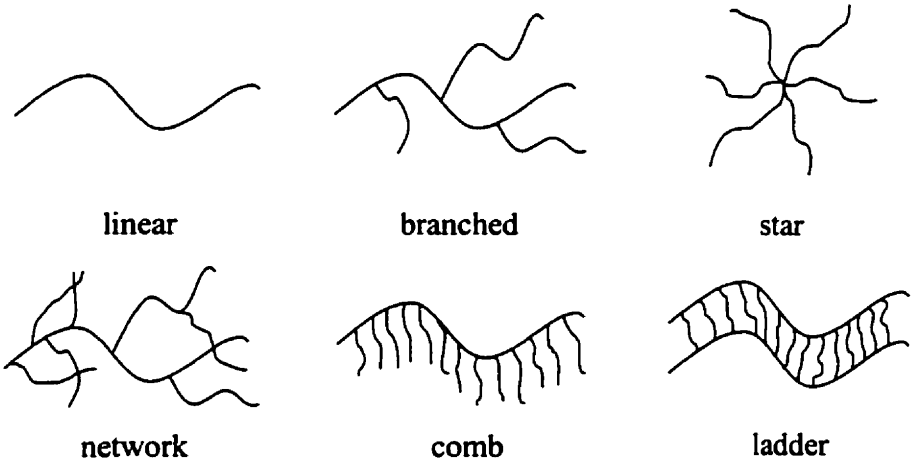

Figure 1.1 Diagrammatic representations of various polymer structures.

Polymers can be composed of a single type, or a number of different types of repeat units. If there are two or more different repeating units present, the polymer is referred to as a copolymer. A random copolymer contains no regularity in the distribution of the different repeating units. In an alternating copolymer, the units are organized in alternating sequence. Block copolymers are composed of sections of polymers joined by covalent bonds. A diblock copolymer contains two different polymer chains whereas triblock copolymer contains three polymer blocks.[9]

random copolymer alternating copolymer

diblock copolymer triblock copolymer

Figure 1.2 Schematic representations of different copolymer arrangements.

1.1.2.1 Polymer Glass Transition Temperature

The glass transition temperature of a polymer is of great importance to its processing and potential applications.[7-10] Similarly, measuring the T_g of a diblock copolymer aggregate is of academic and practical interest. Unfortunately, traditional calorimetric methods of determining the T_g cannot be applied to polymer micelles suspended in solution. The T_g is the temperature at which a non-crystalline polymer undergoes a transition from a glass-like to a rubbery state. Below this temperature, the mobility of the polymer chains is restricted to short-range motions and rotations. In contrast, above this temperature the polymer exhibits greater long-range molecular motion, rotational freedom and segmental motion. There are various theories to explain the T_g phenomenon involving either free volume, thermodynamic or kinetic considerations.[7-10]

1.1.2.2 Molecular Properties and the Glass Transition Temperature

Correlations between the molecular properties of a polymer and its T_g exist. Polymers composed of rigid chains often exhibit increased glass transition temperatures. Similarly, a polymer backbone subjected to high rotational barriers will have a high T_g. The presence of side-groups along the polymer backbone will restrict its rotational freedom and therefore large substituents and multiple side-groups will greatly elevate the T_g. However, when the side-groups are flexible, the T_g decreases.[8,10]

Increasing the molecular weight of a polymer raises the T_g. The middle and end sections of a polymer chain undergo different degrees of motion. As a result, the chain ends contribute a greater free volume. Equation 3 describes the influence of the molecular weight on the glass transition temperature.

$$T_g(M) = T_g(\infty) - {2\rho\theta N_{av}}/{\alpha_f M} \qquad 3$$

$T_g(\infty)$ is the glass transition temperature of the polymer at infinite molecular weight, ρ is the polymer density, θ is the excess free volume per chain end, N_{av} is Avogadro's number, α_f is the free volume expansion coefficient, and M is the polymer molecular weight. The plot of the glass transition temperature as a function of the inverse polymer molecular weight is linear.[10]

Polymer intermolecular forces also affect the glass transition temperature. The cohesive energy density, CED, which is a measure of intermolecular forces, is correlated with the glass transition temperature. Equation 4 shows that intermolecular forces increase the glass transition temperature.[10]

$$CED = 0.5mRT_g - 25m \qquad 4$$

m represents the number of degrees of freedom of the polymer and R is the ideal gas constant.

The diblock nature of the PS-*b*-PAA system complicates the measurement of its T_g by standard techniques, as the presence of more than one type of repeat unit greatly affects this parameter. Random copolymers composed of units, which as homopolymer are of different glass transition temperatures, exhibit a single intermediate T_g value. In polymers where both homopolymers have similar T_g's, both negative and positive deviations from this value have been observed.[10] Block copolymers provide much more complicated systems of study. Often these polymers will form phase-separated materials and two distinct glass transition temperatures will be measured. Intermediate situations are observed where the two different homopolymers have intermediate compatibility.

Mechanical and thermal methods of T_g determinations can only be applied successfully if the T_g's differ by more than *ca.* 30°C.[10]

1.1.2.3 External Forces Affecting the Glass Transition Temperature

It is important to consider the effect of pressure on the T_g as xenon gas will be introduced to PS-*b*-PAA micelle solutions to measure this value by ^{129}Xe NMR spectroscopy. The influence of pressure on the glass transition temperature can be explained by considering the polymer free volume. As pressure is applied on the polymer above the T_g, the free volume of the polymer decreases. Generally, the T_g increases with pressure at a rate of 20°C/1000 atm.[10] Therefore for pressure increases of approximately one atmosphere, changes in the glass transition temperature are negligible. The xenon gas pressure used in the ^{129}Xe NMR study of PS-*b*-PAA micelles is less than 6 atm, therefore, we anticipate a T_g increase of less than 0.12 °C due to the xenon gas.

The addition of plasticizers and diluents to the polymer will also result in changes of the glass transition temperature. Different additives will have varying effects on the T_g; however, most will decrease it.[10] As with the pressure effect, the influence of plasticizers and diluents on the glass transition temperature can be explained using the free volume approach. One possible equation is given below.

$$T_g = \frac{\alpha_{fp} V_p T_{gp} + \alpha_{fd}(1 - V_p) T_{gd}}{\alpha_{fp} V_p + \alpha_{fd}(1 - V_p)} \qquad 5$$

Equation 5 shows the relationship between the glass transition temperature and the plasticizer content in the polymer. α_{fp} is the free volume expansion coefficient of the polymer, V_p is the volume fraction of the polymer, T_{gp} is the glass transition temperature of the polymer, α_{fd} is the free volume expansion coefficient of the diluent, and T_{gd} is the glass transition temperature of the diluent.[10]

1.1.3.1 Polymer Synthesis

To synthesize a polymer, the monomer must have functionality of two or greater to link to two or more other monomers. The two principal methods of polymer synthesis are step-growth and chain-growth polymerization.[7-9]

Step-growth polymerization occurs by the stepwise reaction between species that contain at least two functional groups. This process requires long periods for each macromolecule to form. The monomer is consumed early in the reaction while the molecular weight increases slowly. In addition, there is no termination step and the end groups of the polymers remain reactive throughout the process.[7-9]

Chain-growth polymerization involves the presence of active centers on the end of the growing polymer chains. The chains propagate by the repeated addition of monomers to these active sites. Unlike step-growth polymerization, monomer is consumed throughout the entire reaction. Generally, chain growth occurs at a rapid rate. Chain-growth polymerization involves three distinct mechanisms: initiation, propagation, and a termination.[7-9]

1.1.3.2 Synthesis of Polystyrene-*b*-poly(acrylic acid)

The PS-*b*-PAA copolymers are synthesized by living sequential anionic polymerization.[11,12] The preparation of polymers by living polymerization allows for the control of polymer molecular weight, polydispersity and structure. Care is exercised during the procedure to prevent the premature termination of the polymerization reaction. All active impurities such as water and oxygen must be removed to keep the anionic chain alive. Three steps are involved in this process: initiation, propagation, and termination. The initiation step involves the addition of lithium chloride (LiCl), tetrahydrofuran (THF), and α-methylstyrene to the reaction vessel. α-Methylstyrene acts as both an indicator and an end-capping agent during the reaction. This reaction mixture is cooled to -20°C and titrated with *sec*-butyllithium (*sec*-BuLi) until a light red colour develops. Initially, *sec*-BuLi will eliminate the residual H_2O and O_2 in the reaction system, then it will react with α-methylstyrene to yield the monofunctional initiator (α-methylstyryl)-lithium.

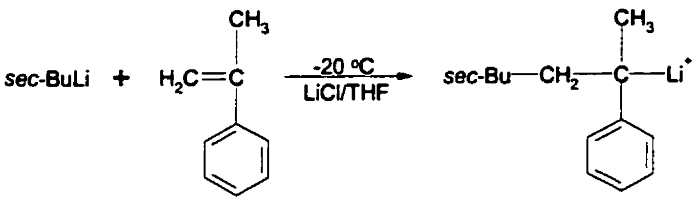

I

This solution of short chain living anions is cooled to –78°C prior to the propagation step. As styrene monomer is added to the solution, the living anions initiate the polymerization reaction and the polymer chain length increases. During this reaction, the red colour changes to a deep orange-yellow colour. Once all of the styrene monomer is consumed, the red colour returns as the α-methylstyrene end-caps the polystyryllithium anions.

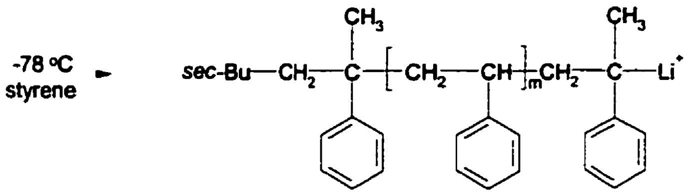

II

Synthesis of the PAA block proceeds with the addition of *tert*-butylacrylate (*tert*-BuA) to the living polystyryllithium anions to form polystyrene-*b*-poly(*tert*-butylacrylate). Similarly, the deep red colour changes to a yellow colour. The LiCl prevents side reactions such as chain transfer and termination from occurring by slightly deactivating the highly reactive styryl anion.

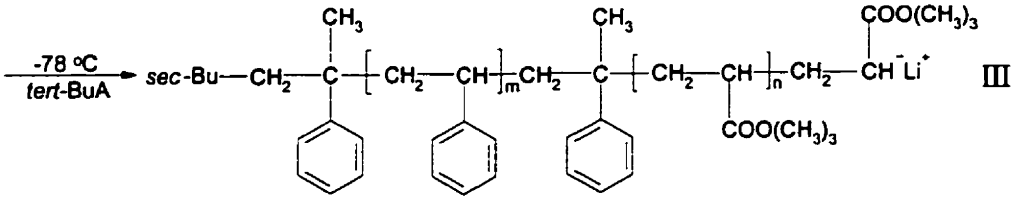

III

Unlike step-growth polymerization, termination of this polymerization reaction occurs by the addition of methanol (MeOH), which provides the labile proton to kill the living anions. The polystyrene-*b*-poly(*tert*-butylacrylate) polymer is recovered by precipitation in a MeOH/H$_2$O mixture. The polymer is finally hydrolyzed to polystyrene-*b*-poly(acrylic acid) by using *p*-toluenesulfonic acid as the catalyst in toluene. The diblock copolymer is recovered by precipitation in MeOH.

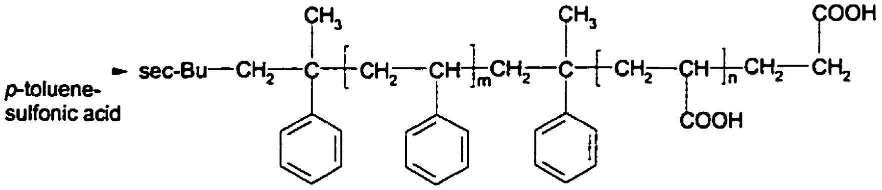

IV

1.2.1 Aggregation Phenomena of Amphiphilic Diblock Copolymers in Selective Solvents

It is well known that diblock copolymers self-assemble to form colloidal size aggregates when dissolved in a selective solvent.[1,2] The bluish and slightly turbid appearance of these solutions served as qualitative evidence for the formation of micelles.[13] Diblock copolymers self-assemble in aqueous media to form regular micelles with a hydrophobic core and a hydrophilic corona. In organic solvents, reverse micelles are formed with a hydrophilic core. The relative block lengths of the copolymer determine if star or crew-cut micelles are formed.[5] A star micelle consists of a small core and a thick corona whereas a crew-cut micelle has a large core and a thin corona. In addition to micelle structure, star and crew-cut micelles differ in their method of preparation. Star micelles are prepared by the direct dissolution of the copolymer in a solvent selective for the long block. Crew-cut micelles cannot be prepared in this fashion since the major component of the copolymer is the insoluble block and the copolymer will not readily dissolve in the selective solvent. In this case, the copolymer is first dissolved in a good solvent for both blocks. Addition of a precipitant for the long block results in the association of the insoluble blocks to form the micelles. Finally, the micelle solution is dialyzed against the selective solvent to remove the initial solvent.[5]

1.2.2.1 Polystyrene-*b*-poly(acrylic acid) Aggregates in Aqueous Media

Our group's research efforts have focused on the preparation and study of diblock copolymer "crew-cut" aggregates. The preparation of micelles from poly(styrene)-*b*-poly(acrylic acid) copolymers in low molecular weight solvents resulted in the first direct observation of multiple morphologies arising from the same block copolymer family.[1,2]

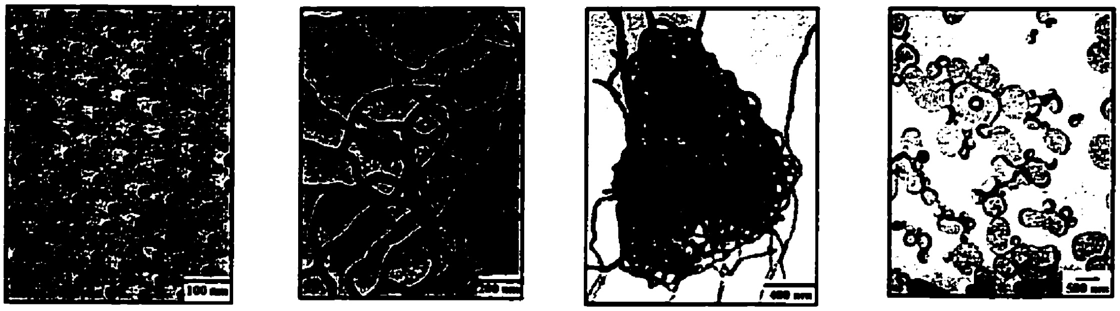

Spheres PS(200)-*b*-PAA(21)
Rods PS(190)-*b*-PAA(20)
Bicontinuous rods PS(190)-*b*-PAA(20)
Lamellae PS(132)-*b*-PAA(20)

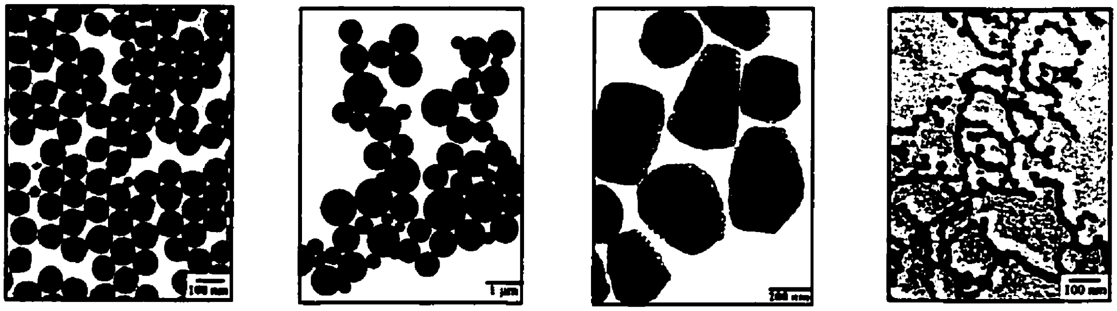

Vesicles PS(410)-*b*-PAA(13)
LCM PS(200)-*b*-PAA(4)
HHH PS(410)-*b*-PAA(13)
Pearl necklace PS(500)-*b*-PAA(60)

Figure 1.3 Transmission electron micrographs of various PS-*b*-PAA aggregate morphologies. The degree of polymerization for each block is noted in parentheses.[5]

In contrast to star micelles, which are spherical structures, these crew-cut aggregates formed various morphologies ranging from spheres, rods, bicontinuous structures, vesicles and other higher order architectures. Changing various micellization conditions, such as the copolymer composition,[1-2,5] the initial copolymer concentration[1-2,5], and the nature and concentration of added ions,[5,14-15] can alter the morphologies.

1.2.2.2 Copolymer Composition

Spherical micelles are formed when the PAA content of the copolymer is relatively high. As the content of the PAA decreases, the micelle morphology changes from spheres to rods, to vesicles or lamellae, and finally to large compound micelles (LCM).[1,2] The core dimensions of spherical micelles depend on the lengths of the soluble PAA and insoluble PS blocks according to equation 6.[16,17]

$$R_{core} \approx N_{PS}^{0.4} N_{PAA}^{-0.15} \qquad 6$$

R_{core} is the number average core radius, and N_{PS} and N_{AA} are the degrees of polymerization for the PS and PAA blocks respectively. Rod-like micelles of varying lengths were formed; however, they exhibited a relatively narrow distribution of cylindrical diameters. The vesicular aggregates had uniform wall thickness, which was independent of the micelle size.

Ultimately, the micelle will adopt the morphology that minimizes the total free energy of the system. It is believed that the optimal morphology is obtained through the force balance between three factors:

i) the stretching of the PS block

ii) the surface tension between the core and the solvent

iii) the repulsion between the corona chains[1,2]

As the content of PAA decreases, the repulsion between the corona chains is reduced and the core size increases. In turn, this increase in core size will augment the stretching of the PS chain. However, the decreased entropy of the PS chains limits the increase of the core dimensions. Therefore, the micelles will change their morphology from spheres to rods, to vesicles and to large compound micelles to minimize the total free energy of the system.[1,2]

The degree of PS chain stretching, S_c, is the ratio of the micelle core radius to the end-to-end distance of the PS chain in an unperturbed state. For spherical micelles in aqueous solution, the degree of PS chain stretching depends on the copolymer composition as:

$$S_c \approx N_{PS}^{-0.1} N_{PAA}^{-0.15} \qquad 7$$

Therefore, as the PS and/or PAA block lengths increase, the degree of stretching decreases. As the morphology changes from sphere to cylinder and to vesicle structures, the value of S_c is reduced.[16]

The area per corona chain at the core/corona interface must be considered as it determines the aggregation number and structure of the micelle. A micelle with a small surface area per corona chain experiences a lower interfacial energy between the core and the solvent, and a stronger steric repulsion among the corona chains. In spherical micelles, if the core is a compact sphere and the density of the PS blocks is homogeneous, the surface area per corona chain, A_c follows the relationship:

$$A_c \propto N_{PS}^{0.6} N_{PAA}^{0.15} \qquad 8$$

A smaller value of A_c will decrease the total surface energy of the micelle core; however, this will increase the stretching of the PS blocks and the repulsive energy between the corona chains. Therefore, a force balance between these three factors will determine the surface area of a corona chain. As the micelle changes from spherical to cylindrical, and to vesicular morphologies, the value of A_c decreases.[16]

1.2.2.3 Additives

The aggregate morphologies can be tailored by the addition of ions to the micelle solution.[14,15] The addition of hydrochloric acid (HCl) to the system had a similar effect on the morphology as reducing the PAA block length. The PAA chains are protonated by the HCl which lowers their degree of ionization. Therefore, the electrostatic interactions due to the partial ionization of the PAA chains, and the steric repulsion associated with their chain dimensions are believed to decrease the overall repulsion among the PAA chains. This decrease in repulsion leads to architectural transitions where spheres transform into rods, vesicles and finally into large compound vesicles (LCVs) or large compound micelles (LCMs).[14,15]

The addition of base in the form of sodium hydroxide (NaOH) results in the opposite morphological trend. The NaOH neutralizes the PAA segments and the degree of ionization along the PAA chain increases. The increased repulsion among the corona chains leads to morphological transitions in the reverse direction.[14,15]

In addition to acids and bases, salt ions can also affect the aggregate structure. The addition of sodium chloride (NaCl) results in shielding of the ionic repulsion, and induces the formation of rods, vesicles, or LCVs from spheres.[14,15]

1.2.2.4 Initial Common Solvent

The initial common solvent has a profound effect on the morphologies for the PS-*b*-PAA micelle system.[18,19] PS-*b*-PAA micelles were prepared using *N,N*-dimethylformamide (DMF), THF or dioxane solvent. The aggregate morphologies formed in DMF were simple spheres even when the PAA content was low. In contrast, preparation of the micelles in THF resulted in the formation of spheres, vesicles and eventually large compound micelles as the PAA content was decreased. The use of dioxane resulted in the formation of spheres, cylinders, vesicles and large compound micelles. Based on theoretical considerations, Nagarajan suggested that changing the solvent content of the core could alter the micelle morphology.[20] In addition, Nagarajan investigated the solubilization of hydrocarbons in poly(ethylene oxide)-*b*-poly(propylene oxide) and poly(*N*-vinylpyrrolidone)-*b*-polystyrene block copolymer micelles.[21] They discovered that the solubilization of hydrocarbons in block copolymer micelles was influenced by the Flory-Huggins interaction parameter, χ. They expressed this relationship with the solubility parameters of the solubilizate and the micelle core.

$$\chi_{s,core} = {(\delta_s - \delta_{core})\upsilon_s}\Big/{k_B T} \qquad 9$$

In equation 9, δ_s and δ_{core} are the solubility parameters for the solubilizate and the polymer forming the core. υ_s is the molecular volume of the solubilizate, k_B is the Boltzmann constant and T is the absolute temperature. For a given copolymer, the preferred micelle structure provides the lowest optimal free energy of solubilization at that core solvent content.

To explain the relationship between the micelle dimensions and the common solvent for the PS-*b*-PAA aggregates, the polymer-solvent interactions were examined.[18,19] The χ parameter, which incorporates the solubility parameters and dielectric constants of the solvent, can be used to estimate the strength of the PS-solvent and PAA-solvent interactions. The PS-solvent interactions should be strongest in THF, intermediate in dioxane and weakest in DMF. As the compatibility between the PS block and the solvent improves, the solubilization of the solvent into the core increases and PS chains are stretched to a greater degree. Therefore, morphological transitions from spheres to rods and vesicles are induced. In contrast, a low solvent polarity produces weak PAA-solvent interactions, which results in weaker repulsive interactions between the corona chains. In this situation, the aggregation number of the micelle increases and the PS chains extended to a greater degree. This modification leads to morphological transitions from spheres to cylinders, vesicles and LCMs. The solvent effect on the PAA chains is quite different from that of the PS block. As expected, increases in the PAA content will heighten the influence of the PAA-solvent interaction on the aggregate morphology.[18,19]

At this point the effect of the common solvent on the PS-*b*-PAA aggregate morphologies can not be fully explained as it involves a combination of complex interactions.

1.2.2.5 Thermodynamics of Polystyrene-*b*-poly(acrylic acid) Aggregate Formation

Thermodynamics of the formation of spherical PS-*b*-PAA crew-cut micelles in DMF/H_2O mixtures were investigated. The effects of water content, PS block length, PAA block length, and NaCl on the thermodynamic functions were studied. Using the closed association model, combined equations for the thermodynamic functions for all these factors were obtained from the experimental data.[3]

Two different mechanisms for micelle formation have been developed: closed and open association models.[13] The closed association model describes the existence of an equilibrium between unimers and micelles, which can be expressed as:

$$nM^{(u)} \leftrightarrow M^{(m)} \qquad 10$$

In equation 10, M is the molar mass, n is the association number, and the superscripts u and m represent the unimer and micelle. The equilibrium constant, K, can be expressed both as amount and mass concentrations:

$$^{a}K = u^{(m)} \big/ (u^{(u)})^{n} \qquad 11$$

$$^{w}K = c^{(m)} \big/ (c^{(u)})^{n} \qquad 12$$

In these equations u is the number concentration and c is the mass concentration.

In contrast, a population composed of a distribution of unimers, dimmers, trimers, up to n-mers, and their corresponding equilibrium constants characterize the open association mechanism. The closed association model implies the existence of a critical micelle concentration whereas the open association model does not.[13]

Thermodynamics of micelle formation involve the relative contributions of the enthalpic and entropic terms to the minimization of the Gibbs free energy.[13] According to the closed association model for aggregate systems with large association numbers, the standard Gibbs free energy change per mole of the solute in a micelle, ΔG°, can be expressed as[3,13]:

$$\Delta G^{\circ} \cong RT \ln CMC \qquad 13$$

In this equation, R is the gas constant, T is the temperature and CMC is the critical micelle concentration. In addition, the standard enthalpy change per mole of the solute in a micelle, ΔH°, can be expressed as:

$$\Delta H^\circ \cong RT^2 (d \ln CMC / dT) \qquad 14$$

Equation 14 is appropriate for cases where the association number n is independent of temperature. If it is assumed that ΔH° is also independent of temperature, integrating equation 14 gives:

$$\ln CMC = \Delta H^\circ / RT + A \qquad 15$$

In this relationship, A is a constant.

If ΔH° and ΔG° are known, then ΔS° can be determined from equation 16.[3,13]

$$\Delta S^\circ = (\Delta H^\circ - \Delta G^\circ) / T \qquad 16$$

Shen *et al.*[3] observed that under the experimental conditions, all the thermodynamic functions were negative and that the standard enthalpy was responsible for the micellization process. Overall, the insoluble block exerted a large effect on all three thermodynamic functions, which is a trend that is observed in star micelles. However, unlike star micelles, the soluble block also had an impact on these functions, where the trend was opposite to that of the PS block. The driving force for micelle formation changed as a function of the water content. In addition, the copolymer composition affected the water content at which this transition occurred. At low water contents, the enthalpy component was the driving force for micellization. The transition from PS/water interactions to PS/PS and water/water interactions was a major contributor to the enthalpy term. At intermediate water contents, both the enthalpy and entropy terms drove the formation of micelles. At high water content, the entropy in the form of hydrogen bonding interactions became the driving force for the aggregation process. The addition of NaCl greatly affected the thermodynamic functions. Here, electrostatic interactions among the corona chains also influenced the enthalpy term.[3]

1.3.1 Characterization of Block Copolymer Micelles

Various techniques such as transmission electron microscopy (TEM),[1,2] static and dynamic light scattering[22,23], fluorescence[24], UV-Vis spectroscopy[4] and small-angle neutron scattering[23] are used to characterize block copolymer aggregate systems. These methods can elucidate numerous micellar properties; however, they cannot be used to study these systems at the sub-micellar level. To circumvent this limitation, we have relied on NMR spectroscopy to probe polystyrene-*b*-poly(acrylic acid) micelle chain dynamics. Solution-state ^{1}H NMR relaxation measurements of PS-*b*-PAA copolymer solutions were acquired at different stages of aggregate formation. ^{129}Xenon NMR spectroscopic experiments provided the means to probe the PS-*b*-PAA micellar environment. In conjunction with the NMR experiments, TEM analysis has been used to verify the morphologies of our PS-*b*-PAA micelles.

1.3.2 Transmission Electron Microscopy

Transmission electron microscopy has proved to be an indispensable technique to study PS-*b*-PAA copolymer aggregate morphologies.[1,2] There are several detailed descriptions of the technique in the literature which can be consulted as this section only provides a brief introduction to TEM.[25-28] TEM is capable of providing atomic resolution of thin films of solid materials because of the strong electron scattering by atoms and the small values of the electron wavelengths produced. The scattering of electrons by matter is principally brought about by a change of phase of the electron wave produced by the electrostatic potential arising from the charges of the nuclei and electrons.[25-28] The principles of electron microscopy can be organized into three aspects:

1. electron scattering in the specimen
2. formation of the diffracted beams at the back focal plane
3. formation of the high resolution image at the image plane

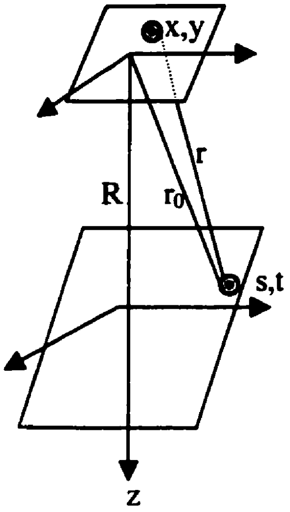

Figure 1.4. Diagrammatic representation of electron scattering in a sample. The electron is moving in the z-direction

For thin samples, electron absorption is neglected, therefore the phase of the electron wave will be modified; however, the amplitude of the wave is unaltered. To describe the electron scatter, the specimen has a transmission function, $q(x,y)$ according to equation 17.

$$q(x,y)=\exp(i\sigma\varphi(x,y)\Delta z) \qquad 17$$

where σ is an interaction constant defined as:

$$\sigma=\frac{2\pi}{V\lambda\left(1+\sqrt{1-B^2}\right)}. \qquad 18$$

In equation 18, V is the acceleration voltage, β is the velocity of the electron relative to the velocity of light, and λ is the wavelength of the electron. $\varphi(x,y)\Delta z$ is the two-dimensional projected potential in the z direction with thickness Δz.[28] For thin specimens, the phase factor in the exponential term is much smaller than 1, therefore this term can be expanded and simplified to the form:

$$q(x,y)\approx 1+i\sigma\varphi(x,y)\Delta z, \qquad 19$$

known as the weak-phase object approximation.[28]

The formation of the diffracted beams at the back focal plane can be described by performing the Fourier transform of equation 19. The scattering amplitude of the electron wave $\Psi(u,v)$ is defined as:

$$\Psi(u,v) \approx \delta(u,v) + i\Im[\sigma\varphi(x,y)\Delta z]\exp(i\chi(u,v)), \qquad 20$$

where the $\exp(i\chi(u,v))$ term represents the phase change of the scattered wave. u and v are defined as:

$$u = {}^{s}\!/_{\lambda r_0} \text{ and } v = {}^{t}\!/_{\lambda r_0} \qquad 21$$

where s, t, and r_0 are defined as illustrated in Figure 1.4.[28]

The scattering amplitude of the electron wave at the image plane, $\psi(x,y)$, is obtained by the Fourier transformation of the scattering amplitude at the back focal plane.

$$\psi(x,y) = \Im[C(u,v)\Psi(u,v)] \qquad 22$$

where $C(u,v)$ is the effect of the objective aperture. The image intensity can be simplified to:

$$I(x,y) \approx 1 - 2\sigma\varphi(-x,-y)\Delta z \qquad 23$$

According to equation 23, the image intensity at a heavy atomic column is lowered while the image intensity at a light atomic column is increased.[28]

In terms of the mechanics of the transmission electron microscope, the thin specimen is irradiated with an electron beam of uniform current density. The electrons are emitted from the electron gun by thermionic, Schottky or field emission, after which condenser lens gather the emitted electrons and focus them on the sample. In addition to focusing the electron beam on the specimen to provide sufficient image intensity, the two or three-stage condenser lens system also varies the illumination aperture and irradiates the specimen illumination area with uniform current density. The lenses in the electron microscope are usually rotationally symmetrical magnetic lenses. The specimen loaded in the gap of the objective lens just above the objective aperture mechanism is imaged and this virtual image is magnified by a three or four-stage projector lens system onto a fluorescent screen. The TEM micrograph is recorded by direct exposure of a photographic emulsion or an image plate inside the vacuum. The image can also be digitally recorded by a fluorescent screen, which is coupled by a fibre-optic plate to a CCD camera.[25-28]

1.3.3.1 An Introduction to Nuclear Magnetic Resonance Spectroscopy

Nuclear magnetic resonance spectroscopy is a powerful and sophisticated technique used in many different scientific areas. High resolution NMR spectrometers are now commonly available and their application ranges from molecular structure, molecular dynamics and particle size determinations. NMR parameters studied include chemical shift data, relative intensities of the signals, constants of spin-spin interaction, and relaxation times.[29-31]

At the most fundamental level, NMR spectroscopy measures the interaction between radio frequency (Rf) electromagnetic radiation and the nuclei of molecules in a strong magnetic field.[29] Nuclei of certain elemental isotopes possess intrinsic angular momentum or spin. The total magnitude of the intrinsic angular momentum, μ, is defined as:

$$\mu = \hbar[I(I+1)]^{1/2} \qquad 24$$

In equation 24, I is the nuclear spin quantum number and $\hbar$ is the reduced Planck's constant. Depending on the isotope, I will have integral or half-integral values. The values of I are quantized, therefore several discrete values of angular momentum may be observable.[29-31] The magnitude of the angular momentum is also defined as:

$$\mu = \hbar m \qquad 25$$

In this expression the quantum number m can take the values $I, I-1, I-2, \ldots, -I$. When these nuclei are placed in a magnetic field, B_o, applied along the z-axis, they give rise to $2I+1$ equally spaced nuclear spin states with angular momentum quantum number I. Each of these quantized orientations corresponds to a certain energy level, E:

$$E = -\mu_z B_o = -m_1 \gamma \hbar B_o \qquad 26$$

In equation 26, m_1 is the magnetic quantum number and γ is the gyromagnetic ratio of the nucleus.[29-31] For ^1H and ^{13}C nuclei, the spin quantum number, I, equals 1/2, therefore there are only two quantized orientations. The lower energy orientation, α, is where the nuclei are aligned parallel to the applied field, and the higher energy orientation, β, is where the nuclei are aligned antiparallel to the applied field. The energy difference between these two states is proportional to the applied field. In terms of frequency, the energy difference, υ_0, is expressed as:

$$\upsilon_o = \frac{\gamma B_o}{2\pi} \qquad (27)$$

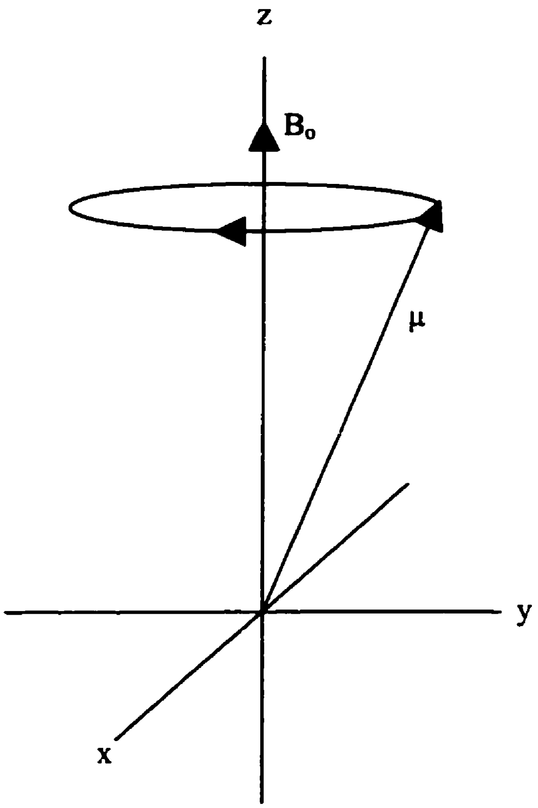

Figure 1.5. Schematic representation of the precession of the magnetic moment, μ, about the axis of the applied magnetic field, B_o, corresponding to the Boltzmann excess in the α energy state.

In the applied magnetic field, the nucleus' motion changes from spinning on a stationary axis to a characteristic wobbling motion. The precessional frequency of this motion is called the Larmor frequency. For the Rf electromagnetic radiation to interfere constructively with the oscillations of the particle, both must be in resonance. To meet this condition, the frequency of the Rf energy must match the Larmor frequency of the nuclei. Only then, will absorption of the Rf energy occur and a nucleus will "flip" from the low energy orientation to the high energy orientation.[29-31] After the absorption of energy, the nucleus can then return to the lower energy state through various relaxation mechanisms. The NMR detector measures the change in impedance of the oscillator coils caused by the relaxation of the nuclei. This signal is in the form of a decaying beat pattern known as a free induction decay (FID), which is Fourier transformed into the conventional NMR spectrum. In its equilibrium state, there is a slight excess of nuclei in the lower energy state, α, than in the upper energy state, β. This difference in populations, shown in equation 28, creates the NMR signal.

$$\frac{N_\beta}{N_\alpha} = \exp\left(\frac{-\Delta E}{kT}\right) \qquad 28$$

N_β and N_α are the nuclear populations in the β and α states, k is the Boltzmann constant, and T is the temperature. This relationship illustrates that the signal intensity is dependent on the gyromagnetic ratio of the nucleus, the strength of the applied magnetic field and the temperature of the system.[31]

1.3.3.2 Molecular Dynamics by NMR Spectroscopy

An extensive area of nuclear magnetic resonance spectroscopy is devoted to investigating the molecular motions of various systems.[32-34] The majority of NMR experiments, which probe molecular dynamics, falls into three basic categories. The first group of experiments involves NMR line shape measurements. NMR line shape measurements provide insight into molecular motions since these dynamics induce changes in the local environment of nuclear spins. These modifications affect the NMR frequencies, and therefore the line shapes are sensitive to molecular motions.[33,35]

The second category involves field gradient methods used to investigate translational motions on length scales that exceed 500 $\mathring{A}$. In these experiments, a magnetic field gradient is applied making the NMR frequencies a function of the position of the spin within the sample. [33,36]

We have employed the final category of NMR techniques to study the local segmental motion of block copolymer micelles by acquiring nuclear spin relaxation measurements. The different nuclear spin relaxation times refer to the characteristic time scales for build-up or decay of various states of nuclear spin order. In this case, relaxation measurements study molecular motion because dynamics produce time dependencies in the forces that act on nuclear spins. These forces induce nuclear spin transitions or perturb nuclear spin energy levels, leading to changes in nuclear spin order. The relaxation times typically range from 100μs to 100 min depending on various factors such as the chemical and physical nature of the sample, the temperature, the nuclear isotope, and the spin order. In contrast, the motions that drive nuclear spin relaxation generally occur on a much shorter time scale, ranging from 1 ps to 1 ms, depending on the same factors.[33,37]

1.3.3.3 Nuclear Magnetic Resonance Relaxation

A perturbed nuclear spin system returns to its equilibrium state by first-order processes characterized by the spin-lattice (T_1) and spin-spin (T_2) relaxation times.[34,38-40] The spin-lattice relaxation process involves the return of the spin system to the equilibrium distribution of spins among the Zeeman levels from its disturbed state. Spin-lattice relaxation involves the exchange of energy from the nucleus to the surrounding molecules, where the lattice serves as a heat sink for the spins.[29] Spin-spin relaxation occurs through energy transfer to neighbouring nuclei and involves the loss of phase coherence amonst spins precessing in phase.[29] Structural and dynamic information can be acquired through NMR relaxation experiments. To have effective interaction between precessing nuclear magnetization and its surroundings an oscillating magnetic field must be present, which provides the link between NMR relaxation and motion. For quadrupole nuclei, an oscillating electric field at the Larmor frequency is also required. According to Bloembergen, Purcell, and Pound, in liquid and gaseous systems, the oscillating field can come from molecules that are undergoing Brownian motion. Fourier analysis of these random motions produces a spectrum of the frequencies present in the system. This continuous and broad distribution of motional frequencies is known as the spectral density function.[29,31] The oscillating field's ability to induce energy exchange and relaxation is determined by the extent of the Larmor frequency's contribution to the spectral density function. The average length of time that a molecule remains in any given position before it changes its state of motion is known as the correlation time, τ_c. The orientation of a molecule at time t, can be described by $Y(t)$, and its position at a later time is described by $Y(t+\tau)$. The correlation function, $k(\tau)$, describes the extent of motion during the period t. This function is shown in equation 29.

$$k(\tau) = \overline{Y(t)Y(t+\tau)} \qquad 29$$

The bar indicates that it is an average over the entire ensemble of molecules.[29,34,38] To connect the relaxation data to the actual motion of a polymer molecule, a dynamic model must be adopted. The simplest interpretation involves assuming that the polymer is a rigid sphere in a viscous medium and the polymer undergoes reorientation via small, random diffusive steps. In this case, the correlation function is assumed to have the exponential form:

$$k(\tau) = k(0)e^{-\tau/\tau_c}. \qquad 30$$

Therefore, according to equation 30, the new position $k(\tau)$ is related to the initial position $k(0)$ in an exponential manner. The spectral density, $J(\omega)$ is the Fourier transform of $k(\tau)$.

$$J(\omega) = A\frac{\tau_c}{1+\omega^2\tau_c^2} \qquad 31$$

In equation 31 A is a constant.[29]

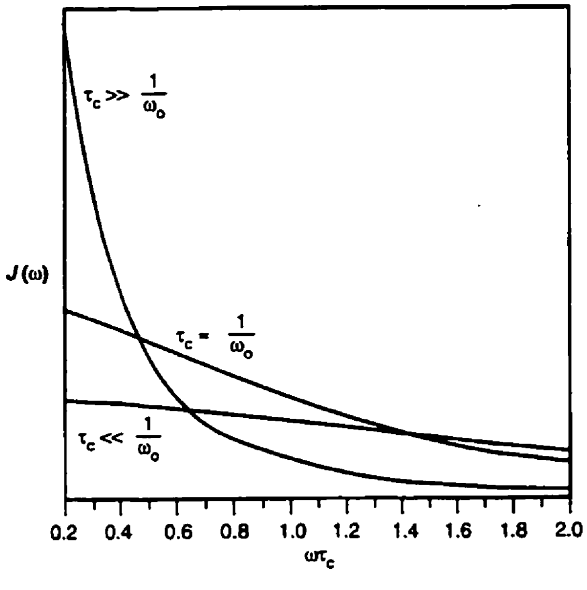

Figure 1.6 Plot of the spectra density function, $J(\omega)$, as a function of $\omega\tau_c$.[29]

When $J(\omega)$ is plotted as a function of $\omega\tau_c$, $J(\omega)$ reaches it maximum when $\tau_c = 1/\omega_0$. At this point, the average molecular tumbling frequency is equal to the Larmor frequency ω_0 and the energy transfer between precessing nuclei and the randomly tumbling molecules is most efficient. When this condition is met, T_1 is at a minimum. It is important to note that for small rigid molecules undergoing isotropic motion, a single correlation time is sufficient to describe the motion.[38] However, it is insufficient to realistically describe the dynamics of a polymer in solution. Macromolecules in reality are undergoing many types of motions with differing rates such as overall tumbling, motions of large portions of the chain and localized segmental motions. In these cases, multiple correlation times or a distribution of correlation times can be used.[38] When multiple correlation times are required, the plot of $J(\omega)$ versus ω is a superposition of several curves.[29]

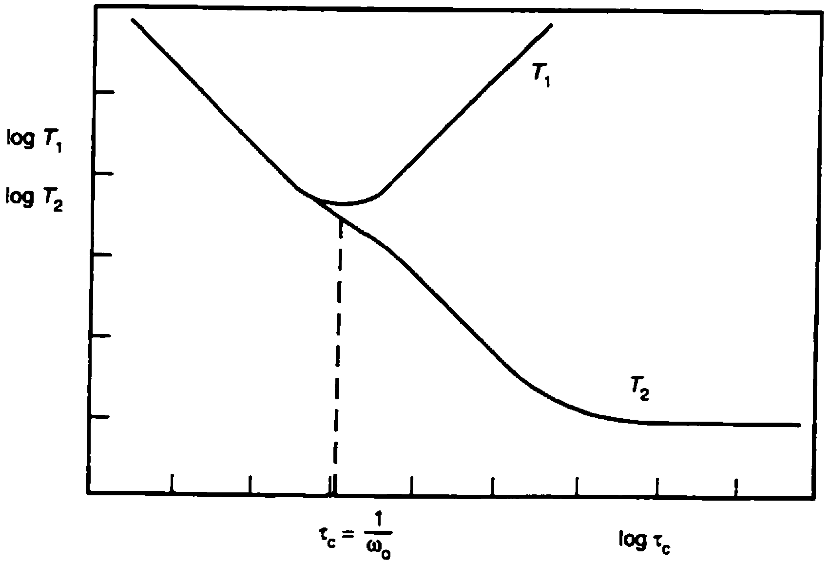

Figure 1.7. Relationship between the relaxation times, T_1, T_2 and the correlation time, τ_c.[29]

In the plot T_1 versus τ_c, T_1 goes through a minimum at $\tau_c = 1/\omega_0$. As the strength of the applied magnetic field increase, the T_1 minimum increases and moves to shorter values of τ_c. For small molecules, their T_1 values will usually be found left to this minimum value except for when the solvent is extremely viscous or the applied field is very low. Under these conditions of motional narrowing, T_1 is independent of the applied field strength. For small polymers, the T_1 value can lie on either side of the minimum value depending on the Larmor frequency.[29,34] In terms of T_2, the dependence on molecular motion is different than that of T_1 since T_2 involves the dephasing of precessing nuclear magnetizations. Unlike T_1, spin-spin relaxation processes involve both the fluctuating local magnetic dipoles and their static components. In addition to high frequency motions, low frequency motions and other low frequency processes significantly shorten T_2. T_2 will decrease monotonically with increasing τ_c and will reach an upper limit characteristic of a rigid solid lattice.[29,34]

1.3.3.4.1 Xenon Nuclear Magnetic Resonance Spectroscopy

Xenon NMR spectroscopy is a powerful technique where the xenon atom is used to probe complex physical, chemical and biological systems.[41-43] In xenon NMR, the physical interaction of the Xe atoms with other Xe atoms and its local environment through collision and overlap is investigated. Numerous xenon NMR techniques are available, including 1D, 2D exchange, diffusion, and cross-polarization experiments. In addition, the development of hyperpolarized Xe NMR has increased the sensitivity of the nucleus by 10^4 fold, which has allowed the study of low sensitivity samples, time resolution experiments and biomedical imaging. Xenon's relative inertness provides a non-invasive technique to study these systems. Xenon is an ideal probe for void spaces and surfaces due to its size of $2\ \mathring{A}$. The two xenon isotopes accessible to NMR investigation are ^{129}Xe and ^{131}Xe; however, the majority of NMR study has been performed on the ^{129}Xe nucleus. [41-43]

Table 1.1. Important Parameters for Xenon NMR Spectroscopy

	^{129}Xe	^{131}Xe
Abundance (%)	26.4	21.2
Spin *I*	½	3/2
Magnetic moment μ	-0.77247	0.68697
Quadrupole moment Q		-0.12×10^{-28}
Magnetogyric ratio γ (rad $T^{-1}s^{-1}$)	-7.4003×10^{7}	2.1939×10^{7}
NMR frequency at 2.3488 T (MHz) (^{1}H at 100 MHz)	27.66	8.199
Relative sensitivity (^{1}H=1)	2.12×10^{-2}	2.76×10^{-3}

Since Xe is a heavy atom bearing a large number of electrons, it possesses a large polarizable electron cloud, which creates a very sensitive probe of local atomic interactions. This sensitivity manifests itself in the large chemical shift range accessible to this nucleus, which is over 7500 ppm. The ^{129}Xe chemical shift is composed of two parts: a diamagnetic and a paramagnetic component. These two contributions produce opposing effects on the chemical shift value. The chemical shift σ can be written:

$$\sigma = \frac{e^2}{3mc^2}\int\frac{\rho}{r}dr - \frac{4}{3\Delta E}\left\langle 0\left|\sum_{j,k} L_j \frac{L_k}{r_k^3}\right|0\right\rangle, \qquad 32$$

where ρ is the electron density, ΔE is the average excited-state energy, L_j and L_k are the angular momentum operators, and r_k is the electron-nuclear distance summed over all excited states. The diamagnetic component arises from the interaction of the electron orbitals with applied magnetic fields where the precession of electrons opposes these fields. This shielding effect on the nucleus from the applied field reduces the resonance frequency of the nucleus.[41-43]

The excited electronic state mixing causes the paramagnetic shift, which is responsible for the observed resonance shift from the interactions of xenon with itself and other species. The resonance frequency of the xenon nucleus is most often increased because of this process. The chemical shift of a lone Xe atom in free space is used as a reference value, where experimentally the shift of Xe gas extrapolated to zero pressure serves this purpose. [41-43]

To our knowledge, this is the first study of block copolymer micelles by xenon NMR spectroscopy. Polymers in solution have rarely been the objects of study by xenon NMR and our system is especially complex as it involves a nanoscale polymer aggregate in a solvent mixture. To fully comprehend the xenon NMR spectra, we must first understand the behaviour of xenon in organic solvents and water. This knowledge must be complemented with the analysis of xenon in condensed phases. The large body of research devoted to the study of polymers in the solid state by xenon NMR must also be discussed.

1.3.3.4.2 ^{129}Xenon NMR of Organic Solvents

The solubility of xenon in most solvents is small, ranging from 4.3 mM in water to 166 mM in isooctane at standard temperature and pressure.[41] This low solubility results in xenon resonance shifts that are independent of the xenon concentration. Therefore, the xenon atoms are at the infinite dilution limit and interact solely with the solvent and not with each other.[41] The chemical shift of xenon in solution is a complicated function of its interaction with neighbouring atoms and molecules, which is further modified by the dynamics of the fluid. The xenon chemical shift, σ, in isotropic liquids results from the contribution of many different interactions:

$$\sigma = \sigma_0 + \sigma_b + \sigma_a + \sigma_w + \sigma_e \qquad 33$$

In equation 33, σ_o is the reference xenon chemical shift, σ_b is the bulk susceptibility correction, σ_a is the nonspecific magnetic anisotropy of the solvent molecules, σ_w is the van de Waals interaction, and σ_e is the solvent electric dipole interaction. In pure solvents, the major contribution to the shielding arises from the dispersive part of the van de Waals interaction and the other contributions can be ignored to a first approximation.[41] There have been several theoretical treatments of xenon NMR in pure solvents. A model proposed by Linder predicts a correlation between the chemical shift and a simple function of the solvent refractive index, since the dispersive component of the van der Waals shift arises in the reaction field that is produced by spontaneous electronic fluctuations of the solute.[44] Fair correlations have been observed between these two parameters; however, notable exceptions exist, particularly in aqueous solutions. Deviations from this trend are minimized when comparisons within groups of related solvents are made. A second model attempts to correlate the xenon shifts with the solubility parameter, δ. The solubility parameter is related to the cohesive energy of the solvent according to:

$$\delta^2 = {}^{\Delta E_v}\!/_{V_m} \qquad 34$$

where ΔE_v is the heat of vaporization at a constant volume, and V_m is the molar volume of the solvent. This model is most accurate for nonpolar solvents.[45]

1.3.3.4.3 ^{129}Xenon NMR of Water

In comparison to other organic solvents, the chemical shift of ^{129}Xe in water is relatively large, *ca.*196 ppm and is dependent on the temperature. The translational diffusion coefficients of Xe in water were measured and were comparable to the diffusion coefficient of water molecules.[42] In mixed solutions of water and organic solvents, an initial sharp increase in the shift at low cosolvent molar ratios is observed. The chemical shift undergoes a steady decrease towards the shift value in the cosolvent alone as the cosolvent molar ratio increases. When ions are present in the aqueous solution, the chemical shift is seen to increase with increasing ion concentration, where the magnitude of the increase is dependent on the activity, charge and hydration of the ions.[42]

1.3.3.4.4 ^{129}Xenon NMR of Condensed Phases

The majority of ^{129}Xe NMR research of condensed phases involves biologically related materials.[41-43] This area of research has been fueled by the anesthetic properties of xenon and the application of magnetic resonance imaging using hyperpolarized xenon techniques. Xenon NMR has been used to study proteins, membranes and vesicles whose spectra are more difficult to interpret than solvent systems due to the heterogeneous nature of the samples. In addition to Xe residing in distinct environments, the spectra are further complicated by the chemical exchange of Xe between these environments.[42] This was observed by Miller *et al.*[46] in aqueous solutions of myoglobin where the presence of one peak indicated that the exchange of xenon between the protein environment and the solvent was fast on the NMR timescale. The influence of temperature on the xenon exchange rate was demonstrated by the presence of two peaks at 35°C and only one peak at 50°C for an aqueous suspension of dimyristoyl lecithin vesicles.

^{129}Xe NMR spectroscopy also been used to elucidate the structural and mechanistic aspects of molecular recognition processes. Cryptophane-A reversibly traps xenon atoms by van der Waals forces to form a host-guest complex. Xenon NMR's extremely sensitive chemical shift can distinguish between deuterium-labeled and non-labeled cryptophane-A xenon complexes. Two dimensional exchange experiments revealed that the exchange of xenon between hosts occurs exclusively by xenon traveling through the solution and that transfer via a collision mechanism does not take place at a measurable rate.[47,48]

Xenon NMR has not been restricted to the study of biological systems. Temperature induced phase transitions in reentrant nematic liquid crystal mixtures were detected by chemical shift, spin-lattice and spin-spin relaxation times. In addition to monitoring the evolution of the different liquid crystal phases, the packing environment of the molecules was also determined.[49]

1.3.3.4.5 ^{129}Xenon NMR of Polymers

^{129}Xe NMR has been applied to polymeric systems to determine various properties such as the glass transition temperature and polymer morphology. The absorption of xenon gas into a polymer is viewed as a dissolution process. This description is especially suited for polymers above their glass transition temperature where the polymer chains exhibit considerable mobility.[41-43] Amorphous polymers absorb xenon gas to a greater extent than crystalline polymers. Stengle and Williamson[50] observed that Xe gas occupied the amorphous regions of polyethylene while the absorption of Xe gas into the crystalline regions was negligible. In the amorphous region, the motion of the polymer chains creates momentary voids which can be occupied by the xenon atom, while the crystalline regions are too tightly packed and do not provide sufficient room to accommodate the probe. The xenon chemical shift is characteristic of a particular polymer and values range from 152 ppm to 250 ppm with most in the 200-230 ppm region at room temperature.[41-43]

The sensitivity of the xenon resonance shift to each different polymer provides an effective method to study phase separation phenomena in polymer blends.[51-55] Generally, phase separation is detected by calorimetric analysis with the observation of multiple glass transition temperatures. However, to resolve different glass transition temperatures, they must differ by at least 20K. Electron microscopy has also been utilized for this application; however, structures smaller than 20 nm are difficult to resolve and often the sample must be stained to produce the phase contrast.[51] The ^{129}Xe NMR spectrum of a phase separated two-component blend will contain two resonance peaks, whereas the spectrum of a miscible blend, will only display a single peak. With two dimensional exchange experiments, diffusion coefficients or average domain sizes in the polymer blends can be measured.[51-55]

The xenon chemical shift does not vary significantly as a function of xenon pressure, as the polymer matrix isolates the individual xenon atoms and the Xe-Xe interaction's contribution to the chemical shift is negligible. In contrast, the xenon chemical shift decreases with increasing temperature.[41-43] This trend is attributed to the decreasing density of the polymer as the temperature is increased. The variation of chemical shift as a function of temperature exhibits two linear regions with a change in the slope at the polymer glass transition temperature. This feature is particularly useful when determining the glass transition temperature of materials, which cannot be measured by conventional calorimetric methods.[41-43] The theoretical basis for the xenon chemical shift dependence on temperature can be described by two different approaches: the free volume model[56] and the van der Waals shift model.[57]

Cheung and Chu[56] developed the free volume model, which explains the discontinuities as being directly related to processes in polymers which result in abrupt changes in the free volume or in the slope of the free volume as a function of the temperature. This model is based on the interaction of the xenon atom in the free volume of the polymer. This interaction is described as a short-range attractive potential between the xenon atom and the polymer; however, the exact nature of the attractive potential is not specified. The free volume of the polymer decreases with decreasing temperature, and this is reflected in the increase in the chemical shift as the temperature is lowered. At the glass transition temperature, the polymer experiences a discontinuity in the volume thermal expansion coefficient, which is marked by a discontinuity in the chemical shift versus inverse temperature relationship. As the exact form of the interaction potential is not specified, this treatment does not provide a quantitative measure of the volume thermal expansion coefficient; however, with this method, the difference between the volume thermal expansion coefficient above and below the glass transition temperature can be calculated. Discrepancies between the model and experimental results were attributed to xenon occupying only the amorphous regions of the polymers, whereas the thermal expansion coefficient reflects changes in the overall volume of the polymer including contributions from both the amorphous and crystalline regions. For poly(4-methyl-1-pentene) studies where xenon can diffuse into both amorphous and crystalline phases, the T_g results were in greater agreement.

Miller et al.[57] proposed the van der Waal's model to describe the chemical shift and temperature relationship observed in xenon NMR spectra. This model describes the local arrangement of polymer chains in the amorphous phase where they lie in parallel on a square lattice. The model assumes that the xenon atom diffuses rapidly through the polymer above the glass transition temperature, and that the xenon atom is larger than the average free volume hole size. As a result, the xenon atom must create the hole in which it resides. Therefore, the work the xenon atom requires to create the hole is proportional to the chemical shift. This work involves breaking the van der Waals' bonds between the neighbouring polymer chains, and a Lennard-Jones 6-12 potential is used to describe the van der Waals interaction. For measurements above the glass transition temperature, the van der Waals model can be used to determine polymer properties such as the van der Waals' chain diameter and the solubility parameter. Unfortunately, both models assume that the xenon is exchanging rapidly amongst all available sites; however, this is not always the case.

In addition to the xenon chemical shift, the line width also changes as a function of temperature.[58] This relationship is marked by a more pronounced change in slope than that of the chemical shift. Below the glass transition temperature, the xenon chemical shift is a broad line. In this situation, the polymer is undergoing slower motions and the trapped xenon atoms reside in a distribution of different sites. The anisotropic chemical shift tensor arises from the distortion of the Xe electron cloud by the surrounding polymer chains. Since polymers are heterogeneous at the atomic scale, a distribution of chemical shift tensors will be produced. The xenon chemical shift depends on the orientation of the chemical shift tensors relative to the magnetic field. Above the glass transition temperature, line widths are narrow since xenon diffuses rapidly through the polymer and samples many sites. This exchange reflects the increased mobility of the polymer. The chemical shift tensor of the xenon atom is constantly changing in size and orientation, therefore this exchange averages away the anisotropy and a single, narrow xenon peak is produced.[41-43]

1.4 Scope of the Thesis

This thesis is devoted to the preparation of PS-*b*-PAA aggregates and their characterization by nuclear magnetic resonance spectroscopy techniques. As NMR spectroscopy comprises a diverse class of experiments, two different NMR methods have been used to study this system. The first technique involves solution state NMR relaxation measurements to elucidate the segmental dynamics of the PS-*b*-PAA micelles. The second technique involves a different approach where a probe, xenon, is introduced to the system and NMR measurements of the probe atom result in information of the micellar environment.

In Chapter 2, ^{1}H NMR spin-lattice and spin-spin relaxation measurements are presented to elucidate the segmental mobility of the PS-*b*-PAA copolymer aggregates during the micellization process.

Chapter 3 discusses the investigation of PS-*b*-PAA block copolymer aggregates in dioxane/water solvent mixtures by ^{129}Xe NMR spectroscopy. The xenon atom provides a non-invasive, sensitive probe of its local environment via resonance shift and line width measurements. Of particular interest is the behavior of these two parameters as a function of temperature to provide information of temperature-induced phase transitions in the copolymer aggregates.

Finally, Chapter 4 contains the general conclusions of the thesis, the original contributions to knowledge and the suggestions for future work.

1.5 References

1. Zhang, L.; Eisenberg, A. *Science* **1995**, 268, 1728-1731.
2. Zhang, L; Eisenberg, A. *J. Am. Chem. Soc.* **1996**, 118, 3168-3181.
3. Shen, H.; Zhang, L.; Eisenberg, A. *J. Phys. Chem. B* **1997**, 101, 4697-4708.
4. Chen, L.; Shen, H.; Eisenberg, A *J. Phys. Chem. B* **1999**, 103, 9488-9497.
5. Cameron, N.; Corbiere, M.K.; Eisenberg, A. *Can. J. Chem.* **1999**, 77, 1311-1326.
6. Allen, C.; Eisenberg, A.; Mrsic, J.; Maysinger, D. *Drug Delivery* **2000**, 7, 139-145.
7. Hamley, I. W. *Introduction to Soft Matter Polymers, Colloids, Amphiphiles and Liquid Crystals*; John Wiley and Sons, Ltd.: New York, 2000.
8. Stevens M. P. *Polymer Chemistry an Introduction,* 2nd ed.; Oxford University Press: New York, 1990.
9. Allcock, H. R.; Lampe, F. W. *Contemporary Polymer Chemistry*, 2nd ed.; Prentice Hall: New Jersey, 1990.
10. Mark, J. E.; Eisenberg, A.; Graessley, W.W.; Mandelkern, L.; Samulski, E. T.; Koenig, J. L.; Wignal, G. D. *Physical Properties of Polymers*, 2nd ed.; United Book Press: Baltimore, 1993; Chapter 2.
11. Hautekeer, J.-P.; Varshney, S.K.; Fayt, R.; Jacobs, C.; Jerome, R.; Teyssie, Ph. *Macromolecules* **1990**, 23, 3893-3898.
12. Zhong, X.F.; Varshney, S.K.; Eisenberg, A. *Macromolecules* **1992**, 25, 7160-7167.
13. Tuzar, Z.; Kratochvil, P. In *Surface and Colloid Science*; Matijevic, E., Ed.; Plenum Press: New York, 1993; Vol. 15, p 1.
14. Zhang, L.; Yu, K.; Eisenberg, A. *Science* **1996**, 272, 1777-1779.
15. Zhang, L.; Eisenberg, A. *Macromolecules* **1996**, 29, 8805-8815.
16. Zhang, L.; Eisenberg, A. *Macromol. Symp.* **1997**, 113, 221-232.
17. Zhang, L.; Barlow, R.J.; Eisenberg, A.; *Macromolecules* **1995**, 28, 6055-6066.
18. Yu, Y.; Eisenberg, A. *J. Am. Chem. Soc.* **1997**, 119, 8383-8384.
19. Yu, Y.; Zhang, L.; Eisenberg, A. *Macromolecules* **1998**, 31, 1144-1154.

20. Nagarajan, R. In *Solvents and Self-organization of Polymers; NATO ASI Series*; E., Webber, S. E., Munk, P., Tuzar, Z., Eds.; Kluwer Academic Publishing: 1996; Vol. 327, p121.
21. Nagarajan, R.; Barry, M.; Ruckenstein, E. *Langmuir* **1986**, 2, 210-215.
22. Zhang, L.; Shen, H.; Eisenberg, A. *Macromolecules* **1997**, 30 1001-1011.
23. Kriz, J. Plestil, J. Tuzar, Z.; Pospisil, H.; Brus, J.; Jakes, J.; Masar, B.; Vlcek, P.; Doskocilova, D. *Macromolecules* **1999**, 32, 397-410.
24. Kabanov, A. V.; Nazarova, I. R.; Astafieva, I. V.; Batrakova, E. V.; Alakhov, V. Y.; Yaroslavov, A. A.; Kabanov, V. A. *Macromolecules* **1995**, 28, 2303-2314.
25. Reimer, L. *Transmission Electron Microscopy Physics of Image Formation and Microanalysis*, 4th ed; Springer-Verlag: Berlin Heidelberg, 1997.
26. Cowley, J. M. In *Electron Microscopy in Imaging Visualization;* Hubbard, A. T. Ed.; CRC Press: Boca Raton, 1995.
27. Kirklan, E. J. *Advanced Computing in Electron Microscopy,* Plenum Press: New York, 1998.
28. Shindo, D.; Hiraga, K. *High-Resolution Electron Microscopy for Materials Science,* Springer-Verlag: Tokyo, 1998.
29. Becker, E. D. *High Resolution NMR Theory and Chemical Applications*, 3rd ed.; Academic Press: San Diego, 2000.
30. Rahman, Atta-ur-; Choudhary, M. I. *Solving Problems with NMR Spectroscopy*, Academic Press Inc.: San Diego, 1996, p 213-279.
31. Hore, P. J. *Nuclear Magnetic Resonance*, Oxford University Press Inc.: New York, 1995.
32. Cerichelli, G.; Mancini, G. *Current Opinion in Colloid and Interface Science.* **1997**, 2, 641-648.
33. Vold, R.R. In *Nuclear Magnetic Resonance Probes of Molecular Dynamis;* Tycko, R. Ed.; Kluwer Academic Publishers: Dordrecht, 1994, Chapter 2.
34. McCall, D. W. *Molecular Relaxation in Polymers* **1971**, 4, 223-232.
35. Kulbaba, K.; Macdonald, P. M.; Manners, I. *Macromolecules* **1999**, 32, 1321-1324.

36. Zhu, X. X.; Masaro, L. *Langmuir* **1999**, 15, 8356-8360.

37. Evertsson, H.; Nilsson, S.; Welch, C. J.; Sundelof, L.-O. *Langmuir* **1998**, 14, 6403-6408.

38. Bovey, F. A.; Jelinski, L. W. *J. Phys. Chem.* **1985**, 89, 571-583.

39. Heatley, F.; Begum, A. *Polymer* **1976**, 17, 399-408.

40. Blum, F. D.; Durairaj, B.; Padmanabhan, A. S. *Macromolecules* **1984**, 17, 2837-2846.

41. Raftery, D.; Chmelka, B. F. In *NMR Basic Principles and Progress*; Springer-Verlag: Berlin Heidelberg, 1994, Vol. 30, p 112.

42. Ratcliffe, C. I. In *Annual Report on NMR Spectroscopy*; Academic Press Limited: 1998, Vol. 36, p 124.

43. Springuel-Huet, M. A. In *Principles Physical Adsorption: Experiment, Theory and Applications*; Fraissar, J. Ed.; Kluwer Academic Publishers: Netherlands, 1997, p 331-348.

44. Linder, B. *J. Chem. Phys.* **1966**, 33, 668-675.

45. Koehler, L. S.; Curley, W.; Koehler, K. A. *Mol. Pharmacol.* **1977**, 13, 113-121.

46. Miller, K. W.; Reo, N. V.; Stengle, D. P.; Stengle, T. R. Williamson, K. L. *Proc. Natl. Acad. Sci. USA* **1981**, 78, 4946-4949.

47. Bartik, K.; Luhmer, M.; Dutasta, J.; Collet, A.; Reisse, J. *J. Am. Chem. Soc.* **1998**, 120, 784-791.

48. Brotin, T.; Lesage, A.; Emsley, L.; Collet, A. *J. Am. Chem. Soc.* **2000**, 122, 1171-1174.

49. Bharatam, J.; Bowers, C.R. *J. Phys. Chem. B* **1999**, 103, 2510-2515.

50. Stengle, T. R.; Williamson, K. L. *Macromolecules* **1987**, 20, 1428-1429.

51. Tomaselli, M.; Meier, B. H.; Robyr, P.; Suter, U.W.; Ernst, R.R. *Chemical Physics Letters* **1993**, 205, 145-152.

52. Walton, J. H.; Miller, J. B.; Roland, C. M.; Nagode, J.B. *Macromolecules* **1993**, 26, 4052-4054.

53. Miyoshi, T.; Takegoshi, K.; Terao, T. *Polymer* **1997**, 38, 5475-5480.

54. Yang, C.; Wen, W.; Jones, A. A.; Inglefield, P. T. *Solid State Nuclear Magnetic Resonance* **1998**, 12, 153-164.

55. Shantz, S.; Veeman, W.S. *Journal of Polymer Science: Part B: Polymer Physics* **1997**, 35, 2681-2688.

56. Cheung, T.T.P.; Chu, P. J. *J. Phys. Chem.* **1992**, 96, 9551-9554.

57. Miller, J. B.; Walton, J. H.; Roland, C. M. *Macromolecules* **1993**, 26, 5602-5610.

Chapter 2

^{1}H Nuclear Magnetic Resonance Studies of the Micellization of Polystyrene-*b*-poly(acrylic acid) Diblock Copolymer in Deuterated Dioxane/Deuterium Oxide Solvent Mixtures

2.1 Introduction

The ability of block copolymers to self-assemble in selective solvents to yield nano-sized aggregates has given rise to an extensive field of research. As discussed in Chapter 1, diblock copolymers forming "crew-cut" aggregates display a variety of morphologies, unlike "star" micelles, which are spherical.[1,2] By tailoring the micellization conditions, different morphologies of uniform size distributions can be formed.[3] The versatility of these systems has made them the object of study involving potential applications such as drug delivery and catalysis.[4,5] The majority of research efforts concerning polystyrene-*b*-poly(acrylic acid) "crew-cut" micelles has been devoted to aggregate structure, thermodynamic and kinetic considerations; however, the analysis of this system's sub-micellar properties such as the copolymer chain mobility has not been undertaken.[7,6]

To form PS-*b*-PAA "crew-cut" aggregates, the copolymer is first dissolved in a common solvent. DMF, THF and dioxane are most frequently used in our group.[3] To induce micelle formation, water is slowly added to the copolymer solution. As the addition of water progresses, the quality of the solvent mixture for the PS block decreases and micellization of the PS block commences when a critical water content (cwc) is reached. At the early stages of micelle formation, thermodynamic equilibrium between the unimers and aggregates exist, and as water is progressively added to the solution, the aggregate structures become kinetically frozen.[8,9] It is our goal to monitor the segmental dynamics of the core PS and corona PAA chains during this process. Micellar dynamics have been studied by nuclear magnetic resonance, electron spin resonance and fluorescence techniques.[10] NMR has achieved wide popularity as a powerful technique to elucidate the molecular dynamics of surfactant colloidal systems and its application to study block copolymer aggregate systems is increasing.[11] The versatility of NMR provides different methods of addressing chain dynamics by measuring a variety of NMR parameters such as chemical shift, line widths, and relaxation times. In addition, different NMR experiments including pulse field gradient methods, and the number of different nuclei accessible to NMR investigation provide effective tools to carry out this investigation.[12-16]

Nuclear magnetic resonance studies of block copolymer micelles are relatively rare; the earliest studies involved block copolymer aggregates in organic solvents. In one such study, analysis of ^1H and ^{13}C NMR spectra of polystyrene-*b*-poly(ethylene/propylene) micelles in paraffinic solvents provided information of the polystyrene chain mobility.[17] The PS chain spanned a range of motion from glass-like to liquid-like as a function of the temperature and solvent. The mobile component of the PS block was identified as the plasticised surface layer at the core-corona interface of the micelle. This study was complemented with ^1H NMR spin-lattice and spin-spin relaxation measurements of polystyrene-*b*-poly(ethylene/propylene) micelles in octane.[18] In this investigation, spin diffusion experiments detected the existence of a core-corona mixed phase. Gao *et al.*[10] used a different approach to study the corona chain dynamics of ionomer aggregates. Here, deuterium NMR measurements were performed on block ionomers into which ^2H labeled segments were incorporated at different sites along the corona chain. The chain mobility of the deuterium label segment was assessed as a function of its distance from the core-corona interface. Also employing ^2H NMR, Xie *et al.*[19] investigated the dynamics of poly(β-deuteriostyrene-*b*-2-vinylpyridine) aggregates in toluene and compared the relaxation time and self-diffusion coefficient data with that of homopolymer poly(α-deuteriostyrene) in the same solvent. Using the Hall-Helfand model for chain dynamics, they determined that the short-range motions were similar for the homopolymer and the copolymer while the long-range motions were different.

Only recently has NMR spectroscopy been used to study aqueous systems of block copolymer aggregates. Cau *et al.*[20] acquired ^{1}H NMR relaxation measurements to study the temperature induced micellization behavior of poly(ethylene oxide)-*b*-polypropylene-*b*-poly(ethylene oxide) (PEO-*b*-PPO-*b*-PEO) triblock copolymers. By monitoring the PPO methyl and PEO methylene relaxation processes, they determined that the PPO blocks were more extended in the micelles than in unimer form. In contrast, the local segmental motions in the PEO block were unaffected by the micellization process and exhibited similar motional processes to PEO homopolymer in dilute solutions. Kriz *et al.*[21-23] studied the solubilization of organic compounds into poly(methyl methacrylate)-*b*-poly(acrylic acid) (PMMA-*b*-PAA) micelles. The PMMA chain mobility decreased to a quasi-glassy state detected by the broadening of the NMR signals. The PAA blocks experienced chain stiffening caused by the neutralization of the corona chains by either Li^+, Na^+ or K^+ counterions.[23] They observed that both the amount of uptake and the rate of solubilization of organic compounds was mainly determined by the Flory-Huggins parameter where solubilization proceeds more readily with organic compounds that are better solvents for the PMMA core. They also observed that the organic compounds were inhomogeneously solubilized into the micelle with more uptake of the solubilizate in the outer region of the micelle core. In a separate study, the possibility of tailoring the solubilization capacity and the uptake/release rate for solubilizates using a multi-layer micelle core was investigated with three-layer micelles of poly(2-ethylhexyl acrylate)-*b*-poly(methyl methacrylate)-*b*-poly(acrylic acid) copolymer in deuterium oxide.[24] Solubilization of solvents resulted in the increased mobility of the polymer chains forming the aggregate core.

This chapter discusses the investigation of the local segmental motions of PS-*b*-PAA copolymer in deuterated dioxane during the micellization process. Aggregate formation is induced by the gradual addition of deuterium oxide to the copolymer solution. Dioxane was chosen as the common solvent since extensive information for this system has been accumulated including critical water contents, morphological phase diagrams and the kinetics of morphological transitions.[7,9,25-26] Analysis of ^{1}H NMR spectra, spin-lattice and spin-spin relaxation times is presented. To improve our comprehension of the unique dynamic behavior of the block copolymer, homopolymer polystyrene solutions were also monitored by ^{1}H NMR measurements. The relaxation data for the PS phenyl ring protons was interpreted using the diamond lattice model developed by Valeur *et al.*[27]

2.2 Experimental Section

2.2.1 Preparation of PS-*b*-PAA Micelle Solutions

The copolymers used in this study were synthesized by anionic polymerization as described in detail elsewhere.[28,29] The polymers are denoted as PS_x and PS_x-*b*-PAA_y where x and y represent the number average degrees of polymerization of the PS and PAA blocks. Poly(acrylic acid) homopolymer was purchased from Aldrich Chemical Company. The deuterated dioxane and deuterium oxide were acquired from Cambridge Isotope Laboratories, Inc. and Isotec Inc. respectively.

Poly(styrene)-*b*-poly(acrylic acid) copolymer micelle solutions were prepared by directly dissolving the polymer in deuterated dioxane in 5-mm NMR tubes. Micellization of the copolymer was induced by the addition of deuterium oxide to the polymer solution. The micelle solutions were stirred and allowed to equilibrate overnight before the NMR measurements. NMR relaxation measurements were performed in duplicate after each deuterium oxide addition in the range of 0 wt % to 40 wt %. In addition to the copolymer solutions, homopolymer polystyrene solutions were prepared and examined by NMR in a similar fashion. To assist with the assignment of the ^{1}H NMR resonance signals, the NMR spectrum of homopolymer poly(acrylic acid) dissolved in deuterium oxide was also acquired.

Table 2.1. Polydispersities and Concentrations of Polymer Samples

Polymer	M_w/M_n	Polymer Concentration wt %
PS_{100}-*b*-PAA_{25}	1.10	1
PS_{100}-*b*-PAA_{25}	1.10	3
PS_{218}-*b*-PAA_{20}	1.08	1
PS_{208}	1.17	1
PAA_{28}		1

2.2.2 Nuclear Magnetic Resonance Measurements

^{13}C NMR experiments were performed on a Varian Mercury 400 MHz spectrometer operating at 100.6 MHz. A pulse width of 8.2 μs and a pulse delay of 1 s were used. Over 30 000 scans were acquired for the ^{13}C NMR spectrum. The Homonuclear Shift-correlated (COSY) and ^{1}H-Detected Heteronuclear Multiple-Quantum Coherence (HMQC) spectra were acquired on a Varian Mercury 400 MHz spectrometer operating at 400.1 MHz. One dimensional ^{1}H NMR experiments were performed on a Varian Unity 500 MHz spectrometer operating at 499.8 MHz. ^{1}H spin-lattice relaxation times, T_1, were measured with the inversion-recovery method. ^{1}H spin-spin relaxation times, T_2, were acquired with the Carr-Purcell-Meilboom-Gill pulse sequence. A pulse delay of at least 5 x T_1 was used to allow the protons to achieve equilibrium magnetization after each data acquisition. For the relaxation time measurements, the temperature was controlled at 298.73 K to within ±0.2 degrees. Before the NMR measurement, the micelle solution was allowed to equilibrate at the sample temperature for 15 minutes. Chemical shifts were measured from the residual protons in the dioxane solvent, while the dioxane signal served for the lock.

2.3 Results and Discussion

The Results and Discussion section contains three parts. Section 2.3.1 discusses the assignment of the ^{1}H and ^{13}C NMR resonance signals using the COSY and HMQC methods. Section 2.3.2 analyzes the features of the ^{1}H NMR spectra of the PS-*b*-PAA copolymer and PS homopolymer solutions as deuterium oxide is progressively added. Section 2.3.3 assesses the ^{1}H NMR relaxation measurements obtained as a function of deuterium oxide content of the copolymer solutions.

2.3.1 Assignment of ^{1}H and ^{13}C Nuclear Magnetic Resonance Peaks

The ^{1}H NMR spectrum of a 3 wt % solution of PS_{100}-*b*-PAA_{25} block copolymer in deuterated dioxane is displayed in Figure 2.1. The assignment of the ^{1}H NMR resonance peaks in the present study corresponds well with previous investigations involving polystyrene and poly(acrylic acid) homopolymers.[30-32]

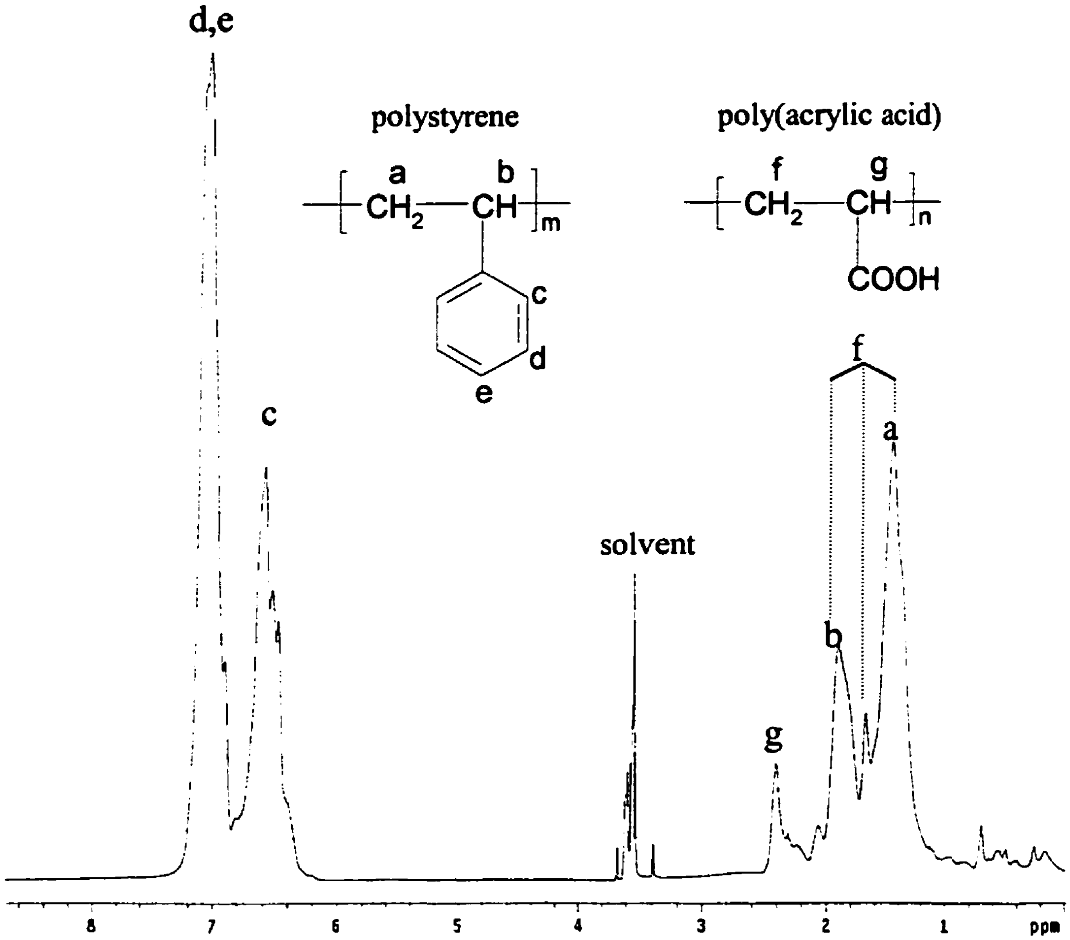

Figure 2.1 ^{1}H NMR spectrum of 3 wt % PS_{100}-*b*-PAA_{25} block copolymer in deuterated dioxane.

The ^{13}C NMR spectrum of a 1 wt % solution of PS_{100}-*b*-PAA_{25} in a 89/11 wt % deuterated dioxane/deuterium oxide solvent mixture is presented in Figure 2.1. ^{13}C NMR peaks were assigned by a combination of two-dimensional NMR measurements and comparisons with literature values.[32-33]

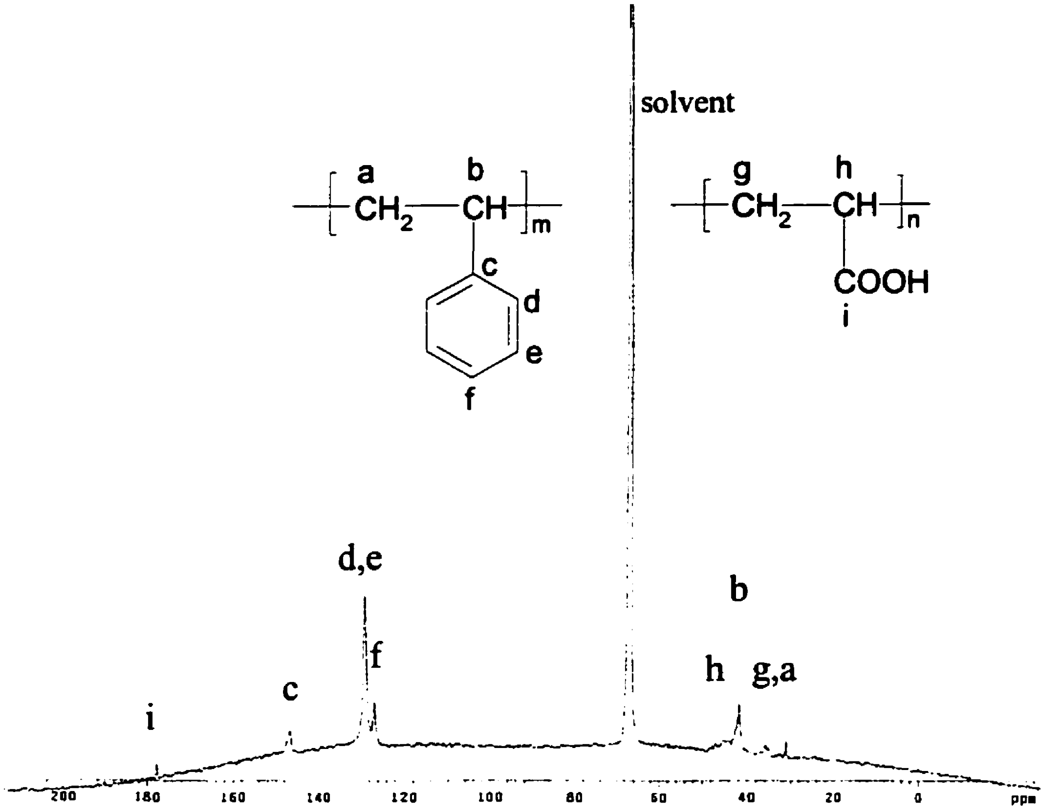

Figure 2.2 ^{13}C NMR spectrum of 1 wt % PS_{100}-*b*-PAA_{25} block copolymer in a 89/11 wt % deuterated dioxane/deuterium oxide solvent mixture.

For both the ^{1}H and ^{13}C NMR spectra, the PS phenyl ring resonance peaks were assigned from previous studies without difficulty, where the ^{1}H chemical shift at 7.02 ppm is attributed to the meta and para protons, and the peak at 6.58 ppm is assigned to the ortho proton. The PAA carboxylic acid carbon resonance shift appears at 180 ppm in Figure 2.2. In contrast, the peaks from the PS and PAA backbone chains were difficult to assess due to the overlapping nature of this spectral region. To assign the PS and PAA backbone chain signals, two-dimensional NMR methods were employed. The Homonuclear Shift-correlation spectrum of a 1 wt % solution of PS_{100}-*b*-PAA_{25} in a 89/11 wt % deuterated dioxane/deuterium oxide solvent mixture is shown in Figure 2.3. In the COSY spectrum, the axes denote the chemical shifts of the coupled nuclei whereas the cross-peaks indicate which nuclei are coupled to each other.[34] The cross-peak at 1.4 ppm and 1.8 ppm indicates coupling between the α proton and the two β protons of the PS block. A second cross-peak observed at 1.7 ppm and 2.3 ppm demonstrates coupling between the protons of the PAA main-chain. Coupling between the ortho proton and the meta and para protons of the PS aromatic group was also observed by the presence of a cross-peak at 6.6 ppm and 7.1 ppm.

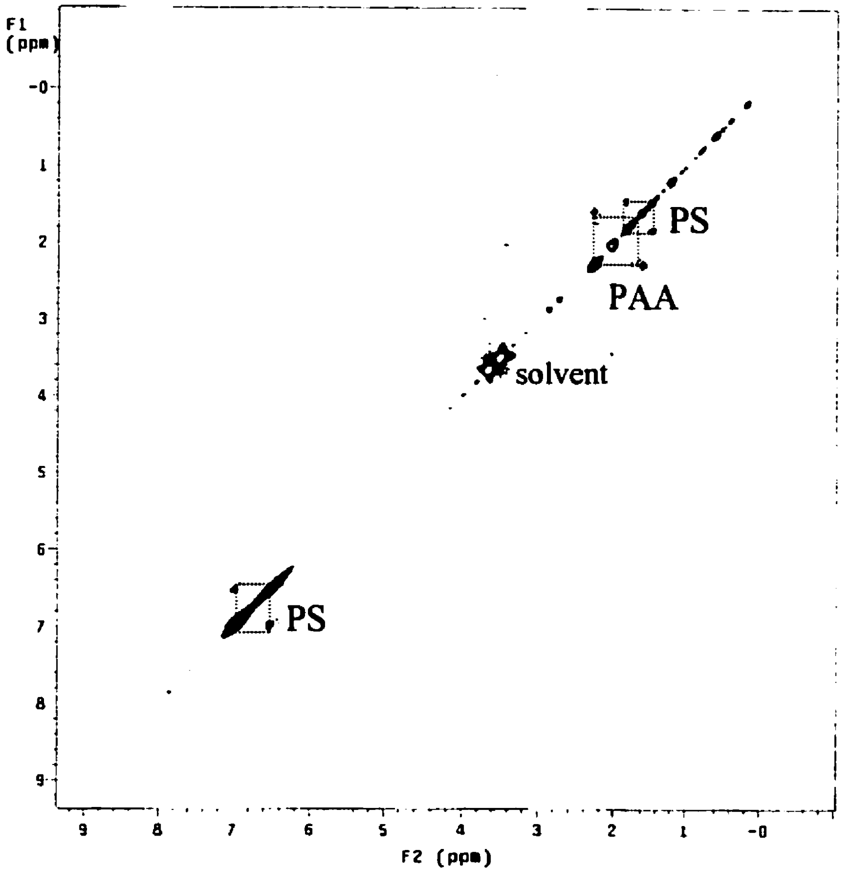

Figure 2.3 COSY NMR spectrum of 1 wt % PS_{100}-*b*-PAA_{25} block copolymer in a 89/11 wt % deuterated dioxane/deuterium oxide solvent mixture.

In addition to the COSY technique, a ^{1}H-Detected Heteronuclear Multiple-Quantum Coherence experiment was also used to assign the ^{1}H and ^{13}C resonance peaks. Figure 2.4 and 2.5 display the relevant sections of the HMQC spectrum of a 1 wt % solution of PS_{100}-*b*-PAA_{25} in a 89/11 wt % deuterated dioxane/deuterium oxide solvent mixture. The HMQC pulse sequence provides a highly sensitive technique to determine one-bond ^{1}H-^{13}C shift correlations where protons directly bonded to ^{13}C nuclei produce cross-peaks in the spectrum.[34] In Figure 2.2, the ^{13}C chemical shifts for the PS ortho and meta carbons were assigned to 128.0 ppm and 128.4 ppm whereas the para carbon was assigned to 126.2 ppm. From the HMQC spectrum, we deduced that the quaternary carbon on the aromatic group appeared at 147 ppm by the absence of a cross-peak for this nucleus.

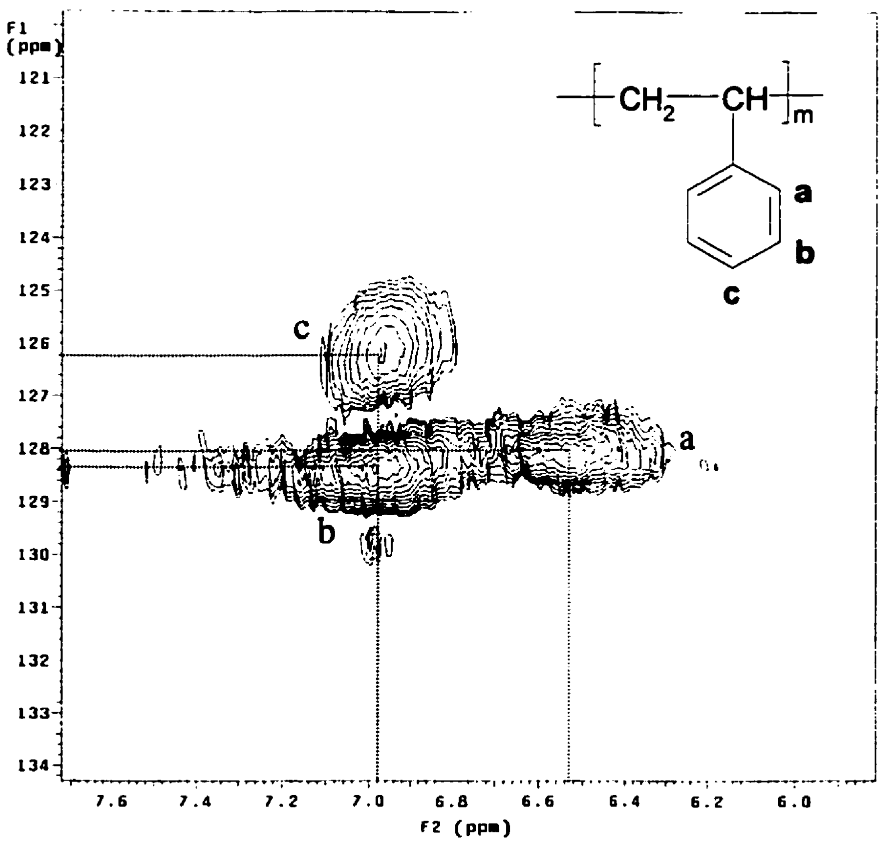

Figure 2.4 HMQC NMR spectrum of the 1 wt % PS_{100}-*b*-PAA_{25} block copolymer in a 89/11 wt % deuterated dioxane/deuterium oxide solvent mixture.

The HMQC experiment was effective in determining the individual resonance peaks for the PS and PAA main-chain proton and carbon nuclei. The PS β proton at 1.44 ppm is correlated with the carbon chemical shift at 35.8 ppm. According to previous measurements and the ^{1}H NMR spectrum of the PAA homopolymer, the PAA β proton resonance splits into three peaks at 1.80 ppm, 1.63 ppm, and 1.52 ppm representing the triad distribution of the *rr*, *mr*, and *mm* sequences.[27] These resonance peaks are observed in the HMQC spectrum with the corresponding carbon resonance shift as 35 ppm. The cross-peak for the PAA α proton at 2.3 ppm corresponds to the carbon resonance peak at 41.7 ppm whereas the α proton for the PS backbone at 1.80 ppm correlates with the carbon resonance peak at 41 ppm.

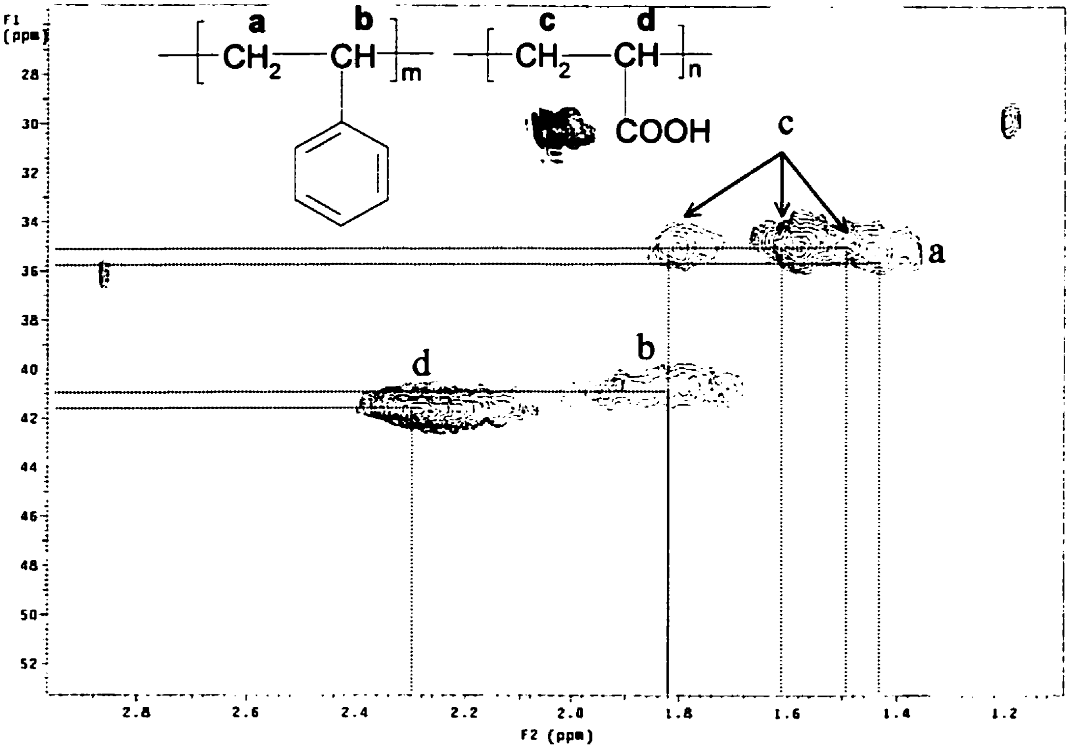

Figure 2.5 HMQC NMR spectrum of the 1 wt % PS_{100}-*b*-PAA_{25} block copolymer in a 89/11 wt % deuterated dioxane/deuterium oxide solvent mixture.

The ^1H NMR spectrum in Figure 2.1 illustrates the desirable high sensitivity of the nucleus; however, all the chemical information is contained within a spectral width of only *ca.* 10 ppm. As a result, acquiring spectra with well resolved resonance shifts is often not possible for polymers in solution. In contrast, ^{13}C NMR spectroscopy provides better chemical resolution with the wider spectral width; however, this is counterbalanced by the decreased sensitivity of the technique due to the low natural abundance of the ^{13}C isotope and its small gyromagnetic ratio. The ^{13}C spectrum in Figure 2.2 was obtained with over 30 000 scans, and regrettably, the weak ^{13}C signals demonstrate that at the polymer concentrations employed to form the PS-*b*-PAA micelle solutions, measuring the ^{13}C relaxation times to monitor the chain dynamics is not feasible.

2.3.2 Analysis of the ^1H NMR Spectra during the Micellization of PS-*b*-PAA Copolymers

The gradual addition of deuterium oxide to the copolymer solutions inducing the formation of aggregates greatly affected the ^1H NMR spectral features. The ^1H NMR spectra of the phenyl ring protons of the PS block with varying amounts of deuterium oxide in the copolymer solution are shown in Figure 2.6. Before the addition of deuterium oxide, the copolymer solutions produce PS and PAA NMR signals with line shapes that are comparable to homopolymer PS and PAA solutions. Most synthetic polymers in solution give fairly well resolved proton spectra and therefore enjoy considerable segmental freedom.[35] Proton NMR line widths for polymers in solution have been found to be independent of molecular weight down to the oligomer level and are almost independent of concentration up to 25 to 30 wt %. Nevertheless, if one compares polymer NMR spectra to their small molecule counterparts, they are still less resolved.[35] As deuterium oxide is added, the PS phenyl ring resonance peaks display weaker intensity and are broadened. For the 1 wt % PS_{100}-*b*-PAA_{25} copolymer in dioxane, at a deuterium oxide content of 32 wt %, these resonance peaks are broadened beyond detection. This process occurs at a deuterium oxide content of 28 wt % for the 3 wt % PS_{100}-*b*-PAA_{25} and 1 wt % PS_{218}-*b*-PAA_{20} copolymers in dioxane. In contrast to these deuterium oxide values for the copolymer samples, the phenyl ring NMR signals for the homopolymer PS_{208} can no longer be detected at a deuterium oxide content of 14 wt %. The aromatic signals for the block copolymer are detectable up to a higher deuterium oxide content than for the homopolymer polystyrene indicating that though the aggregation of the PS blocks greatly restricts their mobility, they do not experience similar motional freedom to that of phase-separated PS homopolymer suspended in solution. Candau *et al.*[17] observed a similar phenomenon for polystyrene-*b*-poly(ethylene/propylene) aggregates, which they attributed to the decreased mobility of the PS block resulting in a broad line width outside the range of the solution-state NMR instrument. In this study, we observe the same process where the PS block undergoes a transition from a mobile liquid-like to a rigid glassy state. The disappearance of the resonance signals for the insoluble block has also been observed for different systems.[18,21] Before the aggregation of the block copolymer, the two PS aromatic resonance peaks are well resolved; however, upon micellization the peaks coalesce. The broadening and coalescence of the aromatic signals occurred for all block copolymers and the PS homopolymer solutions even though the former was forming micelles and the latter was undergoing phase separation as the deuterium oxide was added.

During the micellization of the PS-*b*-PAA copolymer, the resonance peak for the meta and para protons of the PS aromatic group shifted downfield. A similar effect was observed for the ortho proton of the same aromatic group.

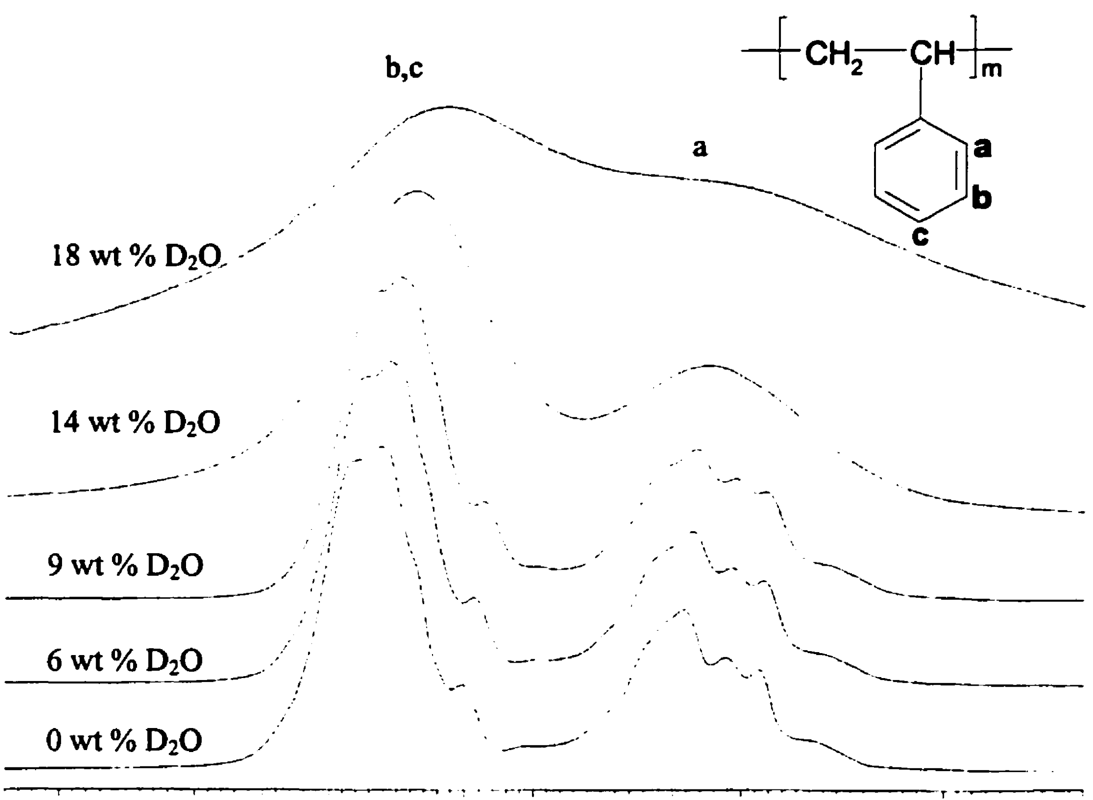

Figure 2.6 Deuterium oxide dependence of the ^{1}H NMR line shapes of the 3 wt % PS_{100}-*b*-PAA_{25} block copolymer in dioxane. The spectral region for the phenyl ring protons of the PS block is shown.

Analysis of the ^{1}H NMR spectral region for the PS and PAA main-chain protons reveals that the PS and PAA blocks undergo different degrees of motion during micelle formation. This region for the 3 wt % PS_{100}-*b*-PAA_{25} copolymer is displayed in Figure 2.7. The most substantial modification of the spectral line shapes occurs for the PS α and β proton resonance peaks at 1.8 ppm and 1.4 ppm. With the gradual addition of deuterium oxide, the intensity of these signals is decreased and their line widths become broad. This transition in line shape is most pronounced after the addition of 12 wt % deuterium oxide to the copolymer solution. As the resonance peaks of the PS block are broadened, the signals for the PAA β protons become more prominent in the spectrum. The PAA α proton at 2.35 ppm remains unchanged during the micellization process indicating that its local environment remains constant. The broadening of the PS α and β resonance signals was observed for all copolymer solutions. The broadening of the line shape is attributed to the decreased mobility of the PS chain.

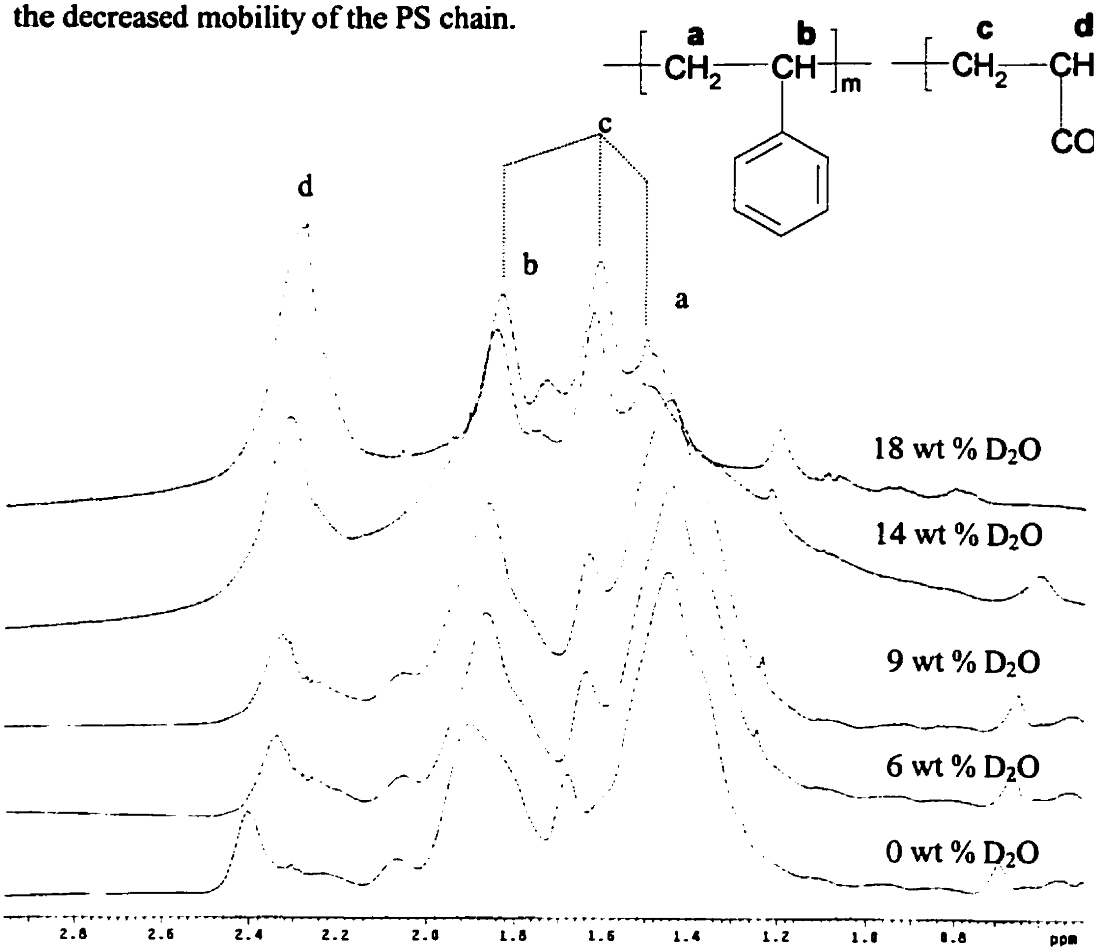

Figure 2.7 Deuterium oxide dependence of the ^{1}H NMR line shapes of the 3 wt % PS$_{100}$-*b*-PAA$_{25}$ block copolymer in dioxane. The spectral region for the aliphatic protons of the PS$_{100}$-*b*-PAA$_{25}$ copolymer is shown.

At high deuterium oxide contents, the further addition of the precipitant does not significantly alter the line shapes of the PS-*b*-PAA copolymer ^{1}H NMR spectrum as shown in Figure 2.8. Broadening of this region can also be attributed to the increased viscosity of the sample caused by the presence of the block copolymer aggregates, which inhibits the block copolymer long-range and segmental motions. In addition, the PAA signals will be broadened due to the PAA units close to the core-corona interface, which should experience restricted mobility upon micellization. Similar effects are observed in the ^{1}H NMR spectra for all block copolymer samples. For the homopolymer PS solution, as deuterium oxide is added, the suitability of the solvent mixture decreases for the polymer and it phase separates out of solution, therefore after the addition of 14 wt %, the intensity of the NMR signals is extremely low.

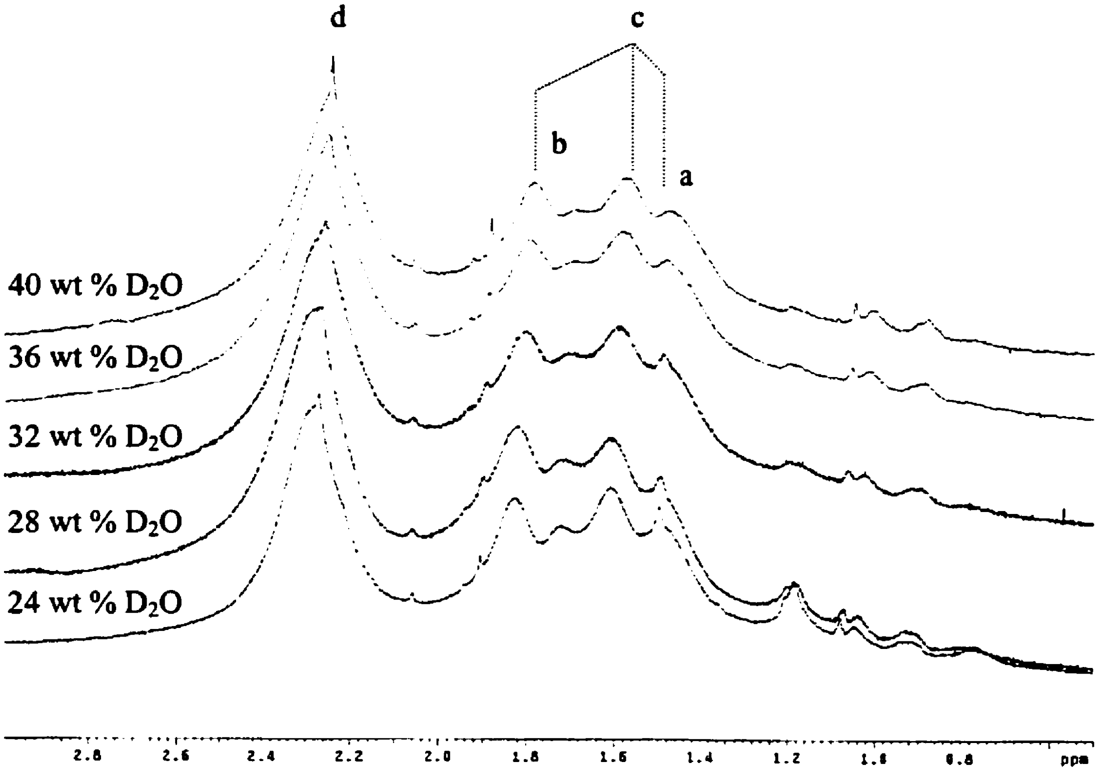

Figure 2.8 Deuterium oxide dependence of the ^{1}H NMR line shapes of the 3 wt % PS_{100}-*b*-PAA_{25} block copolymer in dioxane at high deuterium oxide contents. The spectral region for the aliphatic protons of the PS_{100}-*b*-PAA_{25} copolymer is shown.

2.3.3.1 ^{1}H NMR Relaxation Measurements

To monitor the copolymer chain dynamics during the micellization process, ^{1}H NMR relaxation times were measured. To improve our understanding of the effect of micellization on the copolymer chain dynamics, the relaxation behavior of homopolymer PS was also monitored. The low resolution of the ^{1}H NMR spectrum only allowed the determination of T_1 and T_2 relaxation times of the PS phenyl ring protons and the PAA α proton. The remaining signals could not be resolved due to the overlapping nature of the spectrum. The influence of the micellization process on the spin-lattice relaxation time for the PS aromatic protons is shown in Figure 2.9. At low deuterium oxide contents, the T_1 values are constant; however, at a critical deuterium oxide content between 10-12 wt %, the relaxation times increase abruptly. For the 1 wt % PS_{100}-*b*-PAA_{25} copolymer sample, the T_1 values reach an upper limit and a plateau region after the increase in T_1 at the cwc. It is important to note that relaxation times for these protons were obtainable only up to a specific deuterium oxide content before the PS aromatic resonance peaks coalesced to form one signal. Therefore, the plateau region observed for the 1 wt % PS_{100}-*b*-PAA_{25} copolymer solution was not detected for the 3 wt % PS_{100}-*b*-PAA_{25} or the 1 wt % PS_{218}-*b*-PAA_{20} copolymer solutions. For the 1 and 3 wt % PS_{100}-*b*-PAA_{25} copolymer solutions relaxation measurements were determined up to a deuterium oxide content of 16 wt % while for the 1 wt % PS_{218}-*b*-PAA_{20} and PS_{208} solutions, relaxation values were obtained up to 12 wt % of the precipitant. Even though relaxation data for the PS phenyl ring protons were not measurable up to 40 wt % deuterium oxide, we believe that the large majority of copolymer chains were in aggregate form at these deuterium oxide contents. Previously, Yu *et al.*[9] determined the micelle fraction of PS-*b*-PAA copolymer in various solvents. The micelle fraction is the ratio of the associated polymer to the total polymer. They observed that the micelle fraction increased rapidly within a very narrow range of water contents once microphase separation started at the critical water content. In dioxane, 99.5 % micellization occurred when a water increment of only 2.63 wt % was added after the cwc.[9] This is clearly the situation for the 1 and 3 wt % PS_{100}-*b*-PAA_{25} copolymer solutions where 16 wt % deuterium oxide has been added. Before micellization of the copolymer, the meta and para protons of the PS phenyl ring exhibit different relaxation times from that of the ortho proton of the same side-group; however, with the onset of aggregate formation, their T_1 times become similar. It is expected that as micellization of the block copolymer occurs, the segmental mobility of the polymer chains will become restricted. Therefore as deuterium oxide is progressively added, the correlation time, τ_c, will become longer. For the PS-*b*-PAA copolymer micelles, as the correlation times increase the spin-lattice relaxation times also increase. This behavior indicates that the relaxation behavior of this system is in the slow motion limit, which was discussed in

Section 1.3.3.3. In this region of the T_1-τ_c curve, T_1 is greater than T_2, and T_1 is dependent on the applied magnetic field strength.

The steep increase of the T_1 values at a specific deuterium oxide content correlates well with critical water content determinations by static light scattering experiments.[8,9] It was determined that cwc depends on the polymer concentration, the PS block length and the initial common solvent. In DMF, the cwc was found in the range of 2-9 wt %, 9-11 wt % for dioxane and 16-18 wt % for THF.

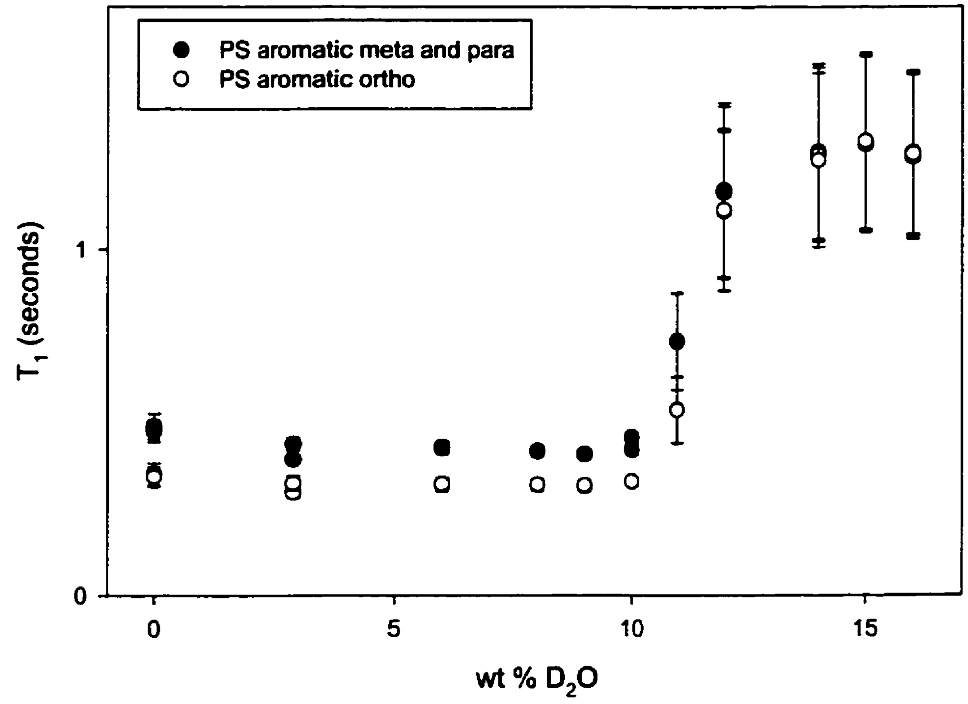

Figure 2.9 Deuterium oxide dependence on the spin-lattice relaxation time for the PS phenyl ring protons of the 1 wt % PS_{100}-*b*-PAA_{25} copolymer in dioxane.

Shen *et al.*[9] also determined that the cwc for homopolymer PS is only slightly lower than that of the block copolymer with the same PS block length in the same initial common solvent. It is clear that the mobility dependence on the deuterium oxide content differs greatly for the block copolymer PS aromatic proton relaxation behavior than that of the homopolymer with a similar PS block length. As displayed in Figure 2.10 for the 1 wt % PS_{218}-*b*-PAA_{20} and 1 wt % PS_{208} solutions, the spin-lattice relaxation times for the PS homopolymer increase at a lower deuterium oxide content than for the copolymer of the similar PS block length. In addition, the homopolymer experiences only a slight gradual increase in T_1 time before it reaches a plateau region. Therefore, upon aggregate formation, the PS block of the copolymer experiences more restricted mobility than the PS homopolymer.

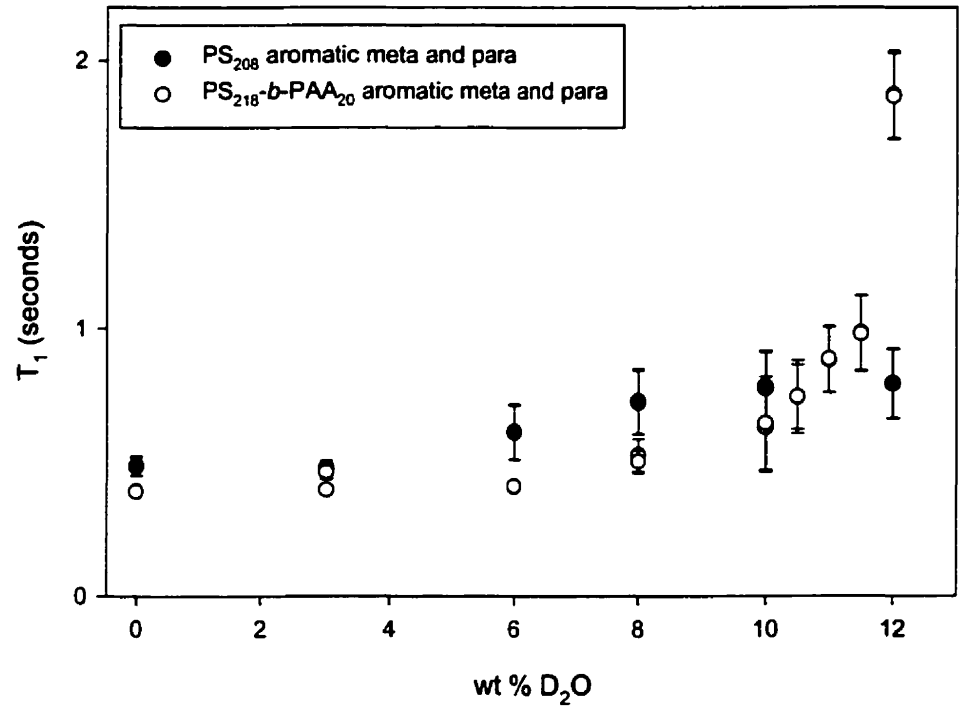

Figure 2.10 Deuterium oxide dependence on the spin-lattice relaxation time for the PS phenyl ring meta and para protons of the 1 wt % PS_{218}-*b*-PAA_{20} copolymer and 1 wt % PS_{208} homopolymer in dioxane.

The spin-spin relaxation time dependence on the correlation time is different from that of the spin-lattice relaxation time. T_2 decreases monotonically with increasing τ_c and reaches a lower limit characteristic of a rigid solid lattice where mobility is highly restricted. The spin-spin relaxation times of the PS phenyl ring protons of the 1 wt % PS_{100}-*b*-PAA_{25} copolymer are tabulated in Table 2.2. The T_2 values were determined by fitting the relaxation data to a single exponential function. It is evident that the progressive addition of deuterium oxide to the copolymer solution greatly influences the spin-spin relaxation times of the PS aromatic protons. With the initial addition of deuterium oxide, the spin-spin relaxation times do not change greatly, and there is a large amount of fluctuation in the T_2 values. Prior to micelle formation, the percent error of the spin-spin relaxation time is greater than 10%. Analysis of the quality of the single exponential fit of the T_2 relaxation data revealed that at low D_2O contents, the spin-spin relaxation does not exhibit single exponential behavior. We fitted the spin-spin relaxation data of the PS phenyl ring protons using a biexponential function; however, the number of data points will need to be increased to determine conclusively if the T_2 values conform to biexponential decay. Clearly, the spin-spin relaxation process detects inhomogeneity in the mobility of the PS phenyl ring before aggregation of the PS-*b*-PAA copolymer. Poor fitting of the spin-spin relaxation times to the single exponential function has been observed for polymers in solution. Mao *et al.*[36] studied the dissolution behavior of concentrated PS solutions in cyclohexane by ^{13}C and ^{1}H NMR spectroscopy. The spin-spin relaxation processes of the PS phenyl ring and main-chain protons were fitted to biexponential functions. They described the spin-spin relaxation behavior as consisting of nuclei undergoing fast and slow relaxation processes. The protons exhibiting slow relaxation are associated with polymer chains which are moving freely in solution while the protons involved in polymer chain entanglements had shorter relaxation times.

It is curious that T_2 detects the motional inhomogeneity of the PS phenyl ring protons before micellization, while T_1 which exhibits single exponential relaxation does not. This contrast can be explained by examining the motional frequencies which affect the T_1 and T_2 processes. Spin-spin relaxation is sensitive to low frequency motions, as a result, T_2 values probe only a small microregion of the polymer solution. Faster motions affect spin-lattice relaxation processes and the scale of the T_1 extends further detecting a larger region. Within the larger scaling region of the spin-lattice relaxation time, spin diffusion between entangled polymer chains occurs, which eliminates the relaxational inhomogeneity among the polymer chains. However, the spin-spin relaxation times, which are much shorter than the spin-lattice relaxation times, are not affected by spin diffusion and this relaxation process detects the motional heterogeneity within the smaller microregion.[37]

As deuterium oxide is progressively added to the PS-*b*-PAA copolymer solution, microphase separation occurs at the cwc and the spin-spin relaxation times decrease drastically and reach a lower limit. The decrease in the spin-spin relaxation times reveal that the mobility of the PS phenyl ring protons is restricted upon aggregate formation. Cau *et al.*[20] observed a sharp decrease in the T_2 values for the methyl protons of the PPO block of PEO-*b*-PPO-*b*-PEO copolymer in D_2O at the critical micellization temperature. The magnitude of the decrease in spin-spin relaxation values is comparable to the change in T_2 values for the PS phenyl ring protons of our PS-*b*-PAA copolymer aggregates. After micelle formation, the spin-spin relaxation data fit the single exponential function. The percent error of the T_2 values is less than 5%. Therefore, the spin-spin relaxation behavior of the PS phenyl ring protons exhibit motional homogeneity in the PS-*b*-PAA micelles. The spin-spin relaxation times decreased sharply at the cwc for all copolymer solutions. In contrast, the decrease of T_2 for the PS homopolymer solution occurred gradually over a range of deuterium oxide contents.

Table 2.2 Spin-spin Relaxation Times for the PS Phenyl Ring Protons of the 1 wt % PS_{100}-*b*-PAA_{25} Copolymer Solution

D_2O content wt %	Meta and Para T_2 seconds	Ortho T_2 seconds
0	0.08±0.03	0.06±0.02
3	0.07±0.02	0.05±0.01
6	0.11±0.03	0.07±0.02
8	0.12±0.03	0.07±0.02
9	0.09±0.02	0.05±0.01
10	0.09±0.02	0.06±0.01
11	0.14±0.02	0.07±0.01
12	0.026±0.002	0.020±0.001
14	0.019±0.001	0.0159±0.0009
15	0.019±0.001	0.016±0.001
16	0.019±0.001	0.0152±0.0005

While the core dynamics could only be monitored before the coalescence of the two aromatic peaks, spin-lattice relaxation times of the coronal PAA chains were measurable for a larger range of deuterium oxide contents. Therefore, the corona dynamics were monitored for deuterium oxide contents well above the cwc. The T_1 values for the PAA α-hydrogen are shown in Figure 2.11. Prior to copolymer association, at low deuterium oxide contents, the spin-lattice relaxation times for the PAA chains decrease slightly. With the onset of copolymer aggregation, the T_1 values increase dramatically indicating that the PAA chains are experiencing restricted segmental motion. However, at high deuterium oxide contents the spin-lattice relaxation times decrease as D_2O is a good solvent for the corona chains. There are various processes occurring during block copolymer aggregate formation including the increased solution viscosity, and the progressive dilution of the copolymer solution with the addition of deuterium oxide. It should also be noted that the mobility of the PAA chain would experience different degrees of segmental freedom with the most rigid components near the core-corona interface as observed by Gao *et al.*[10] for poly(styrene-*b*-sodium acrylate) reverse micelles.

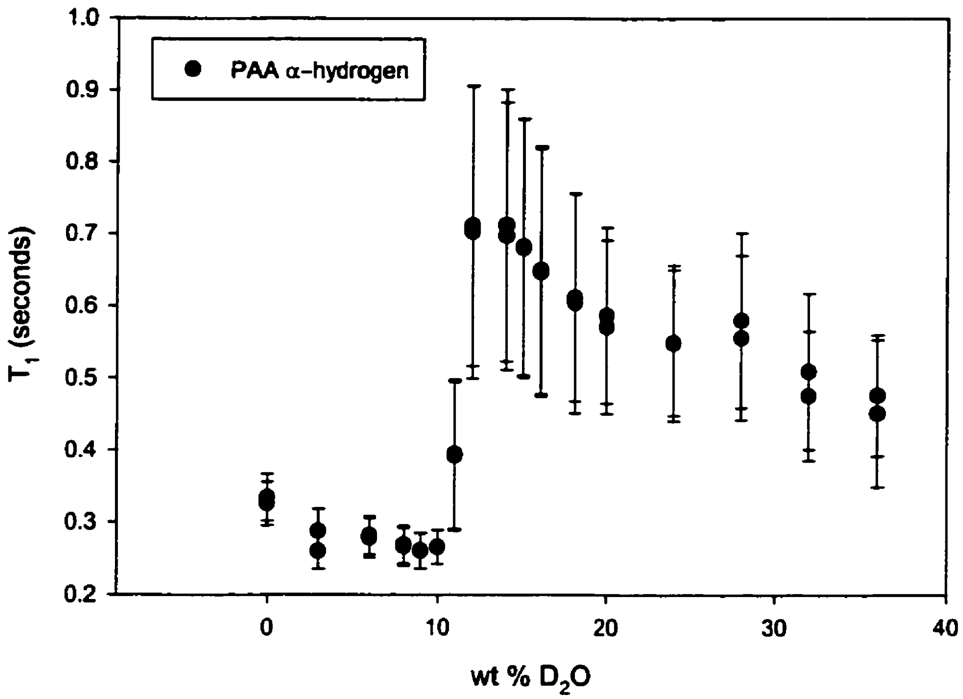

Figure 2.11 Deuterium oxide dependence on the spin-lattice relaxation time for the PAA α proton of the 1 wt % PS_{100}-*b*-PAA_{25} copolymer in dioxane.

The dependence of PAA spin-spin relaxation times on the deuterium oxide content was also observed. However, in this case, due to the sensitivity of the experiment, relaxation times could not be acquired up to 40% deuterium oxide content. The T_2 values are displayed in Table 2.3. Before block copolymer micellization, the T_2 values exhibited a large amount of scatter and did not fit the single exponential function. At the cwc, the spin-spin relaxation times decreased slightly indicating longer correlation times and restricted mobility of the PAA blocks. The chain in the spin-spin relaxation times of the PS blocks at the cwc was much larger in magnitude, reflecting the transformation from freely moving, solvated chain segments to the solid-like environment of the micelle core. While the spin-spin relaxation values for the PS phenyl ring protons exhibited single exponential behavior at the onset of aggregate formation, the T_2 values for the PAA α-hydrogen exhibited motional inhomogeneity at D_2O contents surpassing the cwc. At a D_2O content of 24 wt %, the PAA α-hydrogen spin-spin relaxation data conformed to the single exponential behavior.

Table 2.3 Spin-spin Relaxation Times for the PAA α-hydrogen of 1 wt % PS_{100}-*b*-PAA_{25} Copolymer Solution

D_2O content wt %	α-hydrogen T_2 seconds
0	0.027±0.006
3	0.027±0.005
6	0.031±0.006
8	0.034±0.006
9	0.029±0.005
10	0.031±0.006
11	0.03±0.01
12	0.024±0.004
14	0.025±0.005
15	0.024±0.004
16	0.025±0.005
18	0.025±0.005
20	0.025±0.004
24	0.022±0.002

The ratio of the relaxation times T_1 and T_2 can be used as an indicator of the deviation of the relaxation data from the NMR fast, isotropic motion limit where $T_1 \approx T_2$ and the spin-lattice relaxation time is independent of the applied magnetic field strength.[38] The T_1/T_2 values for the 1 wt % PS_{100}-*b*-PAA_{25} copolymer in dioxane as a function of deuterium oxide content is shown in Figure 2.12. The ratio at low deuterium oxide contents is constant until the cwc is reached whereupon the T_1/T_2 ratio increases dramatically. It is interesting to note that for the spin-lattice relaxation times, at high deuterium oxide contents, the meta/para and ortho resonance signals exhibited similar values; however the T_1/T_2 which are initially similar, become different after the cwc. This trend was observed for all the homopolymer and the block copolymer samples. The T_1/T_2 values increase for the homopolymer PS_{208} gradually as the precipitant is added to the polymer solution where the final values are lower than those recorded for the block copolymer samples.

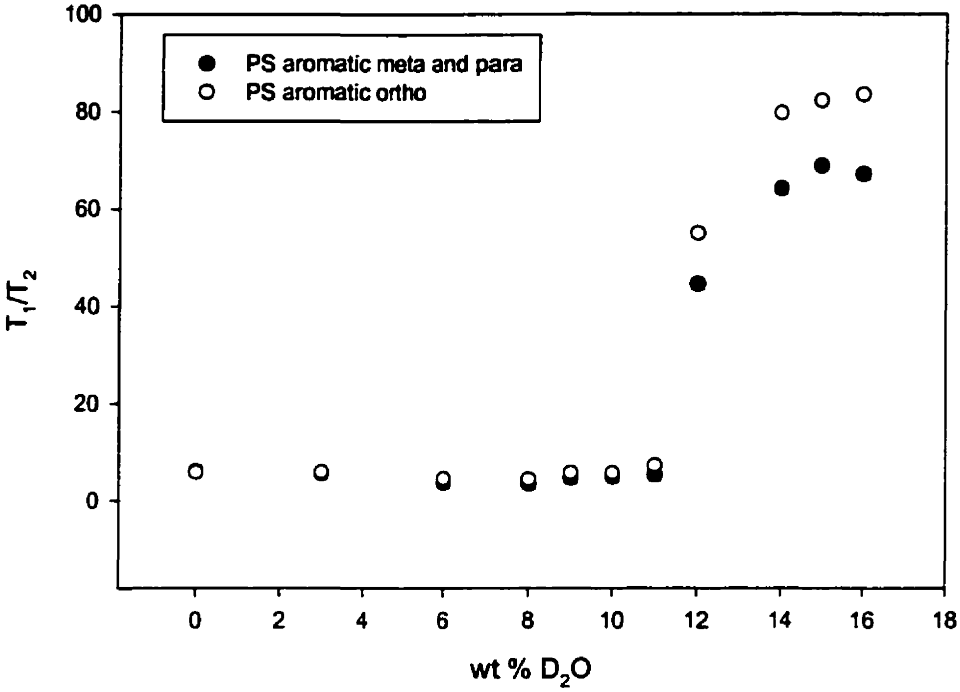

Figure 2.12 T_1/T_2 values for the 1 wt % PS_{100}-*b*-PAA_{25} copolymer in dioxane as a function of deuterium oxide content. Data for the PS phenyl ring protons is shown.

The T_1/T_2 ratios for the PAA block were greater than that of the PS phenyl ring protons before the addition of deuterium oxide; this was expected as dioxane is a better solvent for PS than PAA. The T_1/T_2 values for the PAA α proton also increased at the cwc; however, to a lower final value than the PS phenyl ring signals. As more deuterium oxide was added after the cwc, the ratio for the PAA block decreased as the quality of the solvent mixture for the hydrophilic block improved. In Figure 2.13, the spin-lattice relaxation values for the PAA component also decreased as deuterium oxide was progressively added to the copolymer solution after the cwc value. The large T_1/T_2 values at the high deuterium oxide contents show that even though the T_1 times for the PAA α hydrogen were decreasing, the relaxation behavior of the PAA component was still in the slow motion limit.

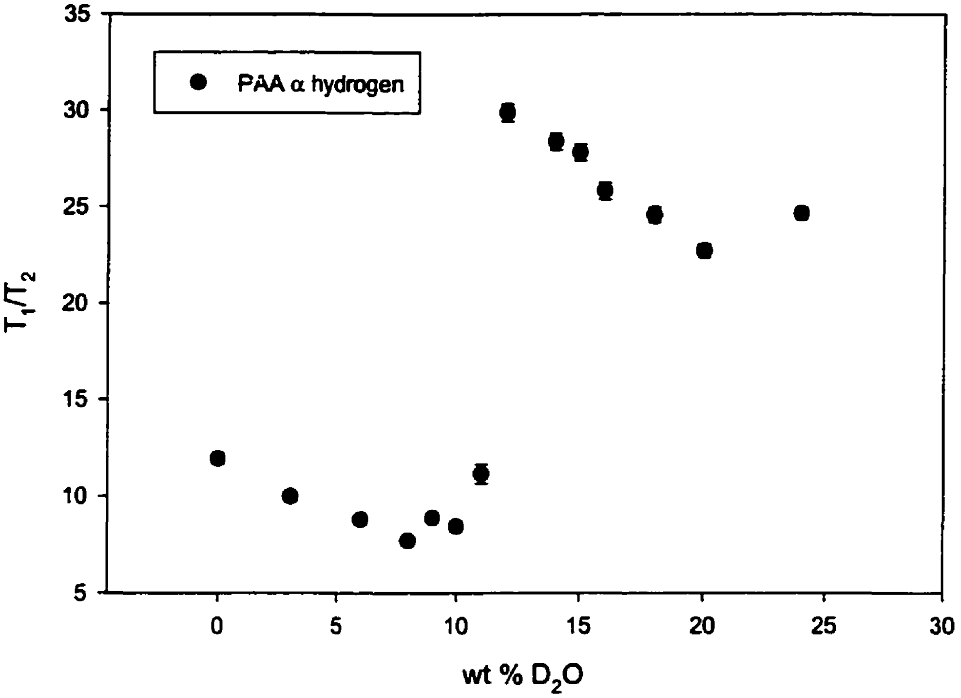

Figure 2.13 T_1/T_2 values for the 1 wt % PS_{100}-*b*-PAA_{25} copolymer in dioxane as a function of deuterium oxide content. Data for the PAA α hydrogen is shown.

2.3.3.2 Interpretation

NMR relaxation measurements have been employed extensively to monitor the molecular motion of polymer solutions; however, study of micelle solutions has mainly entailed surfactants as opposed to polymeric systems.[11] In the former case, the single exponential time correlation function sufficed to interpret the relaxation data. The spectral density function for the single exponential correlation model is expressed as:

$$J(\omega) = \tau \big/ \left(1 + \omega^2 \tau^2\right) \qquad 1$$

where τ is the correlation time and ω is the Larmor frequency. This model provides a useful approximation; however, it does not accurately describe the motion of a random polymer coil in solution.[39] To describe the motion of polymer chains, various models have been developed to interpret the NMR relaxation data.[39-41] The analysis of relaxation data to elucidate the dynamics of polymers in solution requires the study of the relationships between the spin-lattice and spin-spin relaxation times, the internuclear distances, the resonance frequency and the frequency spectra of the molecular motions.[20] The main relaxation mechanism for protons involves the time dependent dipolar interactions, for which the autocorrelation function is inversely proportional to the sixth power of the distance between coupled spins.[42] For the dipolar interaction, the relaxation of protons is described by the following two relationships:

$$\frac{1}{T_1} = \frac{6}{20}\gamma^4\hbar^2 r^{-6}\left[J(\omega_0) + 4J(2\omega_0)\right] \qquad 2$$

and

$$\frac{1}{T_2} = \frac{3}{20}\gamma^4\hbar^2 r^{-6}\left[3J(0) + 5J(\omega_0) + 2J(2\omega_0)\right] \qquad 3$$

In equations 2 and 3, γ is the proton gyromagnetic ratio, $\hbar$ is Planck's constant divided by 2π, r is the internuclear distance, $J(\omega)$ is the spectral density function at different frequencies, and ω_0 is the Larmor frequency.[42] To model the motion of polymer chains in solution, Valeur proposed the diamond lattice model for which the atoms of the polymer chain are assumed to be located on the sites of a diamond lattice.[27] A non-exponential correlation function describes the relaxation process via conformational jumps of the polymer chain positioned on the lattice. The spectral density function for this approach is shown below.

$$J(\omega) = \left[\frac{2T_0T_d(T_0 - T_d)}{(T_0 - T_d)^2 + \omega^2T_0^2T_d^2}\right]\left(\frac{T_0}{2T_d}\right)^{0.5}\left[\frac{(1+\omega^2T_0^2)^{0.5} + 1}{1+\omega^2T_0^2}\right]^{0.5} + \left(\frac{T_0}{2T_d}\right)^{0.5}\left(\frac{\omega T_0T_d}{T_0 - T_d}\right)\left[\frac{(1+\omega^2T_0^2)^{0.5} - 1}{1+\omega^2T_0^2}\right]^{0.5} - 1 \qquad 4$$

The motion is associated with two correlation times, T_0 and T_d where the former characterizes the large-scale motions and the latter represents the local segmental motions. Therefore, T_0 describes a three-bond process on the ideal lattice while T_d characterizes either the isotropic motion of the subchains or the departure of the polymer chains from the ideal lattice. The substitution of equation 4 in equations 2 and 3 yields a set of two equations with two unknowns, T_0 and T_d. Using the spin-lattice and spin-spin relaxation times for the PS phenyl ring protons, the motional correlation times for the PS phenyl ring were calculated with the Newton method. The T_0 and T_d values for the PS phenyl ring protons are displayed in Table 2.4 and 2.5 respectively.

Table 2.4 T_0 and T_d correlation times for 1 and 3 wt % PS$_{100}$-*b*-PAA$_{25}$ copolymer in deuterated dioxane at different deuterium oxide contents. Data for the PS phenyl ring protons. Based on the diamond lattice model.

D$_2$O Content wt %	1 wt % PS$_{100}$-*b*-PAA$_{25}$				3 wt % PS$_{100}$-*b*-PAA$_{25}$			
	Meta and Para		Ortho		Meta and Para		Ortho	
	T_0 (ns)	T_d (ns)	T_0 (ns)	T_d (ns)	T_0 (ns)	T_d (ns)	T_0 (ns)	T_d (ns)
0	81	0.096	45	0.34	11	0.039	7.1	0.096
3	56	0.16	32	0.65	3.8	0.030	1.1	0.081
6	24	0.13	22	0.46	6.4	0.030	2.8	0.063
8	19	0.14	20	0.46				
9	37	0.16	32	0.57	16	0.038	21	0.082
10	46	0.13	37	0.45				
11	83	0.029	140	0.071				
12	9600	0.0099	14000	0.011	890	0.018	3000	0.021
14	21000	0.0079	32000	0.0082	15000	0.0065		
15	24000	0.0076	34000	0.0076	69000	0.0042		
16	23000	0.0080	35000	0.0081				

Table 2.5 T_0 and T_d correlation times for 1 wt % PS$_{218}$-*b*-PAA$_{20}$ copolymer and PS$_{208}$ homopolymer in deuterated dioxane at different deuterium oxide contents. Data for the PS phenyl ring protons. Based on the diamond lattice model.

D$_2$O Content wt %	1wt % PS$_{218}$-*b*-PAA$_{20}$				1 wt % PS$_{208}$			
	Meta and Para		Ortho		Meta and Para		Ortho	
	T_0 (ns)	T_d (ns)	T_0 (ns)	T_d (ns)	T_0 (ns)	T_d (ns)	T_0 (ns)	T_d (ns)
0	43	0.19	23	0.89	59	0.093	37	0.31
3	62	0.14	12	0.36	50	0.10	33	0.32
6	63	0.17	40	0.60	240	0.049	180	0.13
8	150	0.080	120	0.21	540	0.031	460	0.073
9	750	0.044	980	0.063				
10	2100	0.044			1900	0.026	2300	0.039
10.5	4300	0.029	7000	0.031				
11	9900	0.019	16000	0.020				
12					2300	0.025		

As the deuterium oxide content of the PS-*b*-PAA copolymer solution increases and the cwc is reached, the correlation time is expected to increase as micellization is induced. T_0, which is associated with long-range motions, is seen to increase sharply at the cwc indicating decreased motional freedom of the polymer chain. In conjunction with the change in T_0, T_d, which represents short-range motions, decreases at the cwc. The shorter

T_d correlation times point to an increase in the local segmental motions of the PS block. The change in T_0 is approximately 3 orders of magnitude; however, the decrease in T_d is only 1-2 orders of magnitude. Therefore, micelle formation affects the long-range motions of the PS phenyl ring to a greater degree as opposed to the short-range motions. Cau *et al.*[20] also observed a similar trend for the polypropylene segments forming the core of PEO-*b*-PPO-*b*-PEO micelles. The correlation time associated with the long-range motions of the PPO backbone, increased sharply at the critical micelle temperature and reached a plateau region. In contrast, the short-range correlation time increased only slightly at the onset of micellization and steadily decreased as the temperature of the micelle solution was further increased.

Comparing the correlation times of the PS phenyl ring protons for the PS$_{218}$-*b*-PAA$_{20}$ copolymer and the PS$_{208}$ homopolymer, the long-range motions for the homopolymer become restricted at a lower deuterium oxide content than that of the copolymer of similar PS block length. However, once aggregation of the PS$_{218}$-*b*-PAA$_{20}$ copolymer occurs, the copolymer's PS phenyl ring long-range motion is slower than that of the PS phenyl ring for the homopolymer. Similar to the PS$_{218}$-*b*-PAA$_{20}$ copolymer, the T_d values for the PS homopolymer decreases as deuterium oxide is progressively added to the homopolymer solution; however, the decrease in T_d occurs at a lower D_2O content than the cwc of the copolymer solution.

At this point, the limitations to employing the diamond lattice model to elucidate the dynamics of the PS-*b*-PAA copolymer during aggregate formation must be considered. Of concern is the slight decrease in T_d observed for the PS phenyl ring protons at the onset of micellization, which is different from the behavior exhibited by the short-range correlation time of the PPO block of the PEO-*b*-PPO-*b*-PEO aggregates studied by Cau *et al.*[20] Cau and his colleagues detected a small increase in this value at the critical micellization temperature. We anticipated that the short-range motions of the PS block would also become restricted at the critical water content for the PS-*b*-PAA copolymer in dioxane. The discrepancy in the motional correlation times may have resulted from the multi-exponential behavior of the spin-spin relaxation process of the PS-*b*-PAA copolymer before aggregate formation. In addition, the error in the T_0 and T_d

parameters may reflect the limitations of applying this model to describe the motional processes of the PS-*b*-PAA copolymer aggregates. The majority of ^{1}H NMR research involving the dynamics of a polymer chain in solution has been devoted to studying the mobility of the polymer backbone, and in particular, the dipolar interaction between geminal protons has been modeled. Due to the low spectral resolution of the PS-*b*-PAA copolymer ^{1}H NMR spectrum, only relaxation data for the phenyl ring of the PS block and the α proton of the PAA segment was obtained. For these nuclei, the dipolar interaction, which is principally responsible for the proton relaxation, occurs amongst vicinal protons. While determining the internuclear distance between geminal protons is relatively simple, estimating the distance for vicinal protons is complicated by the rotation of the polymer backbone. For this reason, the motional correlation times for the PAA α proton could not be determined. Furthermore, we could not separate the relaxation behavior of the meta and para protons of the PS phenyl ring. A third concern pertaining to the analysis of the relaxation data to extract the dynamic behavior of the PS-*b*-PAA copolymer is the use of the diamond lattice model which is normally employed to describe the polymer backbone. To extend our knowledge of the dynamics of the PS block in a quantitative fashion, the relaxation data for the phenyl ring of the PS block was fitted to the diamond lattice model. While the limitations of applying this model to analyze the mobility of a side-chain group, are understood, we believe that the resulting motional correlation times still provide a valuable picture of the motions of the PS block during the micellization process.

2.4 Conclusions

^{1}H NMR spectroscopy has been used to monitor the segmental chain dynamics of PS-*b*-PAA copolymer aggregates during the micellization process. PS-*b*-PAA block copolymer solutions in deuterated dioxane were analyzed as deuterium oxide was progressively added to the samples. Analysis of the NMR spectral line shapes indicates the level of motional freedom experienced by PS and the PAA block forming the micelle core and corona respectively. Relaxation measurements provided a quantitative means to assess the influence of the precipitant on the dynamics experienced by the copolymer. In addition, study of homopolymer PS showed that the copolymer does exhibit contrasting dynamic behavior to that of the homopolymer.

2.5 Acknowledgments

The author would like to thank Dr. Yisong Yu for the PS homopolymer and the PS-*b*-PAA copolymer synthesis. The author is also indebted to Carl Bartels for programming the source code used to calculate the correlation times for the relaxation data.

2.6 References

1. Zhang, L.; Eisenberg, A. *Science* **1995**, 268, 1728-1731.
2. Zhang, L.; Eisenberg, A. *Journal of the American Chemical Society* **1996**, 118, 3168-3181.
3. Cameron, N. S.; Corbierre, M. K.; Eisenberg, A. *Can. J. Chem.* **1999**, 77, 1311-1326.
4. Allen, C.; Eisenberg, A.; Mrsic, J.; Maysinger, D. *Drug Delivery* **2000**, 7, 139-145.
5. Antonietti, M.; Forster, S.; Oestreich, S. *Macromol. Symp.* **1997**, 121, 75-88.
6. Shen, H.; Zhang, L.; Eisenberg, A. *J. Phys. Chem. B* **1997**, 101, 4697-4708.
7. Chen, L.; Shen, H.; Eisenberg, A *J. Phys. Chem. B* **1999**, 103, 9488-9497.
8. Zhang, L.; Shen, H.; Eisenberg, A. *Macromolecules* **1997**, 30, 1001-1011.
9. Yu, Y.; Zhang, L.; Eisenberg, A. *Macromolecules* **1998**, 31, 1144-1154.
10. Gao, Z.; Zhong, X.; Eisenberg, A. *Macromolecules* **1994**, 27, 794-802.
11. Evertsson, H.; Nilsson, S.; Welch, C. J.; Sundelof, L.-O. *Langmuir* **1998**, 14, 6403-6408.
12. Cerichelli, G.; Mancini, G. *Current Opinion in Colloid and Interface Science.* **1997**, 2, 641-648.
13. Vold, R.R. In *Nuclear Magnetic Resonance Probes of Molecular Dynamis;* Tycko, R. Ed.; Kluwer Academic Publishers: Dordrecht, 1994, Chapter 2.
14. McCall, D. W. *Molecular Relaxation in Polymers* **1971**, 4, 223-232.
15. Kulbaba, K.; Macdonald, P. M.; Manners, I. *Macromolecules* **1999**, 32, 1321-1324.
16. Zhu, X. X.; Masaro, L. *Langmuir* **1999**, 15, 8356-8360.
17. Candau, F.; Heatley, F.; Price, C.; Stubbersfield, R.B. *Eur. Polym. J.* **1984**, 20, 685-690.
18. Godward, J.; Heatley, F.; Price, C. *J. Chem. Soc. Faraday Trans.*, **1993**, 89, 3471-3475.
19. Xie, M.; Blum, F. D. *Macromolecules* **1990**, 29, 3862-3867.
20. Cau, F.; Lacelle, S. *Macromolecules* **1996**, 29, 170-178.
21. Kriz, J.; Masar, B.; Pospisil, H.; Plestil, J.; Tuzar, Z.; Kiselev, M.A. *Macromolecules* **1996**, 29, 7853-7858.
22. Kriz, J.; Masar, B.; Dybal, J.; Doskocilova, D. *Macromolecules* **1997**, 30, 3302-3308.

23. Kriz, J.; Masar, B.; Doskocilova, D. *Macromolecules* **1997**, 30, 4391-4397.

24. Kriz, J.; Masar, B.; Plestil, J.; Tuzar, Z.; Pospisil, H.; Doskocilova, D. *Macromolecules* **1998**, 31, 41-51.

25. Yu, Y.; Eisenberg, A. *J. Am. Chem. Soc.* **1997**, 119, 8383-8384.

26. Shen, H.; Eisenberg, A. *J. Phys. Chem. B* **1999**, 103, 9473-9487.

27. Valeur, B.; Jarry, J. P.; Geny, F.; Monnerie, L. *J. Polym. Sci., Polym. Phys. Ed.* **1975,** 13, 667.

28. Hautekeer, J.-P.; Varshney, S.K.; Fayt, R.; Jacobs, C.; Jerome, R.; Teyssie, Ph. *Macromolecules* **1990**, 23, 3893-3898.

29. Zhong, X.F.; Varshney, S.K.; Eisenberg, A. *Macromolecules* **1992,** 25, 7167.

30. Hautekeer, J.-P.; Varshney, S. K.; Fayt, R.; Jacobs, C.; Jerome, R.; Teyssie, Ph. *Macromolecules* **1990**, 23, 3893-3898.

31. Crowther, M. W.; Cabasso, I.; George, C. L. *Macromolecules* **1988,** 21, 2924-2928.

32. Garces, F. O.; Sivadasan, K.; Somasundaran, P.; Turro, N. J. *Macromolecules* **1994,** 27, 272-278.

33. Stilbs, P.; Moseley, M. E.; *Polymer* **1981**, 22, 321-326.

34. Rahman, Atta-ur-; Choudhary, M. I. *Solving Problems with NMR Spectroscopy;* Academic Press Inc.: San Diego, 1996, 213-279.

35. Laupretre, F. Noel, C.; Monnerie, L. *Journal of Polymer Science: Polymer Physics Edition* **1977**, 15, 2127-2142.

36. Mao, S.-Z.; Feng, H.-Q. Colloid Polym Sci. 1998, 276, 247-251.

37. Mao, S. –Z.; Zhang, X. –D.; Dereppe, J.-M.; Du, Y.-R. Colloid Polym Sci. 2000, 278, 264-269.

38. Xie, M.; Blum, F. D. *Macromolecules* **1996**, 29, 3862-3867.

39. Bovey, F. A.; Jelinski, L. W. *J. Phys. Chem.* **1985**, 89, 571-583.

40. Heatley, F.; Begum, A. *Polymer* **1976**, 17, 399-408.

41. Blum, F. D.; Durairaj, B.; Padmanabhan, A. S. *Macromolecules* **1984**, 17, 2837-2846.

42. Solomon, I. *Phys. Rev.* **1955**, 99, 559.

Chapter 3

^{129}Xenon NMR Study of Polystyrene-*b*-poly(acrylic acid) Copolymer Micelles in Dioxane/Water Solvent Mixtures

3.1 Introduction

A substantial area of research involving the physical characterization of polymers is devoted to the study of temperature-induced transitions since these properties often dictate the polymer's suitability in potential applications.[1] As discussed in Chapter 2, nuclear magnetic resonance measurements of PS-*b*-PAA copolymer aggregates provide information of the motional behavior of the polymer chains since relaxation phenomena are related to molecular motion.[2] However, NMR experiments where the sample itself is studied cannot elucidate the glass transition temperature of polymeric materials. Previous investigations have shown that the 'glass transition' temperatures (T_{gNMR}) determined by conventional NMR spectroscopy do not coincide with glass transition temperatures (T_g) measured by differential scanning calorimetry (DSC).[3,4] T_{gNMR} values are measurable since NMR spectral features are influenced by changes in temperature as demonstrated by the NMR line widths of bulk polymers.[3] The ^{13}C NMR spectrum of bulk polyisobutylene at low temperatures shows a broad peak; however, as the temperature is increased, spectral collapse occurs and the line shape becomes narrow. For this sample, the spectral collapse temperature, T_c, was observed at –10 °C whereas, the glass transition temperature measured by DSC was –70 °C.[3] Similar discrepancies were observed for ^{2}H NMR studies of deuterated acrylates for which NMR glass transition temperatures were determined via line shape and spin-spin relaxation data.[4] The T_{gNMR} values were also consistently higher than the glass transition temperatures determined by DSC. The difference in T_g and T_{gNMR} can be explained by the frequency of observation and time scale of the two different methods, as DSC probes the low frequency region of motions and NMR probes the MHz frequency region of motions. T_g is a dynamic process and depends on the frequency at which it is being measured, therefore it is not surprising that T_{gNMR} is higher than T_g. Unfortunately, the difference between these two temperatures cannot be predetermined in a simple fashion as the relationship between T_g and T_{gNMR} is different for each polymer. In addition, determining T_{gNMR} of a polymer is difficult as it can depend on the instrumental parameters of the NMR experiment.[3,4]

To our knowledge, there are no determinations of T_g for block copolymer micelles; however, T_{gNMR} has been determined for one block copolymer system. Candau *et al.*[5] studied the dynamic structure of micelles formed from polystyrene-*b*-poly(ethylene/propylene) block copolymers in paraffinic solvents by solution-state ^1H NMR spectroscopy. They observed a sharp line width transition for the PS core at 50 °C, which they attributed to increased segmental motions of the polymer chain. They referred to this transition as the T_{gNMR} of the aggregate core.

^{129}Xe NMR spectroscopy is an alternative method to conventional NMR techniques where the properties of a probe introduced into the sample are monitored. Recently, the use of ^{129}Xe NMR spectroscopy to elucidate structural and dynamic properties of molecules in complex chemical and biological systems has increased.[6-8] The xenon atom is an ideal non-invasive probe of its surroundings whose large chemical shift range gives it great sensitivity to its local environment.[6-8] In terms of ^{129}Xe NMR studies of polymers, generally the resonance shift is correlated with a molecular parameter such as the polymer pore size or density. In particular, this method has been effective for studying morphology and phase transitions of polymer blends.[9] In these investigations, the glass transition temperatures were detected as the temperature dependencies of the NMR resonance shifts were analyzed. Temperature-induced transitions in polymers led to discontinuities in the slope of the chemical shift-inverse temperature relationship. To explain this phenomenon, the free volume and van de Waals theories were applied to ^{129}Xe NMR data for a range of amorphous and semi crystalline polymers.[10,11] In addition to the ^{129}Xe NMR chemical shift, the line shapes yield information on polymer morphology as the line width for a polymer is significantly narrower above its glass transition temperature.[12] The collapse of the broad signal as the temperature is increased results from the rapid diffusion of xenon among various sites in the polymer at a rate that is faster than the NMR time scale. Simpson *et al.*[13,14] determined the diffusion coefficient of xenon in micron-size polystyrene beads as a function of temperature. They observed a sharp increase in the xenon diffusion coefficient above the glass transition temperature of the PS bead. Bharatam *et al.*[15] employed ^{129}Xe NMR to detect phase transitions in binary and tertiary reentrant nematic liquid crystal mixtures. They observed discontinuities in the slopes of the chemical shift, T_1 and T_2 as a function of temperature curves at the phase transitions. The relaxation measurements in this study were particularly sensitive in detecting these temperature-induced processes.

PS-*b*-PAA copolymer aggregates in dioxane/water solvent mixtures have undergone intense investigation resulting in morphological, thermodynamic and kinetic information; however, the study of the temperature-induced transitions of the micelle core has not been pursued.[16-20] The question was raised by Zhang *et al.*[21] whether the glass transition temperature of the core-forming blocks is above room temperature during micelle formation. Should this be the case, it is more likely that thermodynamic equilibrium may not be operative between the unimer and the aggregates. Therefore, the structures should be called micelle-like aggregates under these circumstances. They believed that after the formation of the copolymer aggregates and the removal of the co-solvent, the micelles become structurally locked because the PS chains are below their glass transition temperature and they are no longer in thermodynamic equilibrium. Measuring the glass transition temperature of the polystyrene core of PS-*b*-PAA aggregates in solution is not possible by traditional calorimetric methods and conventional NMR spectroscopy can only provide T_{gNMR} values; therefore, we have used ^{129}Xe NMR spectroscopy to study transitions in the polystyrene core as a function of temperature. Dioxane was selected as the co-solvent for two reasons. The first advantage of using dioxane as the initial solvent involves its melting and boiling points, which are similar to those of water. The high freezing point of both dioxane and water permit the observation of the morphology of the PS-*b*-PAA copolymer aggregates in dioxane/water mixtures by TEM, as the solid solvent mixture can be sublimed during TEM sample preparation.[17] In addition to verifying the PS-*b*-PAA aggregate structure, our rationale for using dioxane involved the ^{129}Xe NMR chemical shifts of xenon in dioxane, water and polystyrene. We hoped to decrease the likelihood that the resonance shift of the probe in the solvent phase would overlap with xenon absorbed in the PS core. The ^{129}Xe NMR resonance shifts of xenon in dioxane, water and polystyrene are 187.7 ppm, 196 ppm, and 220 ppm respectively.[22]

This chapter describes the characterization of polystyrene-*b*-poly(acrylic acid) copolymer aggregates in dioxane/water mixtures using the xenon atom to probe the PS core. ^{129}Xe NMR resonance shifts and line shapes are analyzed to study the effect of temperature on the micelles. The aggregate morphologies are verified by TEM and the thermal behavior of PS homopolymer plasticized with dioxane is analyzed by DSC.

3.2 Experimental Section

3.2.1 Materials

Polystyrene homopolymer and polystyrene-*b*-poly(acrylic acid) diblock copolymers were synthesized by sequential anionic polymerization. A detailed description of the synthetic procedures can be found elsewhere.[23,24] Xenon gas at natural abundance was purchased from Air Liquide. Polystyrene beads were generously donated by Christian Krueger from the Max Planck Institute for Polymer Research in Mainz.

3.2.2 Study of the Thermal Behavior of PS Homopolymer

Specific amounts of PS_{208} homopolymer and dioxane were placed in a tube-shaped flask attached to a two-way stop-cock. The flask was attached to a vacuum line and immersed in liquid nitrogen to freeze the dioxane. The flask was evacuated for 5 seconds and removed from the vacuum assembly to return to ambient temperature. The evacuated flask was heated in a water bath from 25 °C to 80 °C with a heating rate of 5 °C per 15 minutes. When the final temperature of 80 °C was attained, the flask was allowed to remain at this temperature for 3 hours. After the heating period, the flask was removed from the water bath and allowed to cool to ambient temperature. The glass transition temperature of the PS samples was measured using a Seiko II DSC, model DSC 220. The samples were heated from 10 °C to 120 °C at a rate of 5 °C per minute over a single heating cycle. The T_g was determined as the temperature at the inflection point of the glass transition endotherm.

3.2.3 Preparation of PS-*b*-PAA Micelle Solutions

To prepare the PS-*b*-PAA aggregates, the block copolymer was first dissolved in dioxane, which is a common solvent for both the polystyrene and poly(acrylic acid) blocks. To induce micelle formation, deionized water was added to the copolymer solutions at a rate of one drop every 15 seconds with vigorous stirring. The addition of water continued until 75 wt % of water had been added. The final copolymer concentration in the dioxane/water mixture was 1 wt %. To remove the dioxane, the micelle solutions were dialyzed against deionized water over three days. To increase the copolymer concentration of the micelle solutions, water was removed slowly by rotary evaporation until the polymer concentration exceeded 10 wt %. At this point, the micelle solution was divided evenly into vials. To each portion, an aliquot of a different dioxane/water mixture was added producing micelle samples of the same copolymer concentration with varying ratios of dioxane and water. For PS-*b*-PAA micelle solutions with sodium hydroxide, NaOH was added to the copolymer/dioxane solutions during the addition of the deionized water.

Approximately 1.25g of the PS-*b*-PAA micelle sample were transferred to a 10 mm heavy-walled NMR tube (Wilmad N.J.). The NMR tube was attached to a vacuum line and the samples underwent several freeze-pump-thaw cycles to remove gaseous impurities. Xenon was added to the samples by condensation and the NMR tubes were flame sealed under vacuum. It is important to note that as a safety precaution, loading of the xenon gas into the NMR tubes was performed behind a protective shield. In addition, a metal canister with a lid containing a vent was made to store the NMR tube while it returned to ambient temperature immediately after it was sealed. The samples were allowed to equilibrate prior to the NMR measurement. For the NMR variable temperature measurements, the samples were heated in a water bath before the NMR experiment to ensure the structural integrity of the NMR tube at the elevated pressures.

Table 3.1 Properties of PS-*b*-PAA copolymer samples.

Polymer	Polymer Concentration wt %	Dioxane wt %	NaOH / PAA R value mole ratio
PS_{218}-*b*-PAA_{20}	10	10	0
PS_{218}-*b*-PAA_{20}	10	20	0
PS_{218}-*b*-PAA_{20}	10	40	0
PS_{218}-*b*-PAA_{20}	10	10	0.015
PS_{218}-*b*-PAA_{20}	10	20	0.015
PS_{218}-*b*-PAA_{20}	10	30	0.015
PS_{100}-*b*-PAA_{25}	5	0	0.0064
PS_{100}-*b*-PAA_{25}	9	0	0.030
PS_{100}-*b*-PAA_{25}	9	5	0.030
PS_{100}-*b*-PAA_{25}	9	10	0.030
PS_{100}-*b*-PAA_{25}	9	20	0.030
PS_{100}-*b*-PAA_{25}	9	30	0.030

3.2.4 ^{129}Xenon NMR Measurements

^{129}Xe NMR spectra were acquired on a Varian Unity-500 spectrometer operating at a ^{129}Xe Larmor frequency of 138.3 MHz using a 10 mm broadband probe. The samples were not spun. The single 90° pulse experiments were acquired with a 25 μs pulse width and a pulse delay of 10 seconds. For the single pulse experiments at ambient temperature, at least 8000 acquisitions were recorded to obtain sufficient signal to noise in the NMR spectra.

For the variable temperature ^{129}Xe NMR measurements, the samples were allowed to equilibrate for 30 minutes at the acquisition temperature prior to the NMR experiment. Before each ^{129}Xe NMR measurement, the xenon standard sample was run at 20 °C and the gas signal was referenced to 0 ppm. For these experiments, at least 3000 acquisitions were recorded. Chemical shifts and line widths were obtained from Lorentzien fitting of the resonance signals.

3.2.5 Transmission Electron Microscopy

Transmission electron micrographs were obtained on a Jeol JEM-2000 microscope operating at an acceleration voltage of 80 kV. Copper EM grids, which had been precoated with a thin film of Formvar (J. B. EM Services Inc.) and then coated with carbon were prepared. A small drop of the aggregate solution was deposited on the EM grid and the thin layer of liquid was immediately frozen by placing the grid on a metal block cooled to liquid nitrogen temperature. The solvent was removed by freeze-drying under vacuum for one day.

3.3 Results and Discussion

The Results and Discussion section is divided into four parts. Section 3.3.1 describes the PS-*b*-PAA aggregate morphologies observed by TEM. Section 3.3.2 describes the thermal analysis of PS homopolymer by DSC. Section 3.3.3 discusses the ^{129}Xe NMR spectra of the samples acquired at ambient temperature. The final section focuses on the effect of temperature on the ^{129}Xe NMR spectra for two PS-*b*-PAA aggregate solutions.

3.3.1 Morphologies of the PS-*b*-PAA Crew-Cut Aggregates

It was necessary to verify the PS-*b*-PAA aggregate morphologies by TEM because of the high copolymer concentrations in our samples. Traditionally, our research group prepares aggregate solutions with low copolymer concentrations rarely exceeding 5 wt %; however, our copolymer concentrations exceeded this value because of the low sensitivity of the ^{129}Xe NMR technique.[16-21] Figure 3.1 shows three TEM micrographs of the aggregates formed from the 10 wt % PS_{218}-*b*-PAA_{20} copolymer in different dioxane/water solvent mixtures. All three samples yielded aggregates which were vesicular in nature with a large polydispersity of diameters. The vesicular nature of the structure can be seen from the higher transmission in the center of the aggregates than around their periphery. The size of the vesicles ranged from 50 nm to 230 nm in diameter for the largest structures. The thickness of the vesicle walls was *ca.* 20 nm. TEM micrographs also provided an estimate of the domain size of the PS environment in which the xenon atom resides. Simple spheres approximately 35 nm in diameter were also present in this sample. Yu *et al.*[17,18] also observed the formation of vesicular aggregates from PS-*b*-PAA copolymers in dioxane/water mixtures. The PAA content of this sample is 9 mol %, which corresponds well to previous studies where PS-*b*-PAA copolymers with PAA contents of 9.5 mol % gave rise to vesicles with outer diameters of 150-500 nm.

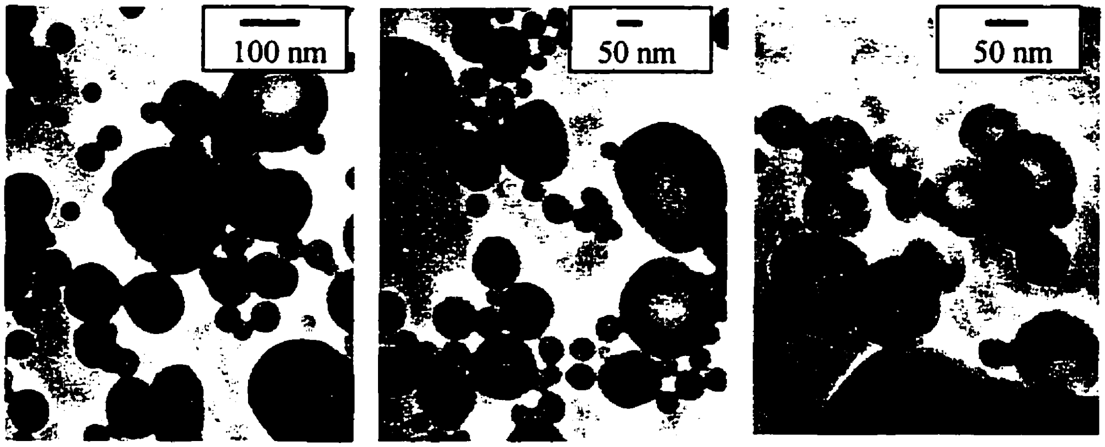

10 wt% PS_{218}-*b*-PAA_{20} in 10/90 wt% dioxane/H_2O

10 wt% PS_{218}-*b*-PAA_{20} in 20/80 wt% dioxane/H_2O

10 wt% PS_{218}-*b*-PAA_{20} in 40/60 wt% dioxane/H_2O

Figure 3.1 TEM micrographs of aggregates from the 10 wt % PS_{218}-*b*-PAA_{20} copolymer in different dioxane/water solvent mixtures.

It has been determined that morphologies are influenced by many variables, *e.g.*, the composition of the block copolymer,[16,21] the copolymer concentration,[16,21] the common solvent,[17,18] and the type and concentration of added ions.[25,26] To prepare aggregates with a different type of architecture, PS_{218}-*b*-PAA_{20} micelles with sodium hydroxide were prepared. Figure 3.2 shows the TEM micrographs of the 10 wt % PS_{218}-*b*-PAA_{20} copolymer aggregates in different dioxane/water mixtures. Sodium hydroxide has been added so that the NaOH/PAA mol ratio, R=0.015. The addition of NaOH yielded vesicular aggregates of varying size. The structures' diameters ranged from 45 nm to 220 nm, with a wall thickness of 20 nm. Spheres, 30 nm in diameter, were also present with the vesicles.

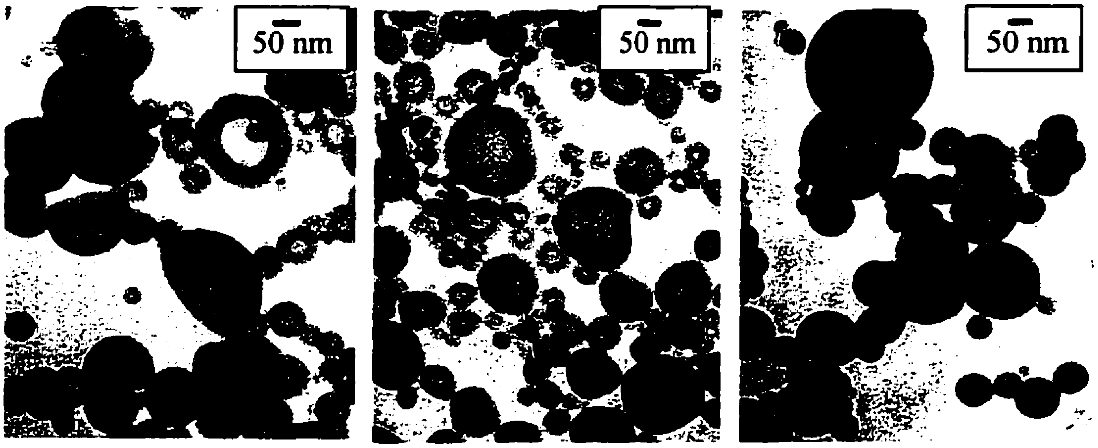

10 wt% PS_{218}-*b*-PAA_{20} in 10/90 wt% dioxane/H_2O R=0.015

10 wt% PS_{218}-*b*-PAA_{20} in 20/80 wt% dioxane/H_2O R=0.015

10 wt% PS_{218}-*b*-PAA_{20} in 30/70 wt% dioxane/H_2O R=0.015

Figure 3.2 TEM micrographs of aggregates from the 10 wt % PS_{218}-*b*-PAA_{20} copolymer in different dioxane/water solvent mixtures with NaOH added. R=0.015

Yu *et al.*[17,18] observed that as the PAA content of the block copolymer increased, the PS-*b*-PAA copolymer aggregates prepared in dioxane, formed vesicles, rods and finally spheres.[15,16] The PAA content of the PS-*b*-PAA copolymer was increased from 9 mol % to 20 mol % by using PS_{100}-*b*-PAA_{25} copolymer. Figure 3.3 shows TEM pictures of PS_{100}-*b*-PAA_{25} copolymer aggregates in various dioxane/water solvent mixtures. Sodium hydroxide has been added to the copolymer solutions prior to micellization. The first TEM picture shows the 5 wt % PS_{100}-*b*-PAA_{25} copolymer in water with NaOH added so the NaOH/PAA mole ratio, R= 0.0064. This sample yielded a mixture of spheres, cylinders and vesicles, which indicates that the block copolymer is in the rod to bilayer coexistence region. The spheres were approximately 40 nm in diameter while the thickness of the cylindrical structures was *ca.*18 nm. The vesicles were approximately 70 nm in diameter. The five subsequent micrographs display samples of the 9 wt % PS_{100}-*b*-PAA_{25} copolymer in different dioxane/water solvent mixtures with NaOH added so that R=0.03. Beyond the copolymer concentration of 9 wt % the viscosity of the solution was too high to handle the sample without difficulty. At 0 wt % dioxane (pure water), the aggregate structures were spheres fusing into cylinders of varying lengths. Branched rods were formed with a relatively uniform diameter of 17 nm. Hemispherical caps can be seen at the ends of the cylinders. As the dioxane content was increased to 5 wt %, the aggregate structures were still branched cylinders; however, the individual spheres were not clearly distinguishable as in the 0 wt % dioxane micrograph. The diameter of the cylinders was *ca.* 17 nm. As the dioxane content was increased to 10, 20 and 30 wt %, the structures remained as branched cylinders of varying lengths, and diameters of 17 nm.

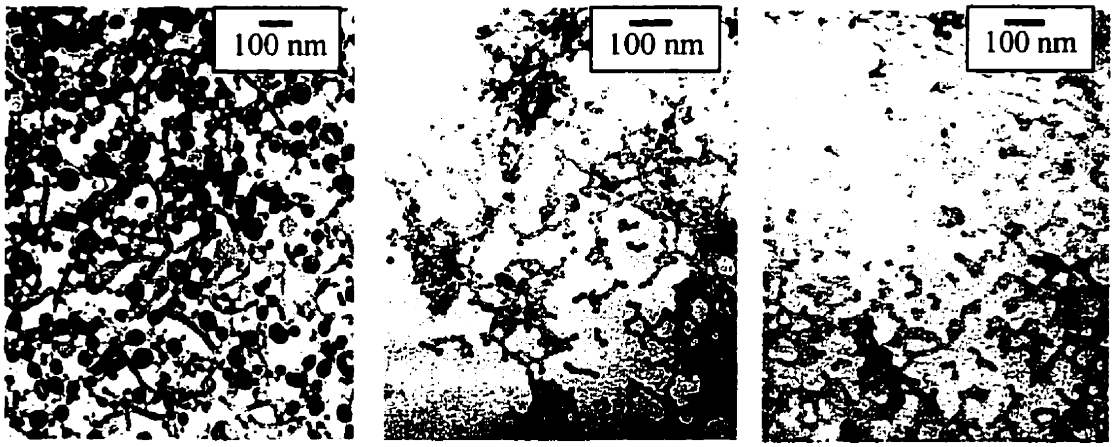

5 wt% PS_{100}-*b*-PAA_{25} in H_2O R=0.0064

9 wt% PS_{100}-*b*-PAA_{25} in H_2O R=0.03

9 wt% PS_{100}-*b*-PAA_{25} in 5/95 wt% dioxane/H_2O R=0.03

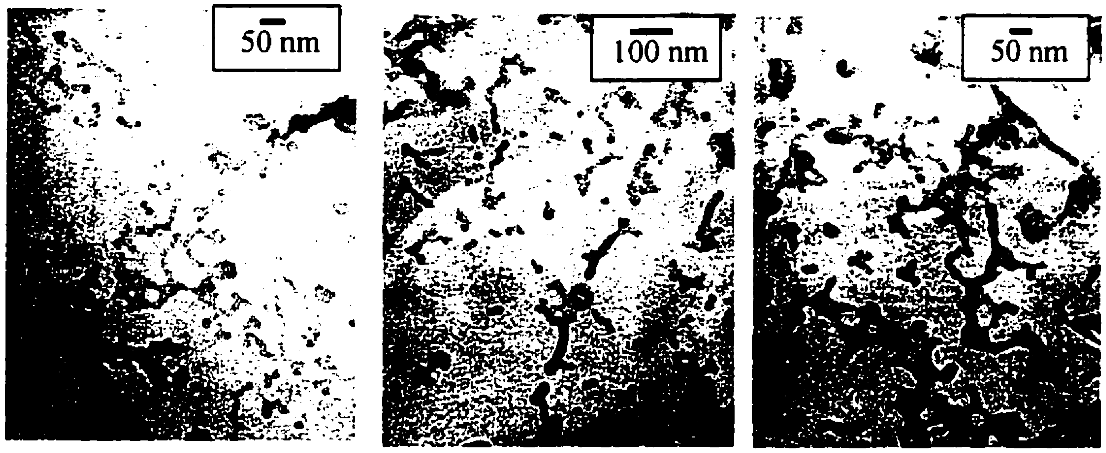

9 wt% PS_{100}-*b*-PAA_{25} in 10/90 wt% dioxane/H_2O R=0.03

9 wt% PS_{100}-*b*-PAA_{25} in 20/80 wt% dioxane/H_2O R=0.03

9 wt% PS_{100}-*b*-PAA_{25} in 30/70 wt% dioxane/H_2O R=0.03

Figure 3.3 TEM micrographs of aggregates from the PS_{100}-*b*-PAA_{25} copolymer in different dioxane/water solvent mixtures with NaOH added. R is the mole ratio of NaOH/PAA.

3.3.2 Thermal Behavior of PS Homopolymer

Differential scanning calorimetry measurements were performed on PS_{208} homopolymer plasticized with different amounts of dioxane as T_g values for this system are not available in the literature. It was important to determine the glass transition temperatures of plasticized PS homopolymer samples to model the plasticization of the micellar PS core by dioxane in the solvent mixture. Yu *et al.*[18] determined the dioxane content in PS homopolymer of a phase-separated ternary system of PS, dioxane and water as a model for the solvent content in the core of the PS-*b*-PAA aggregates. Of particular interest was the effect of water on this parameter. Unfortunately, due to the increased viscosity of the PS phase at high water contents, measurements were only obtained up to a water content of 17 wt % in the study. They observed that as water was gradually added to the polystyrene solution, the dioxane content in the polymer decreased steeply to the point where at 17 wt % water content, the dioxane content in the PS homopolymer was 0.4 v/v. As our PS-*b*-PAA copolymer aggregate solutions contain at least 60 wt % water, the dioxane content in the core of our micelles is considerably less than 0.4 v/v. Therefore, PS_{208} plasticized with dioxane contents from 0 to 0.23 v/v were prepared. The glass transition temperatures of the PS samples are shown in Figure 3.4. The pure PS homopolymer has a glass transition temperature of 103 °C and as dioxane is added, the T_g decreases. PS plasticized with 0.11 v/v dioxane underwent the glass transition at 76.0 °C and increasing the dioxane content to 0.17 v/v and 0.23 v/v decreased the T_g to 70.8 °C and 59.4 °C respectively. The rate of change of the glass transition temperature as a function of the dioxane content (v/v), $\frac{dT_g}{dc} = -190^{\circ}C$, with a standard error of 20 °C.

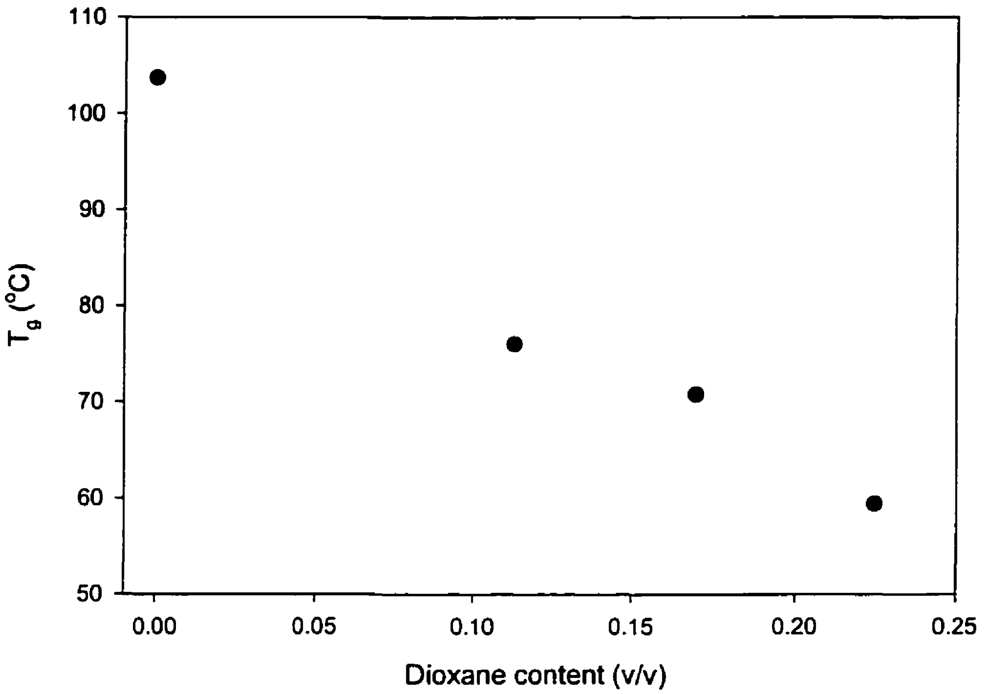

Figure 3.4 Glass transition temperature of PS_{208} homopolymer as a function of dioxane content (v/v).

3.3.3 ^{129}Xenon NMR Measurements at Ambient Temperature

Polymers in the solid-state have been studied extensively by ^{129}Xe NMR spectroscopy; however, polymers in solution have not been investigated by this method.[6-8] Therefore, it was important to examine polymer samples in the solid-state prior to investigating the PS-*b*-PAA aggregate solutions. ^{129}Xe gas was introduced to PS beads 518 nm in diameter and examined by NMR spectroscopy. Figure 3.5 displays the ^{129}Xenon NMR spectrum for this sample. The sharp peak referenced at zero ppm is the ^{129}Xe gas phase peak. Overlapping with the gas phase peak in the upfield direction is a weaker signal arising from ^{129}Xe gas occupying the void spaces of the polymer. The broad peak at 218 ppm is that of ^{129}Xe sorbed into the PS beads. This chemical shift is comparable to previous studies of polystyrene beads for which the resonance shift separation between the gas phase and the PS signals was *ca.* 220 ppm.[13,14] The line width of ^{129}Xe sorbed in the PS beads was *ca.* 787 Hz, and it is important to note that this spectrum was measured at a temperature below the glass transition temperature of PS, which is *ca.* 100°C. This line width is comparable to previous measurements at the same applied magnetic field strength by Simpson *et al.*[13,14] where the line widths for PS beads in the micron range gave rise to NMR line widths at 25 °C ranging from 657 Hz to 817 Hz.

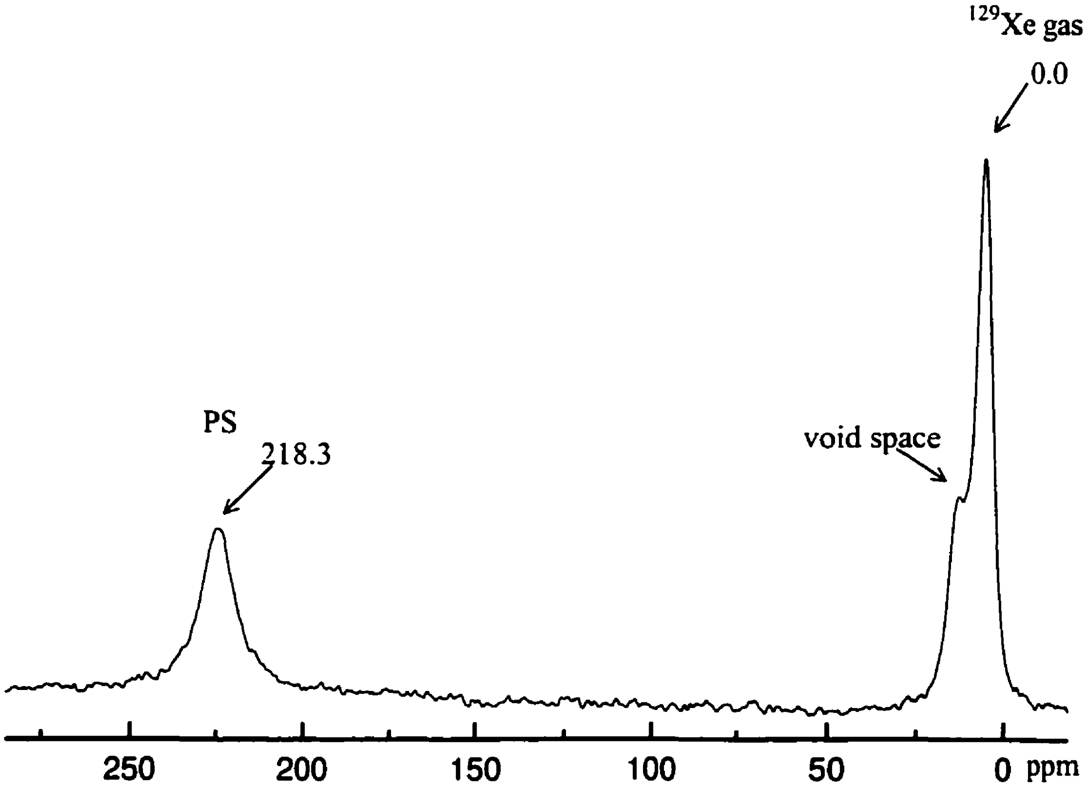

Figure 3.5 ^{129}Xe NMR spectrum of polystyrene beads 518 nm in diameter acquired at ambient temperature.

PS_{218}-*b*-PAA_{20} aggregates in the solid-state were also analyzed by ^{129}Xe NMR spectroscopy. PS_{218}-*b*-PAA_{20} aggregates were prepared and the solvent was removed by freeze-drying the copolymer solution under vacuum. The ^{129}Xe NMR spectrum of freeze-dried PS_{218}-*b*-PAA_{20} aggregates is shown in Figure 3.6. We see a broad peak at *ca.* 218 ppm for the ^{129}Xe gas in the PS component of the freeze-dried aggregates. A signal for xenon in the gas phase is also observed which was set to 0 ppm. A broad, intense peak is also present upfield from the gas phase peak, which was assigned to xenon gas residing in the void spaces of the freeze-dried copolymer aggregates. The signal for xenon occupying these sites is stronger in the freeze-dried aggregates than in the PS bead sample. This spectrum was also obtained at a temperature well below the glass transition temperature of the

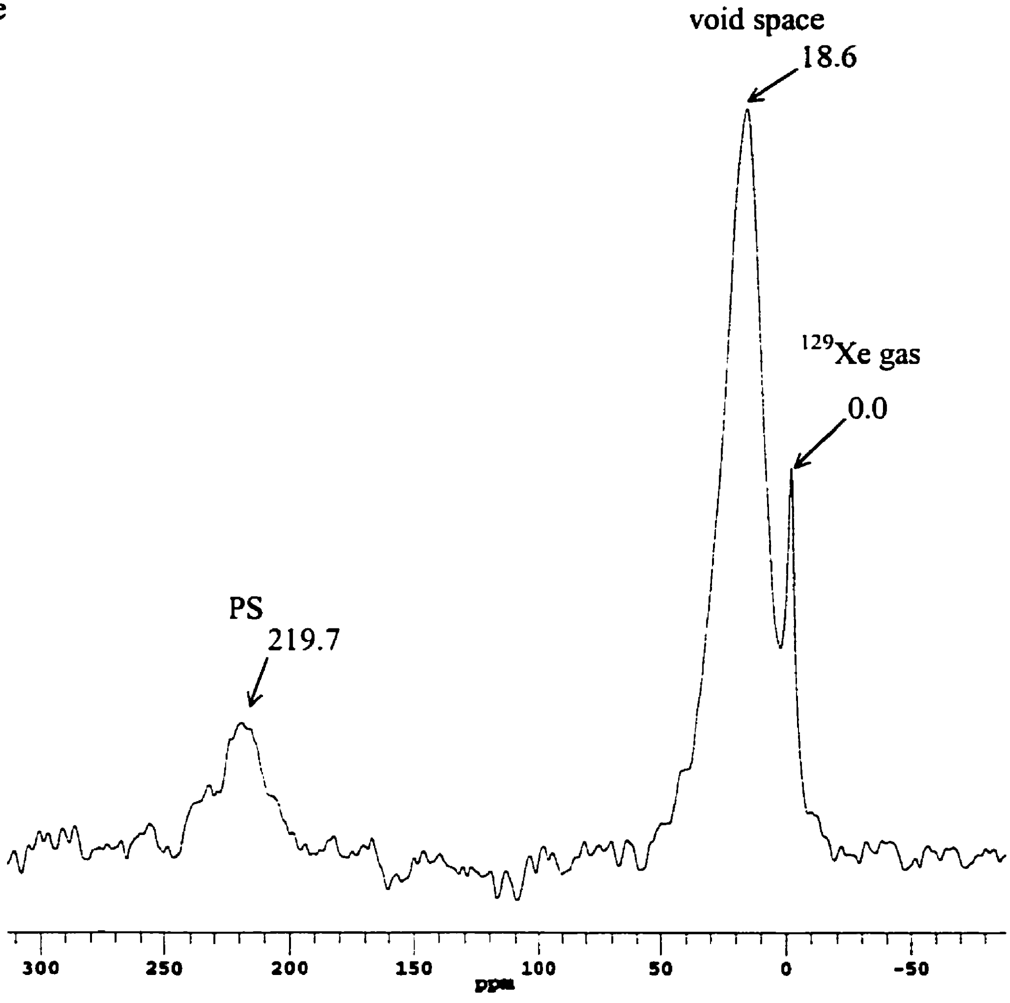

Figure 3.6 ^{129}Xe NMR spectrum of freeze-dried PS_{218}-*b*-PAA_{20} aggregates acquired at ambient temperature.

The ^{129}Xe NMR spectra of the PS-*b*-PAA aggregates in solution displayed different features from that of the PS-*b*-PAA aggregates in the solid-state. The most noticeable difference is the absence of the gas phase peak at 0 ppm in the solution samples. Therefore, it was necessary to run a xenon standard sample where the gas phase peak was used as a reference at 0 ppm prior to each ^{129}Xe NMR measurement. Figure 3.7 displays the ^{129}Xe NMR spectra of the 10 wt % PS_{218}-*b*-PAA_{20} aggregates in different dioxane/water solvent mixtures. The intense peak at *ca.* 196 ppm is assigned to xenon in the solvent phase while the broad, weak peak at *ca.* 218 ppm is that of xenon sorbed in the PS component of the PS-*b*-PAA aggregates. In previous studies involving ^{129}Xe NMR of solvents, the resonance shift of xenon in water was *ca.* 195 ppm.[22] The resonance shift of xenon sorbed in the PS block of the aggregates corresponds well with the spectra of the PS beads and the freeze-dried PS_{218}-*b*-PAA_{20} micelles displayed in Figure 3.5 and 3.6. As expected, the signal for the PAA block is not observed in the ^{129}Xe NMR spectra. The PAA content of the block copolymer is low, therefore the overall concentration of PAA in the aggregate solution is too low to result in an NMR signal.

As the dioxane content of the sample increases, the separation between the solvent and the PS peak decreases up to the point where at 40 wt % dioxane, there is only one broad peak in the spectrum. To account for the single signal in the 40 wt % dioxane sample, either the chemical shifts of xenon in the PS and solvent phases are similar or the xenon atom is moving rapidly between these two phases. The change in solvent resonance shift is not attributed to the increase in dioxane content of the solvent mixture as the xenon chemical shift in pure dioxane is *ca.* 187 ppm and the resonance shift of the solvent mixture would be seen to shift downfield, which is contrary to what was observed. A possible explanation for the decrease of the PS resonance shift involves the increase of the free volume of the PS core caused by the addition of dioxane. An increase in the free volume of the xenon atom's environment manifests itself as a downfield shift of the ^{129}Xe resonance signal. Another consideration is the exchange of xenon between the two sites. The dioxane content of 40 wt % may have plasticized the PS block to the extent that at ambient temperature, the micelle core is above its glass transition temperature. As a result, the diffusion of xenon between the polymer and solvent will occur at a rate, which is faster than the NMR timescale. Miller *et al.*[27] observed two distinct environments for xenon in a sample of dimyristoyl lecithin vesicles and the chemical exchange of xenon between these two sites. Miller *et al.*[27] observed an increase in the rate of chemical exchange was exhibited in the NMR spectra at elevated temperatures as two peaks were visible at 35 °C and only one peak was present at 50 °C. To ascertain the cause of the shift and coalescence of the PS and solvent signals, further investigations will be required to quantify the rate of xenon exchange between the PS and solvent environments of the PS_{218}-*b*-PAA_{20} micelle solution.

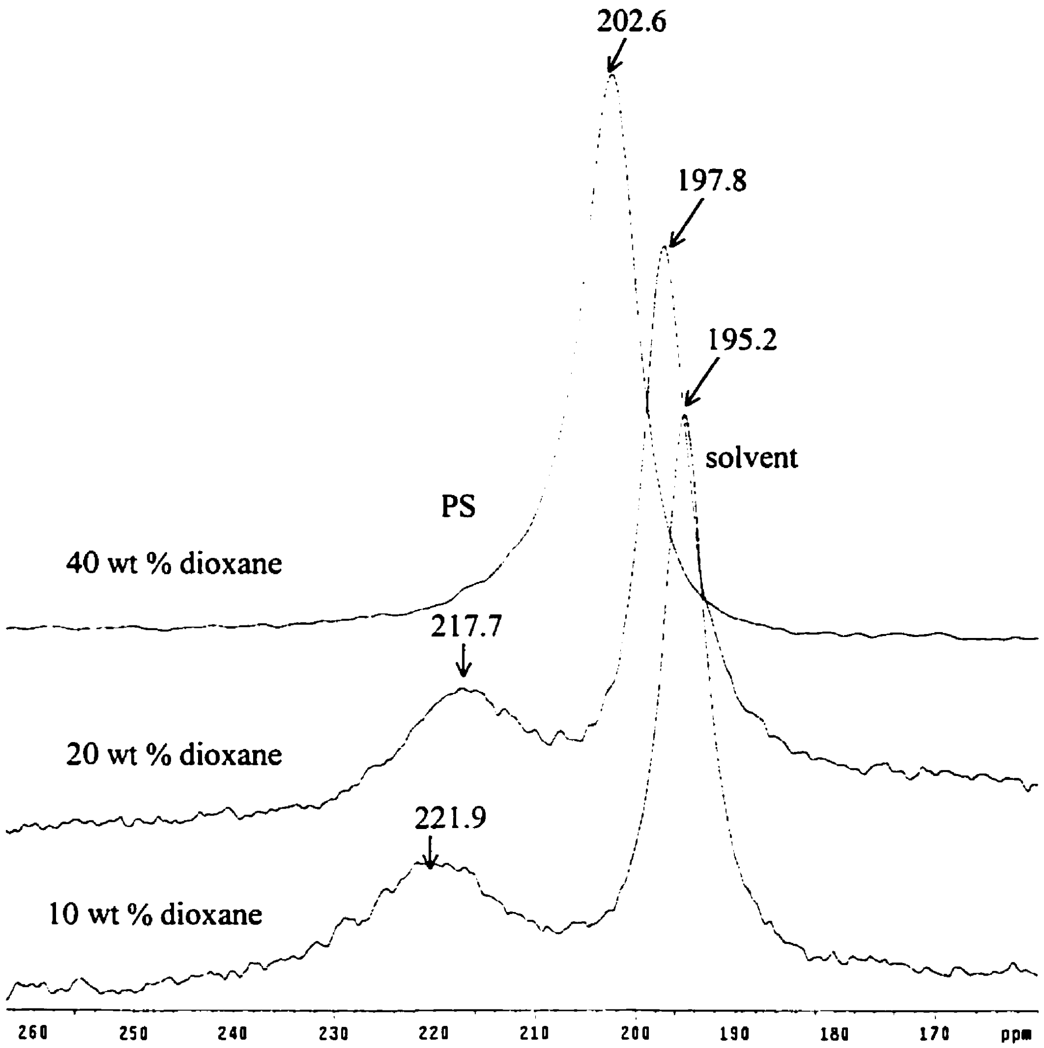

Figure 3.7 ^{129}Xe NMR spectra of 10 wt % PS_{218}-*b*-PAA_{20} aggregates in different dioxane/water solvent mixtures at ambient temperature.

The ^{129}Xe NMR spectra of the 10 wt % PS_{218}-*b*-PAA_{20} aggregates in different dioxane/water solvent mixtures with NaOH added (R=0.015) are shown in Figure 3.8. The spectra are similar to the 10 wt % PS_{218}-*b*-PAA_{20} aggregates shown in Figure 3.7, which indicates that the NaOH added to the copolymer solution did not significantly alter the ^{129}Xe NMR resonance shifts.

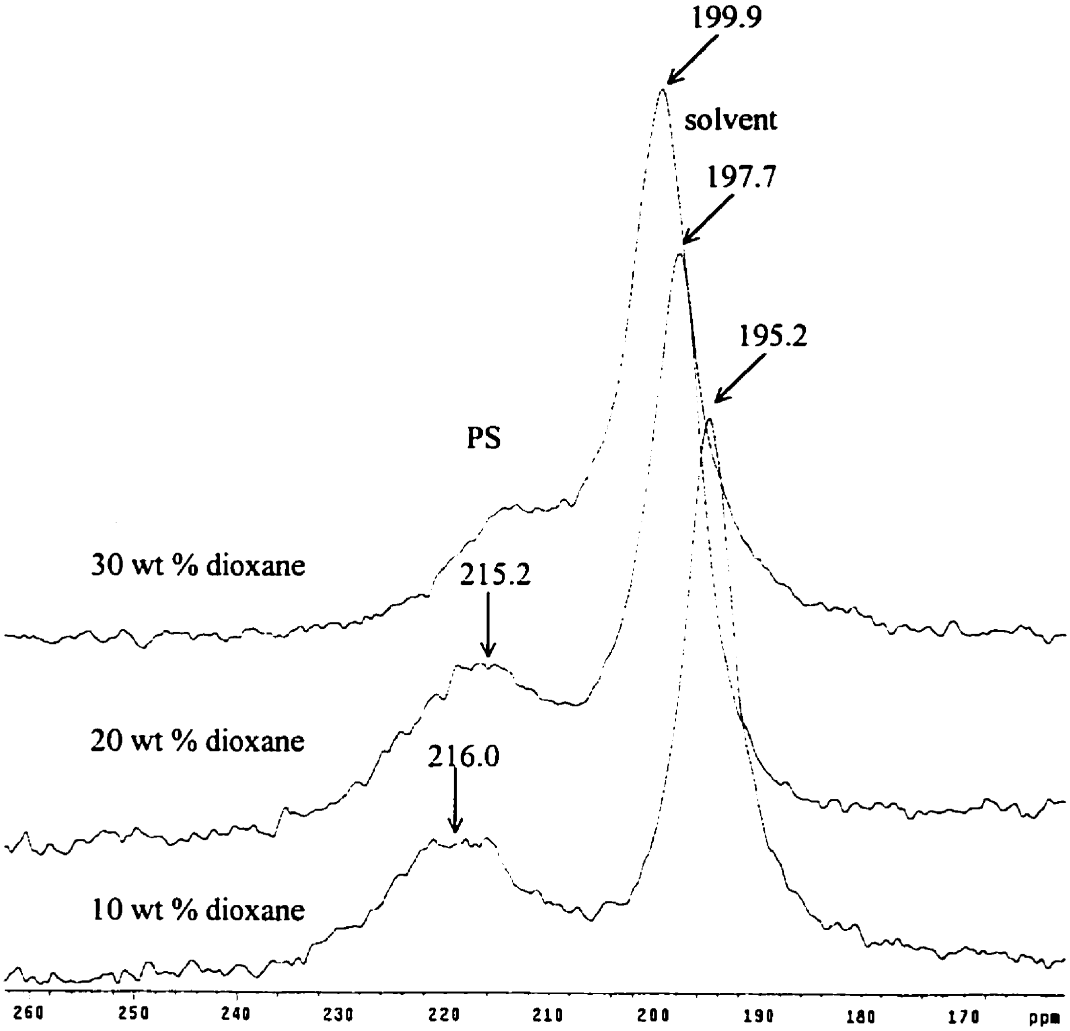

Figure 3.8 ^{129}Xe NMR spectra of 10 wt % PS_{218}-*b*-PAA_{20} aggregates in different dioxane/water solvent mixtures with NaOH added (R=0.015). The NMR spectra were acquired at ambient temperature.

Figure 3.9 shows the ^{129}Xe NMR spectrum of the 5 wt % PS_{100}-*b*-PAA_{25} copolymer in water with NaOH added so that R=0.0064. This sample consists of a mixture of cylindrical and vesicular structures. The xenon probe yields a strong solvent peak at *ca.* 192.4 ppm and a broad PS peak at *ca.* 214.0 ppm. To improve the sensitivity of the ^{129}Xe NMR experiment, the copolymer concentration was increased in subsequent samples.

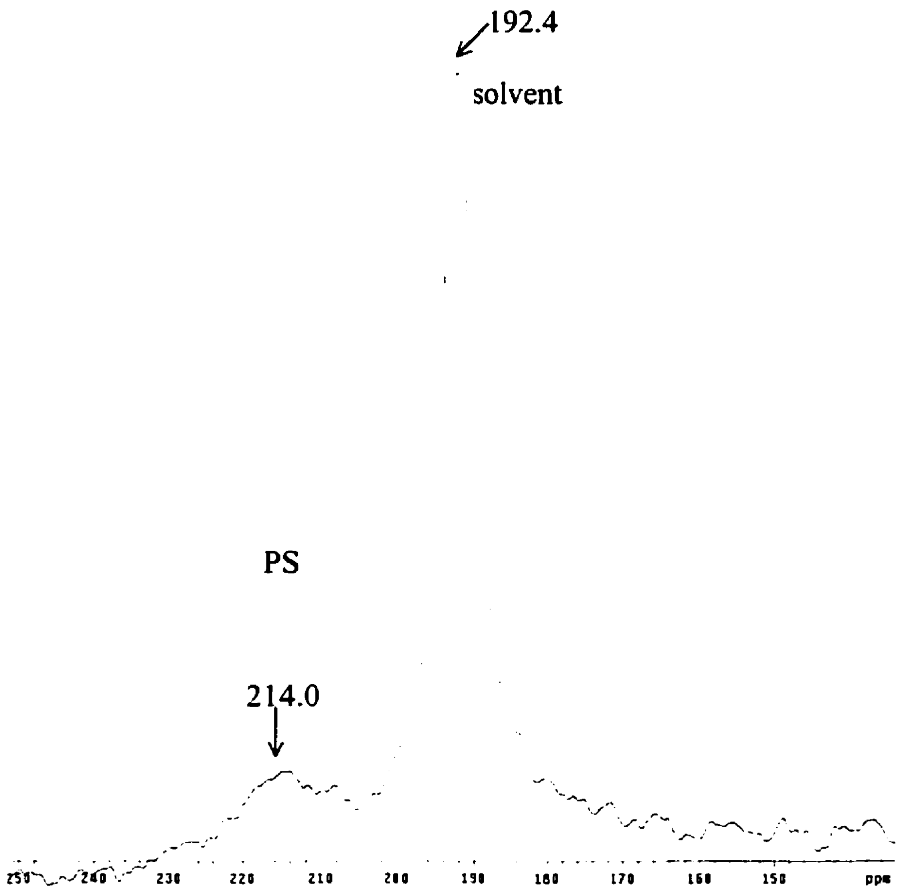

Figure 3.9 ^{129}Xe NMR spectrum of the 5 wt % PS$_{100}$-*b*-PAA$_{25}$ copolymer solution in water with NaOH added (R=0.0064).

The ^{129}Xe NMR measurements of the branched cylindrical aggregates formed from 9 wt % PS_{100}-*b*-PAA_{25} copolymer in different dioxane/water solvent mixtures with NaOH are shown in Figure 3.10. The increase in polymer concentration improved the signal intensity of xenon occupying the PS phase. There is a stark contrast between the samples with 0-20 wt % dioxane and the 30 wt % dioxane solution where the former exhibits a large separation between the solvent phase and the polymer phase peaks. The line shape of xenon in the solvent is narrower for these samples whereas the solvent line width of the 30 wt % dioxane aggregate solution is broad. These differences are attributed to the phase separation of the PS_{100}-*b*-PAA_{25} copolymer aggregates in this sample, which occurred when the NMR tube was cooled to liquid nitrogen temperature during the NMR tube sealing process. Phase separation of the copolymer solution occurred to a smaller extent for the sample with 30 wt % dioxane. It is interesting to note that for the 10 wt % PS_{218}-*b*-PAA_{20} solutions which formed vesicular structures, phase separation of the copolymer did not occur even when these samples were cooled to the same temperature. If the freeze-pump-thaw degassing cycle cannot be eliminated from the sample preparation process, there may be an upper limit to the copolymer concentration that can be investigated for cylindrical structures to avoid phase separation of the copolymer solution. The use of ^{129}Xe NMR to study protein solutions has revealed that these samples can be degassed without freezing the solutions as the cold temperatures would denature the proteins.[27] A similar degassing technique could be applied to the preparation of block copolymer micelle solutions to prevent phase separation of the copolymer aggregates.

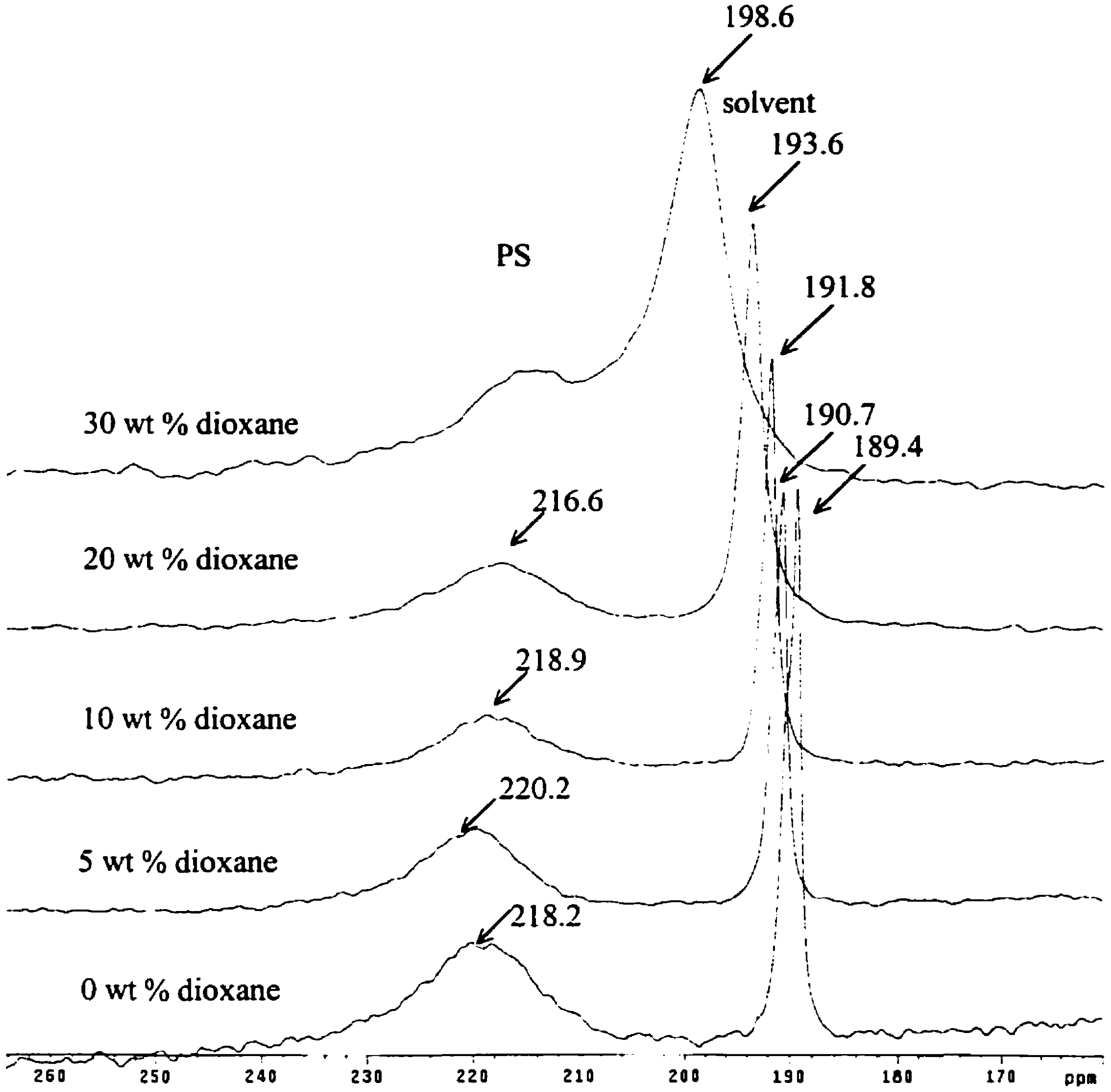

Figure 3.10 ^{129}Xe NMR spectra of 9 wt % PS_{100}-*b*-PAA_{25} copolymer solution in different dioxane/water solvent mixtures with NaOH added (R=0.03).

Table 3.2 ^{129}Xe NMR Data for the PS-*b*-PAA Copolymer Solutions Measured at Ambient Temperature

Polymer	Polymer Concentration (wt %)	Dioxane (wt %)	NaOH/PAA R value mole ratio	^{129}Xe in PS (ppm)	^{129}Xe in solvent (ppm)
PS_{218}-*b*-PAA_{20}	10	10	0	221.9	195.2
PS_{218}-*b*-PAA_{20}	10	20	0	217.7	197.8
PS_{218}-*b*-PAA_{20}	10	40	0		202.6*
PS_{218}-*b*-PAA_{20}	10	10	.015	216.0	195.2
PS_{218}-*b*-PAA_{20}	10	20	.015	215.2	197.7
PS_{218}-*b*-PAA_{20}	10	30	.015		199.9*
PS_{100}-*b*-PAA_{25}	5	0	0.0064	214.0	192.4
PS_{100}-*b*-PAA_{25}	9	0	.030	218.2	189.4
PS_{100}-*b*-PAA_{25}	9	5	.030	220.2	190.7
PS_{100}-*b*-PAA_{25}	9	10	.030	218.9	191.8
PS_{100}-*b*-PAA_{25}	9	20	.030	216.6	193.6
PS_{100}-*b*-PAA_{25}	9	30	.030		198.6*

* Individual peak assignments not possible due to the overlap of the PS and solvent ^{129}Xe NMR signals

3.3.4.1 Variable Temperature (VT) ^{129}Xenon NMR Measurements

Variable temperature ^{129}Xe NMR measurements were acquired for the 9 wt % PS_{100}-*b*-PAA_{25} copolymer in the 30/70 wt % dioxane/water solvent mixture and for the 10 wt % PS_{218}-*b*-PAA_{20} copolymer in the 20/80 wt % dioxane/water solvent mixture. The chemical shifts and peak line shapes of xenon in the PS core and in the solvent phase were monitored as a function of temperature. Due to the absence of the gas phase peak in the ^{129}Xe NMR spectrum, the gas phase peak of the xenon standard sample acquired at 20 °C was referenced to 0 ppm before the NMR spectrum of the aggregate solution was obtained.

3.3.4.2 VT ^{129}Xe NMR of PS_{100}-*b*-PAA_{25} Copolymer Aggregates in the 30/70 wt % Dioxane/Water Mixture

The ^{129}Xe NMR spectra of the PS_{100}-*b*-PAA_{25} copolymer in the 30/70 wt % dioxane/water solvent mixture acquired at different temperatures is shown in Figure 3.11. The copolymer concentration of 9 wt % and the addition of sodium hydroxide to give an R value of 0.03 gave rise to branched cylindrical aggregate structures as shown in Figure 3.3. The strong peak at *ca.* 197 ppm is that of xenon dissolved in the solvent phase and the weaker peak upfield is that of xenon in the PS component. Dissimilar to the PS_{218}-*b*-PAA_{20} micelle solution, this sample showed evidence of phase separation where solid PS_{100}-*b*-PAA_{25} copolymer aggregates were observed at the bottom of the NMR tube in addition to the aggregates still suspended in solution. The effect of phase separation of the PS_{100}-*b*-PAA_{25} aggregates on the ^{129}Xe NMR spectral features can be discerned by comparing the temperature dependence of the PS signal for the PS_{100}-*b*-PAA_{25} and PS_{218}-*b*-PAA_{20} aggregate samples. The major difference in the NMR spectral features between the two samples is observed at the higher temperatures. The PS_{100}-*b*-PAA_{25} sample, composed of both phase separated aggregates and aggregates suspended in solution, shown in Figure 3.11 gives rise to two peaks even at the highest temperature. In contrast, the PS_{218}-*b*-PAA_{20} sample consisting only of aggregates suspended in solution, showed one peak in the ^{129}Xe NMR spectrum at 50 °C in Figure 3.13.

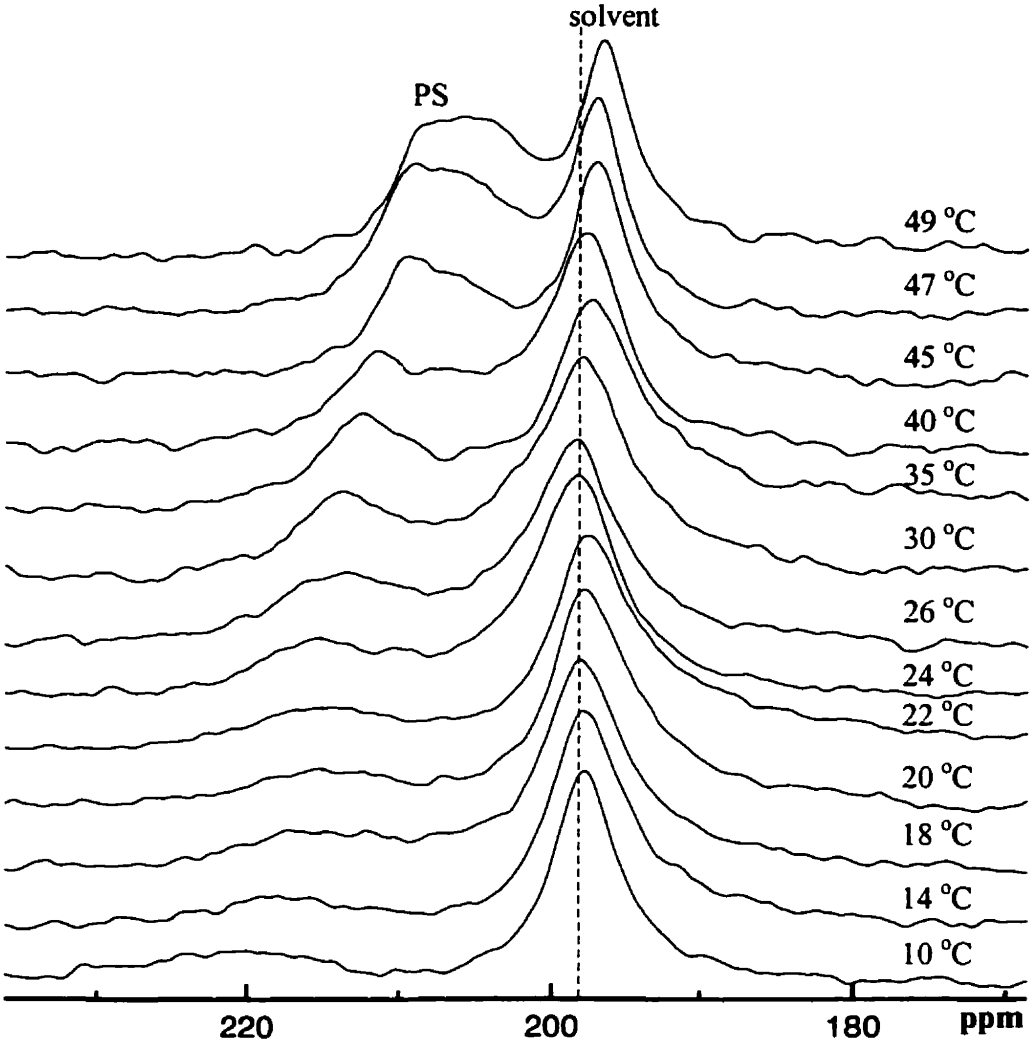

Figure 3.11 ^{129}Xe NMR spectra of the 9 wt % PS_{100}-*b*-PAA_{25} copolymer aggregates in the 30/70 wt % dioxane/water solvent mixture obtained at different temperatures. R=0.03 This sample is composed of both aggregates in solution and phase separated aggregates.

The line shapes of the xenon signals were determined by Lorentzian fitting of the spectra and are tabulated in Table 3.3. Unfortunately, due to the presence of both the PS-*b*-PAA copolymer aggregates and phase separated aggregates in the sample, it was difficult to fit the PS peak composed of two components. A clear trend cannot be associated with the line width data and the effect of temperature.

Previous studies have shown that the line shape of the xenon signal is broad above the glass transition of the polymer and narrow below this temperature. The anisotropic chemical shift tensor is influenced by the distortion of the xenon electron cloud in contact with the polymer and as the polymer sample is composed of different environments at the atomic scale, a distribution of chemical shift tensors will result. For polymers above the glass transition temperature, the xenon atom diffuses rapidly and experiences different sites in the sample. As a result, the chemical shift tensor is changing in size and orientation, and the anisotropy is averaged away resulting in the narrow lineshape.[28,29] Brownstein *et al.*[30] observed that the ^{129}Xe NMR spectrum of the block copolymer polystyrene-*b*-polyisoprene showed two superimposed peaks belonging to xenon dissolved in the two polymer environments. At room temperature, the PS component was below its glass transition temperature; however, the polyisoprene phase was above the glass transition. Therefore, the line width for xenon in the PS phase was broad whereas it was narrow for xenon dissolved in the PI component. Both line shapes were broader than their respective pure homopolymers, and this was interpreted as being caused by rapid the diffusion of the xenon atoms between the two different phases.

The line widths of the signal for xenon dissolved in the solvent of the PS_{100}-*b*-PAA_{25} copolymer solution and their dependence on temperature are displayed in Table 3.3 Unlike the line width measurements, assessing the resonance frequencies of xenon sorbed in the PS and solvent phases of the PS_{100}-*b*-PAA_{25} sample was more reliable. Figure 3.12 shows the effect of temperature on the chemical shift of the probe in the phase separated block copolymer aggregates and the solvent mixture. Clearly, the chemical shift dependencies on the temperature are different for xenon in the PS and solvent. The chemical shift for the solvent varies *ca.* 1.5 ppm over the entire temperature range with no significant influence from the temperature. In contrast, the chemical shift of xenon in the

PS component decreases in a linear fashion over the entire temperature range; however, there is a discontinuity in the slope of the chemical shift-temperature curve between 40 °C and 45 °C where the slope of this relationship decreases at this temperature. The rate of change of the xenon chemical shift, δ, as a function of the temperature before the discontinuity, $\frac{d\delta}{dT}$, is -0.234 ± 0.008 ppm/°C, whereas, $\frac{d\delta}{dT} = -0.66\pm0.01$ ppm/°C after the transition. The discontinuity of the chemical shift-temperature curve determined from the intersection of the two linear curves is 41 °C.

To determine the contributing factors to the chemical shift dependence on the temperature for the PS_{100}-*b*-PAA_{25} copolymer aggregate sample, the temperature dependencies of the polymer free volume must be considered, and the exchange of xenon between the solvent and polymer phases. Cheung *et al.*[10] proposed that the phenomenon of the ^{129}Xe chemical shift dependency on temperature in solid polymers could be explained by applying the free volume approach. As the temperature of a polymer is elevated, the free volume of the sample increases and this modification manifests itself in the ^{129}Xe NMR spectrum as a decrease in the resonance frequency. Using examples of isotactic poly(4-methyl-1-pentene) and isotactic polypropylene, they showed that transitions in polymers led to discontinuities in the slope of the chemical shift-T^{-1} curve. Of particular interest is that at the glass transition, the discontinuity in the slope is directly related to the discontinuity in the thermal expansion coefficient of the polymer. They also noted that the slope of the chemical shift-T^{-1} will decrease going from the high temperature side to the low temperature side of the glass transition temperature.

A further complication to interpreting the resonance shift data arises as the exchange of xenon between the PS phase of the PS_{100}-*b*-PAA_{25} aggregates and the solvent will also lead to a decrease in the chemical shift value of xenon in the PS component. However, the clear separation of the two signals in the ^{129}Xe NMR spectrum acquired at 49 °C shows slow exchange of xenon between the PS core and the solvent. Therefore, the decrease of the chemical shift for xenon sorbed in the PS component can be attributed to the change of polymer free volume and not the exchange of xenon between the two sites.

We believe that the glass transition temperature of the phase separated PS_{100}-*b*-PAA_{25} copolymer aggregates is in the region of 40 °C and 45 °C.

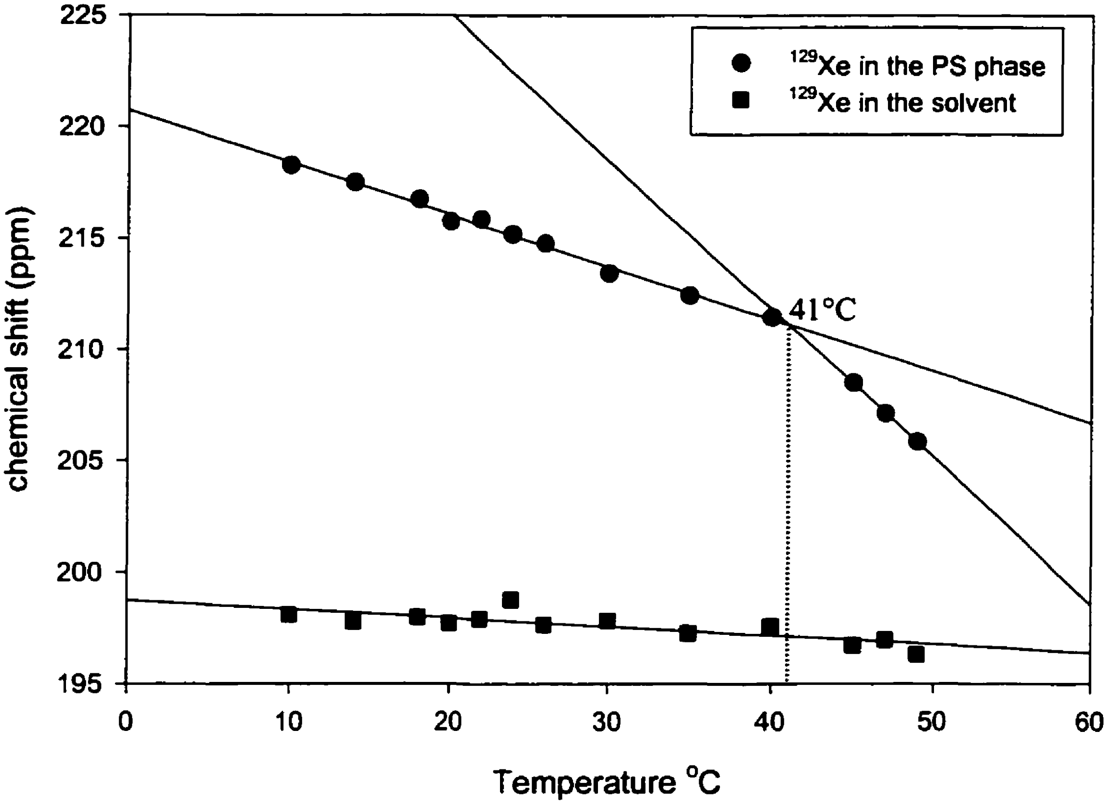

Figure 3.12 ^{129}Xe NMR resonance shifts of the 9 wt % PS_{100}-*b*-PAA_{25} copolymer aggregates in the 30/70 wt % dioxane/water solvent mixture as a function of temperature.

Table 3.3 ^{129}Xe NMR Data as a Function of Temperature for the 9 wt % PS$_{100}$-*b*-PAA$_{25}$ Copolymer Aggregates in the 30/70 wt % Dioxane/Water Solvent Mixture.

Temperature	Solvent		Polystyrene	
	δ	Line width	δ	Line width
°C	(ppm)	(Hz)	(ppm)	(Hz)
10	198.1	707	218.2	2112
14	197.8	1030	217.5	1143
18	198.0	1039	216.7	1098
20	197.7	933	215.7	1179
22	197.9	1192	215.9	1804
24	198.8		215.2	1736
26	197.6	1282	214.8	1147
30	197.8	1197	213.4	1141
35	197.3	1260	212.4	958
40	197.6		211.5	
45	196.7	1052	208.5	953
47	196.8	582	207.5	1239
49	196.3	641	205.8	1079

3.3.4.3 VT ^{129}Xe NMR of PS$_{218}$-*b*-PAA$_{20}$ Copolymer Aggregates in the 20/80 wt % Dioxane/Water Mixture

The ^{129}Xe NMR spectra of the 10 wt % PS$_{218}$-*b*-PAA$_{20}$ copolymer aggregates in the 20/80 wt % dioxane/water solvent mixture are shown in Figure 3.15. This sample consisted of vesicular structures of various sizes ranging from 50 nm to 230 nm in diameter. The thickness of the vesicle walls was 20 nm for the aggregates. In addition to these architectures, simple spheres 35 nm in diameter were also observed by TEM. In Figure 3.13, the strong peak at *ca.* 197 ppm is that of xenon in the solvent mixture while the broad signal upfield from the solvent peak is that of xenon sorbed in the PS phase. For vesicular structures, the PS component of the copolymer is found in the interior portion of the vesicular walls. The most noticeable feature of these spectra is that at 10°C, two distinct peaks are observed; however at 50°C, only one broad peak is present. Due to the coalescence of these two signals, extracting data from the spectra was possible only within the 10°C to 40°C temperature range. Unlike the 9 wt % PS$_{100}$-*b*-PAA$_{25}$ copolymer aggregate sample in which phase separation occurred, the PS$_{218}$-*b*-PAA$_{25}$ copolymer micelle solution did not contain phase separated aggregates, which can explain the presence of only one peak in the NMR spectrum acquired at 50 °C. Xenon gas can exchange more readily between the PS core and the solvent in the block copolymer aggregates suspended in solution as opposed to the phase separated copolymer aggregates.

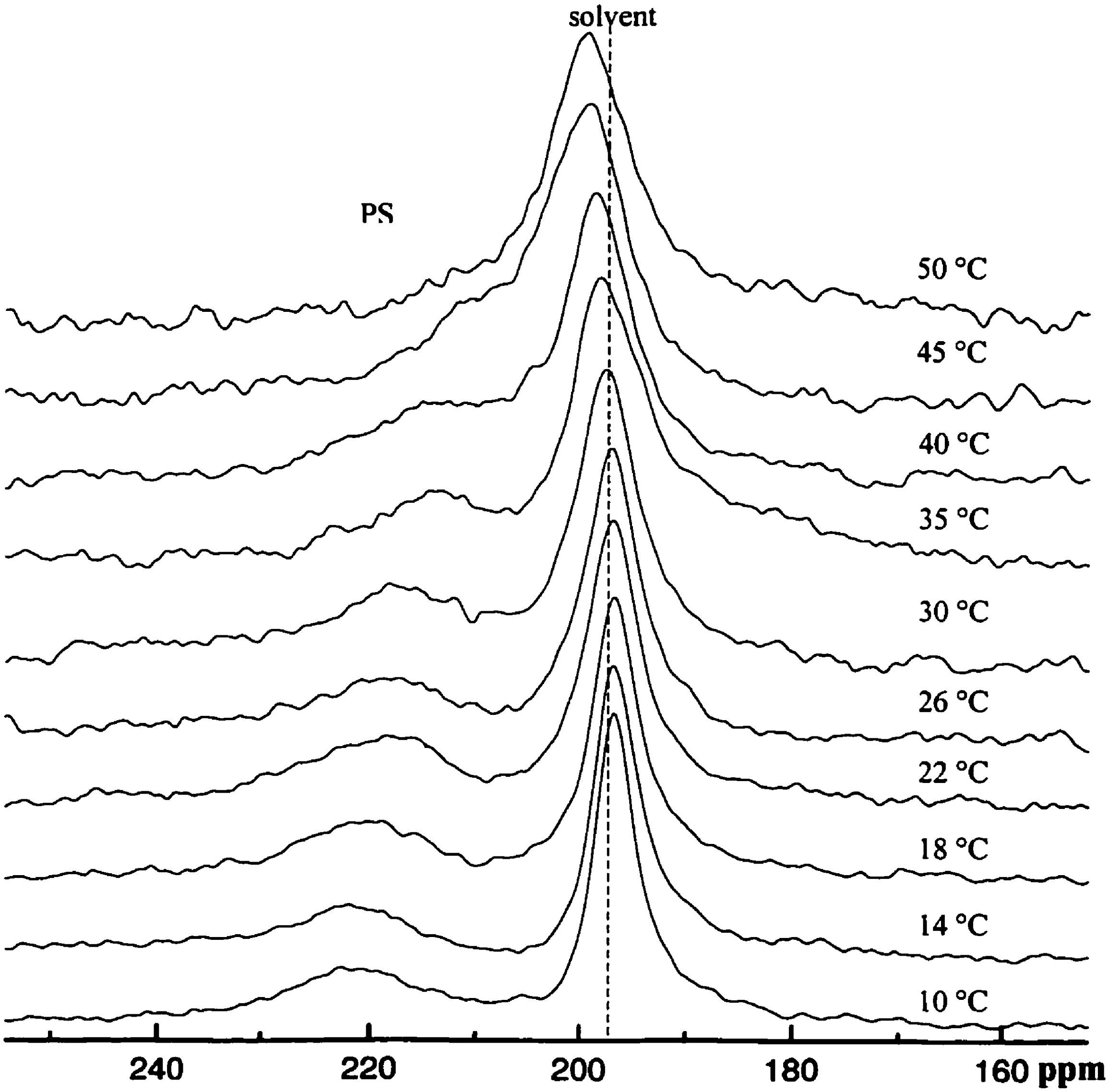

Figure 3.13 ^{129}Xe NMR spectra of the 10 wt % PS_{218}-*b*-PAA_{20} copolymer aggregates in the 20/80 wt % dioxane/water solvent mixture obtained a different temperatures. The micelles are suspended in solution.

The line shapes of the ^{129}Xe NMR signals were fitted with Lorentzian curves. Line width data was extracted from the spectra for temperatures between 10 °C and 37 °C since above this range, the overlap of the PS and solvent signals made deconvoluting the line shapes difficult. The line width of the ^{129}Xe NMR signal for xenon in the solvent phase increased as the temperature of the sample was elevated as shown in Figure 3.14. As the temperature was increased from 10 °C to 30 °C, the line width of the peak gradually increased from 657 Hz to 885 Hz; however, between 30 °C and 35 °C, the line width increased significantly from 885 Hz to 1396 Hz. The increase of line width of the solvent peak can be attributed to the increased exchange of xenon between the two phases. Simpson *et al.*[13,14] ascertained that the diffusion coefficient of xenon in PS beads increased dramatically at the glass transition temperature of the polymer. Therefore the presence of a single peak with a line width of 1723 Hz at 50 °C may have resulted from the fast exchange of xenon between the PS and solvent environments.

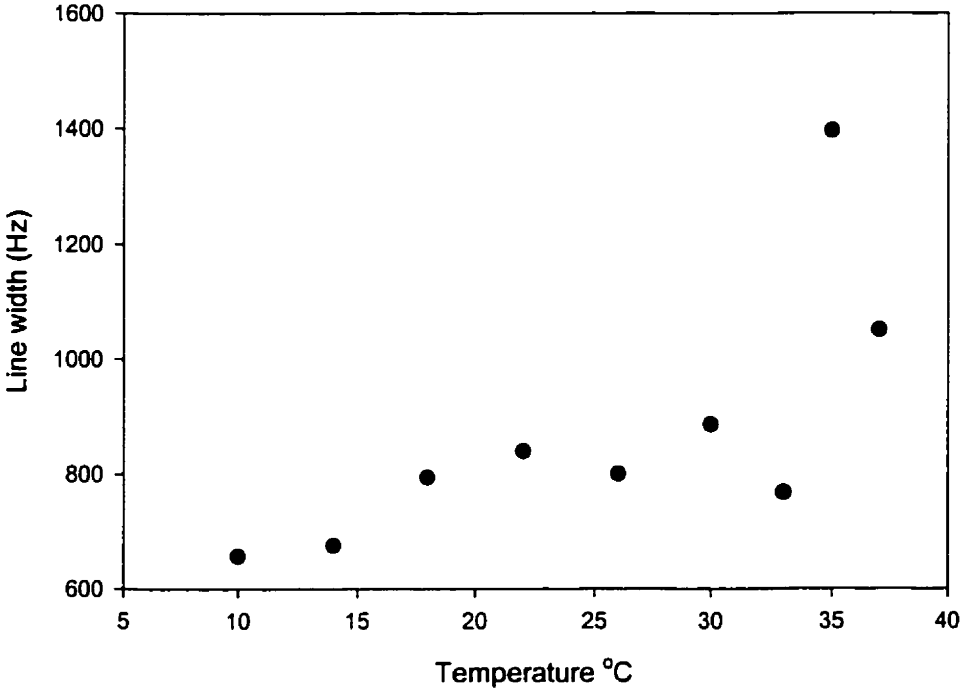

Figure 3.14 ^{129}Xe NMR line widths of xenon in the solvent phase of the 10 wt % PS_{218}-*b*-PAA_{20} copolymer aggregates in the 20/80 wt % dioxane/water solvent mixture as a function of temperature.

The ^{129}Xe NMR signal for xenon sorbed in the PS core of the micelles showed different behavior to temperature than that of xenon dissolved in the solvent phase. The line width of the PS phase signal decreased from 2393 Hz to 1397 Hz as the temperature was increased from 18 °C to 37 °C; however, at the lower temperatures of 10 °C and 14 °C, the line widths were 2027 Hz and 1724 Hz respectively. This result was surprising, as we would expect the signals at these two lower temperatures to be broader than those acquired at 18 °C. In the temperature range of 10 °C to 30 °C, all the peak line widths were greater than 1724 Hz; however, at 35 °C, the line width was only 1397.1 Hz.

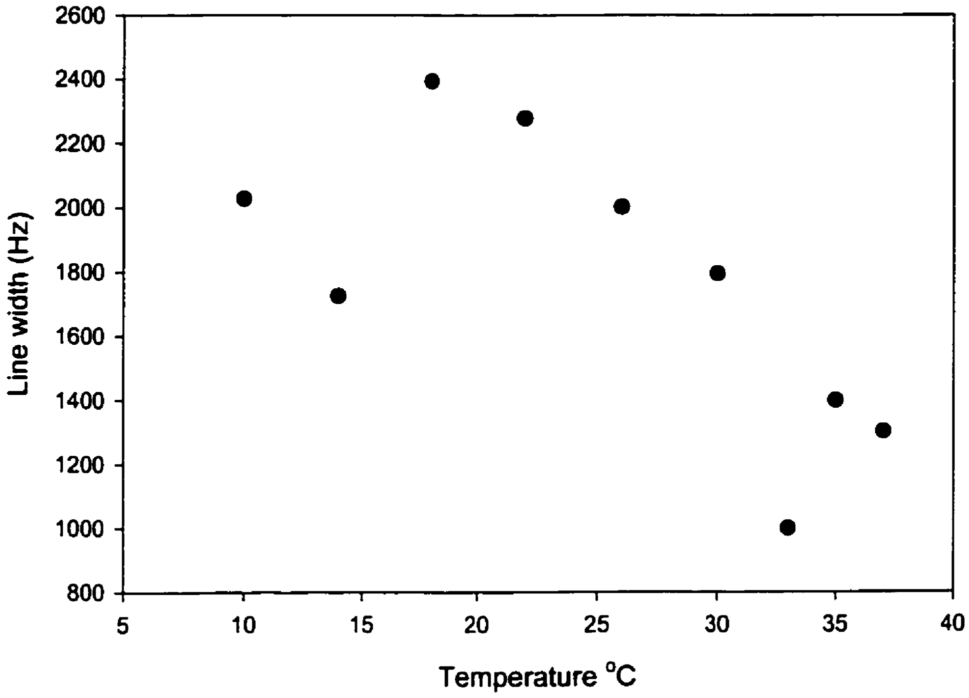

Figure 3.15 ^{129}Xe NMR line widths of xenon in the PS component of the 10 wt % PS_{218}-*b*-PAA_{20} copolymer aggregates in the 20/80 wt % dioxane/water solvent mixture as a function of temperature.

The temperature dependence of the ^{129}Xe NMR resonance shifts were also monitored for the PS_{218}-*b*-PAA_{20} copolymer aggregate solution. Figure 3.16 shows the influence of temperature on the ^{129}Xe NMR resonance shift of xenon in the solvent mixture. The chemical shift of this signal did not vary significantly in the temperature range of 10 °C to 26 °C. However, at 30 °C the signal at 197.6 ppm increased steadily to 199.2 ppm as the temperature was raised to 50 °C. Figure 3.16 displays the behavior of the ^{129}Xe NMR chemical shift for the PS component as a function of temperature. The resonance shift decreases linearly from 221.6 ppm to 218.2 ppm as the temperature is increased from 10 °C to 33 °C. The slope of this linear relationship is -0.18 ± 0.02 ppm/°C. When the temperature is raised from 33 °C to 35 °C, there is a discontinuity in the slope of the chemical shift and temperature relationship as the resonance shift decreases dramatically to 214.0 ppm. At 40 °C, the resonance shift is 213.5 ppm and at higher temperatures, the solvent and PS signals coalesce to form one broad peak at 199.2 ppm at 50 °C. It is important to note that the effect of temperature on the ^{129}Xe NMR resonance shift is more substantial for xenon in the PS phase opposed to the probe in the solvent mixture. The chemical shift for xenon sorbed in the PS component changed from 221.6 ppm at the lowest temperature to overlap with the solvent peak at 199.2 ppm, in contrast, the resonance shift for the solvent component only changed by 2.6 ppm over the same temperature range of 10 °C to 50 °C. Once the transition between 33 °C and 35 °C was passed, the chemical shift of the PS component decreased more sharply as a function of temperature. At temperatures greater than 37 °C, the chemical shift of xenon sorbed in the PS phase decreased to the extent that it overlapped significantly with the solvent peak. Consequently, the determination of the resonance shift values of xenon residing in the PS core is less reliable at these temperatures. The empty circles in Figure 3.16 are the chemical shifts of xenon in the PS component acquired at 37 °C and 40 °C. These values are conservative estimates indicating the upper limit to the chemical shift of these signals.

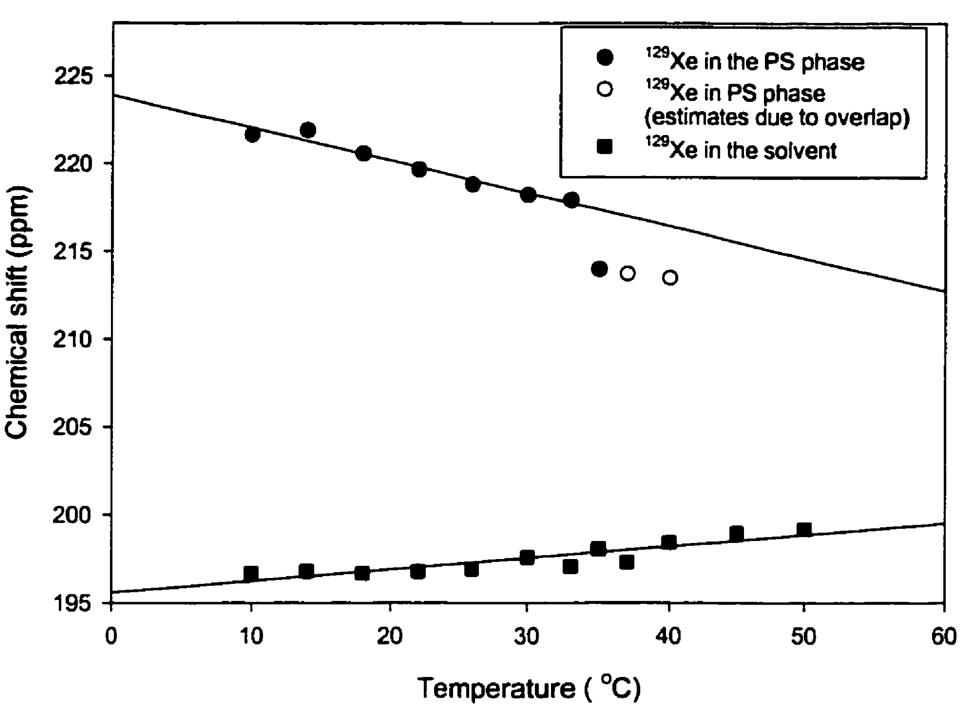

Figure 3.16 ^{129}Xe NMR resonance shifts of xenon in the solvent and PS components of the 10 wt % PS_{218}-*b*-PAA_{20} copolymer aggregates in the 20/80 wt % dioxane/water solvent mixture as a function of temperature.

To interpret the chemical shift data, xenon exchange within the micelle solution must be considered in addition to the free volume change of the PS core, as both processes will affect the resonance shifts of xenon in the PS phase.

NMR of xenon in different systems shows that the probe undergoes varying degrees of exchange from slow exchange exhibited in solid polymers to fast exchange in protein solutions. An example of the former is the ^{129}Xe NMR spectrum of the PS beads displayed in Figure 3.5 where two signals are separated by 220 ppm. At the other extreme, only one peak is observed in the ^{129}Xe NMR spectrum of horse metmyoglobin in aqueous solution.[31] The study of the temperature dependence of ^{129}Xe NMR resonance shifts is easier for solid polymers because of the large chemical shift separation between the polymer and the xenon gas phase peaks. The ^{129}Xe NMR spectra of the 9 wt % PS_{100}-*b*-PAA_{25} copolymer aggregates exemplify this characteristic as two distinct peaks are displayed for xenon sorbed in the PS phase of the phase separated copolymer aggregates and the solvent mixture. However, xenon in the 10 wt % PS_{218}-*b*-PAA_{20} copolymer aggregate solution underwent an intermediate rate of exchange between the PS and solvent sites. For this reason, determining the glass transition temperature of the core of copolymer aggregates in solution by ^{129}Xe NMR spectroscopy will be difficult as xenon exchange plays a prominent role in the spectra. Of particular concern is that above the T_g of a polymer, the xenon diffusion coefficient increases significantly and the signal will shift in the direction of the solvent peak. To apply this technique effectively, the chemical shift separation between xenon in the polymer and solvent components must be relatively large to accurately obtain the line width and resonance shift data.

Determining the glass transition temperature of the core of block copolymer aggregates from line width data will also be difficult since xenon exchange between the core and solvent is not in the slow exchange limit. The line width for xenon sorbed in a polymer will decrease as the temperature is raised above T_g because the xenon atom can move rapidly within sites in the polymer. However, above the glass transition temperature, the substantial increase of the xenon diffusion coefficient results in increased xenon exchange between the polymer and the solvent phases. The rapid exchange of xenon between the polymer and solvent sites leads to an increase in the peak line width. Therefore the temperature increase influences the ^{129}Xe NMR line shapes of copolymer aggregate solutions in two competing directions.

Table 3.4 ^{129}Xe NMR Data as a Function of Temperature for the 10 wt % PS$_{218}$-*b*-PAA$_{20}$ Copolymer in the 20/80 wt % Dioxane/Water Solvent Mixture.

Temperature	Solvent		Polystyrene	
	δ	Line width	δ	Line width
°C	(ppm)	(Hz)	(ppm)	(Hz)
10	196.7	656	221.6	2027
14	196.8	675	221.9	1724
18	196.7	793	221.6	2392
22	196.8	838	219.7	2277
26	197.0	799	218.8	2000
30	197.6	885	218.2	1793
33	197.1	767	217.9	997
35	198.1	1396	214.0	1397
37	197.3	1049	213.7	1301
40	198.4		213.5	
45	199.0*			
50	199.2*			

* at 45 °Cand 50 °C, the PS and solvent phase signals cannot be deconvoluted due to overlap

According to our thermal analysis of the PS homopolymer samples plasticized with dioxane, we would anticipate that the dioxane content of the PS core of the PS$_{100}$-*b*-PAA$_{25}$ and PS$_{218}$-*b*-PAA$_{20}$ copolymer aggregates is 0.30 v/v and 0.35 v/v respectively. However, with the high water content in the solvent mixture of our PS-*b*-PAA copolymer aggregates samples, the dioxane content in the PS core of our micelles should be considerably less than the two values stated above. This discrepancy would suggest that the depression of the glass transition temperature of the micellar PS core is not solely the result of the plasticization of polystyrene by dioxane in the solvent mixture.

3.4 Conclusions

Preliminary results have shown that ^{129}Xe NMR spectroscopy is a promising method to probe the solvent phase and the PS core of PS-*b*-PAA copolymer micelle solutions. Analysis of ^{129}Xe NMR line shapes and resonance shifts as a function of temperature have demonstrated temperature-induced transitions in the PS component of the block copolymer solutions. The ^{129}Xe NMR measurements of the phase separated PS$_{100}$-*b*-PAA$_{25}$ copolymer aggregates exhibited a transition in the temperature region of 40 °C to 50 °C. The PS$_{218}$-*b*-PAA$_{20}$ copolymer aggregates underwent a transition at 33 °C to 35 °C. Further investigations are needed to determine the extent of xenon exchange between the PS and solvent phases of the PS-*b*-PAA copolymer aggregate solutions.

3.5 Acknowledgments

The author thanks Dr. Yisong Yu for the synthesis of the PS homopolymer and PS-*b*-PAA copolymers. Christian Krueger's synthesis of the PS beads is also gratefully acknowledged. The author wishes to thank Antisar Hlil for the DSC analyses of the PS homopolymer. Alfred Kluck's assistance in fashioning the materials for the xenon loading apparatus is appreciated. The author also benefited from George Kopp's glass blowing expertise and Dr. Paul Xia's NMR knowledge.

3.6 References

1. Stevens M. P. *Polymer Chemistry an Introduction,* 2nd ed.; Oxford University Press: New York, 1990.
2. Vold, R.R. In *Nuclear Magnetic Resonance Probes of Molecular Dynamis;* Tycko, R. Ed.; Kluwer Academic Publishers: Dordrecht, 1994, Chapter 2.
3. Komoroski, R. A. In *High Resolution NMR Spectroscopy of Synthetic Polymers in Bulk;* Komoroski, R. A., Ed.; VCH Publishers, Inc.: Florida, 1986, pp 135-136.
4. Colletti, R. F.; Mathias, L. J. In *Solid State NMR of Polymers*; Mathias, L. J., Ed.; Plenum Press: New York, 1991, pp 34-35.
5. Candau, F.; Heatley, F.; Price, C.; Stubbersfield, R. B. *Eur. Polym. J.* **1984**, 20, 685-690.
6. Raftery, D.; Chmelka, B. F. In *NMR Basic Principles and Progress*; Springer-Verlag: Berlin Heidelberg, 1994, Vol. 30, p 112.
7. Ratcliffe, C. I. In *Annual Report on NMR Spectroscopy*; Academic Press Limited: 1998, Vol. 36, p 124.
8. Springuel-Huet, M. A. In *Principles Physical Adsorption: Experiment, Theory and Applications*; Fraissar, J. Ed.; Kluwer Academic Publishers: Netherlands, 1997, p 331-348.
9. Tomaselli, M.; Meier, B. H.; Robyr, P.; Suter, U.W.; Ernst, R.R. *Chemical Physics Letters* **1993**, 205, 145-152.
10. Cheung, T. T. P.; Chu, P. J. *J. Phys. Chem.* **1992**, 96, 9551-9554.
11. Miller, J. B. Walton, J. H. Roland, C. M. *Macromolecules* **1993**, 26, 5602-5610.
12. Stengle, T. R.; Williamson, K. L. *Macromolecules* **1987**, 20, 1428.
13. Simpson, J. H.; Wen, W.-Y.; Jones, A. A.; Inglefield, P. T.; Bendler, J. T. Appl. Magn. Reson. **1995**, 8, 349-360.
14. Simpson, J. H.; Wen, W.-Y.; Jones, A. A.; Inglefield, P. T.; Bendler, J. T. *Macromolecules* **1996**, 29, 2138-2142.
15. Bharatam, J.; Bower, C. R. *J. Phys. Chem. B* **1999**, 103, 2510-2515.
16. Zhang, L.; Eisenberg, A. *Science* **1995**, 268, 1728-1731.
17. Yu, Y.; Eisenberg, A. *J. Am. Chem. Soc.* **1997**, 119, 8383-8384.

18. Yu, Y.; Zhang, L.; Eisenberg, A. *Macromolecules* **1998**, 31, 1144-1154.
19. Shen, H.; Eisenberg, A. *J. Phys. Chem. B* **1999**, 103, 9473-9487.
20. Chen, L.; Shen, H.; Eisenberg, A. *J. Phys. Chem. B* **1999**, 103, 9488-9497.
21. Zhang, L.; Eisenberg, A. *Journal of the American Chemical Society* **1996**, 118, 3168-3181.
22. Grishin, Y. K.; Mazitov, R. K.; Panov, A. N. *Appl. Magn. Reson.* **1998**, 14, 357-366.
23. Hautekeer, J.-P.; Varshney, S. K.; Fayt, R.; Jacobs, C.; Jerome, R.; Teyssie, Ph. *Macromolecules* **1990**, 23, 3893-3898.
24. Zhong, X. F.; Varshney, S. K.; Eisenberg, A. *Macromolecules* **1992**, 25, 7167.
25. Zhang, L.; Yu, K.; Eisenberg, A. *Science* **1996**, 272, 1777-1779.
26. Zhang, L.; Eisenberg, A. *Macromolecules* **1996**, 29, 8805-8815.
27. Miller, K. W.; Reo, N. V.; Stengle, D. P.; Stenble, T. R.; Williamson, K. L. *Proc. Natl. Acad. Sci. USA* **1981**, 78, 4946-4949.
28. Walton, J. H. *Polymer and Polymer Composites* **1994**, 2, 35-41.
29. Kentgens, A. P. M.; van Boxtel, H. A.; Verweel, R.-J.; Veeman, W. S. *Macromolecules* **1991**, 24, 3712-3714.
30. Brownstein, S. K.; Roovers, J. E. L.; Worsfold, D. J. *Magnetic Resonance* **1988**, 26, 32.
31. Locci, E.; Dehouck, Y.; Casu, M.; Saba, G.; Lai, A.; Luhmer, M.; Reisse, J.; Bartik, K. *Journal of Magnetic Resonance* **2001**, 150, 167-174.

Chapter 4

Conclusions, Original Contributions to Knowledge and Suggestions for Future Work

4.1 Conclusions and Original Contributions to Knowledge

This thesis describes the preparation of PS-*b*-PAA copolymer aggregates and their characterization by nuclear magnetic resonance spectroscopy. ^{1}H NMR solution-state measurements elucidated the dynamics of the copolymer chains during the micellization process. In addition, ^{129}Xe NMR measurements of PS-*b*-PAA copolymer aggregates in dioxane/water mixtures probed the micellar environment.

Chapter 2 describes the study involving ^{1}H NMR relaxation measurements obtained for both PS-*b*-PAA copolymer and PS homopolymer in deuterated dioxane as deuterium oxide was progressively added to the polymer solutions. Our main goal was to determine the segmental mobility of the PS and PAA chains, which formed the aggregate core and corona respectively. Despite the limited resolution of the ^{1}H NMR experiment, the mobility of the core and corona could be separately monitored via the relaxation parameters of the PS phenyl ring protons and the PAA α proton. Analysis of the ^{1}H NMR line shapes revealed broadening of the signals assigned to the PS phenyl ring protons as deuterium oxide was added to the copolymer and homopolymer solutions. As the deuterium oxide content of the copolymer solutions exceeded 28 wt %, the PS aromatic peaks were no longer detectable. At a deuterium oxide content of 14 wt %, the homopolymer PS aromatic signals were not observed in the NMR spectrum. The line shapes of the NMR signals assigned to the PAA blocks exhibited contrasting behaviour to that of the micelle core. These signals displayed a lesser degree of broadening and were still observed at higher deuterium oxide contents. Spin-lattice and spin-spin relaxation times determined that the PS-*b*-PAA copolymer and PS homopolymer were experiencing relaxation behaviour in the slow motion limit. The motional freedom of the PS segments of the copolymer decreased significantly at a critical deuterium oxide content whereas the mobility of the PS homopolymer decreased over a range of deuterium oxide contents. The dynamic behavior of the PAA blocks during the micellization process is more complicated. Initially, the PAA mobility increases with added deuterium oxide whereas that of the PS blocks decreased. This trend reflects the fact that water is a highly favorable solvent for PAA and highly unfavorable for PS. At the critical deuterium oxide content, the mobility abruptly decreased as the PAA segments formed the corona of the micelles, effectively transforming them into pinned chains with more restricted mobility. The mobility than again continues to increase with deuterium oxide content due to the increasing solvation of the PAA corona.

This picture of the micellization dynamics is drawn from the spin-lattice relaxation parameters. As explained in Chapter 2, the spin-spin relaxation measurements indicate the complexity of the local dynamics of the copolymer before micellization. The dynamic heterogeneity, as reflected by the absence of a simple single exponential decay, may be due to the presence of some aggregates before the actual micellization.

Preliminary results from the investigation of PS-*b*-PAA copolymer aggregates in dioxane/water solvent mixtures by ^{129}Xe NMR spectroscopy are discussed in Chapter 3. Two distinct NMR signals were observed in the spectra, which were assigned to xenon dissolved in the solvent and PS phases. The analysis of the line shapes and resonance shifts of xenon occupying the PS core and solvent as a function of temperature are also described. Obtaining accurate line width values from the spectra was difficult due to the overlap of the PS and solvent signals and the presence of phase separated copolymer aggregates in the PS_{100}-*b*-PAA_{25} solution. The resonance shifts of xenon occupying the PS core of the PS-*b*-PAA aggregates displayed a discontinuity in the slope of the chemical shift-temperature curve indicating the presence of a temperature-induced phase transition. The phase separated PS_{100}-*b*-PAA_{25} copolymer aggregates underwent the glass transition in the temperature region of 40 °C to 45 °C whereas the PS_{218}-*b*-PAA_{20} copolymer aggregates exhibited a T_g in the region of 33 °C to 35 °C.

4.2 Suggestions for Future Work

This research involved the first investigations of PS-*b*-PAA "crew-cut" aggregates using NMR spectroscopy and clearly, we have only touched the surface of the possibilities of this characterization technique. PS-*b*-PAA aggregates are challenging to study by NMR since they are not ideal systems for both solution and solid-state techniques. While the PS core experiences restricted mobility, which broadens the NMR signals beyond the detection of solution-state instruments, the copolymer aggregates are still suspended in solution.

One major obstacle to acquiring dynamic information for the entire block copolymer chain is the overlapping nature of the ^{1}H NMR spectrum. There are two different ways to overcome this challenge. The first involves exploiting the greater spectral resolution of ^{13}C NMR spectroscopy to obtain relaxation data from the copolymer backbone. However, the low sensitivity of this nucleus due to its low natural abundance and weak gyromagnetic ratio will require the synthesis of ^{13}C labeled copolymer samples. Labeled polymers will be required for ^{13}C NMR relaxation measurements where the signal intensity cannot be enhanced by protons, a practice used to acquire 1D ^{13}C NMR spectra. The second approach consists of two-dimensional inversion recovery NMR experiments to measure the spin-lattice relaxation times of the main-chain copolymer signals. This method does not require the synthesis of labeled copolymers; however, the NMR experiment itself is more complex. The inversion recovery pulse sequence can be combined with the homonuclear correlated spectroscopy experiment and the spin-lattice relaxation times can be determined from the intensity of the cross-peaks which correspond to the J-coupled nuclei. These experiments have been employed to study the dynamics of proteins solutions, which also give rise to complex NMR spectra.[1-3]

A significant limitation to the study discussed in Chapter 2 is our inability to distinguish the relaxation behaviour of protons from different sites along both the PS and PAA chains. Gao *et al.*[4] determined that a mobility gradient existed along the corona chains in poly(styrene-*b*-sodium acrylate) reverse micelles. It would be advantageous to elucidate the dynamics of the PAA block at different points along the polymer chain as the micelle corona should also exhibit a motional gradient where the PAA units closest to the core-corona interface will experience greater motional restriction. Using Gao's method, deuterium-labeled segments could be incorporated at different sites along the copolymer chain and the dynamics of the corona as a function of the distance from the core-corona interface can be monitored by ^{2}H NMR measurements. In addition to the synthetic requirements, a complication may arise due to the low sensitivity of ^{2}H NMR spectroscopy as high copolymer concentrations will be used to prepare the aggregate solutions.

It was apparent that at *ca.* 30 wt % deuterium oxide content in the copolymer solutions, the NMR signals assigned to the PS block were not detectable. This points to the serious limitation of using a solution-state instrument to characterize the PS core of the copolymer aggregates in solution. Sample inserts, specifically designed to hold liquid samples, for solid-state NMR sample rotors are available which will permit the analysis of copolymer aggregate solutions by solid-state NMR experiments. Solid-state NMR techniques have been used extensively to characterize a wide range of polymers. We believe that solid-state NMR techniques will be effective in characterizing PS-*b*-PAA copolymer aggregates since the PS cores are expected to be in a glassy state. The 2D Wideline Separation experiment correlates structural and motional information where the ^{13}C dimension provides the isotropic chemical shift and the ^{1}H dimension provides the dynamic information via the line shape.[5-7] This technique may reveal the existence of a mixed PS and PAA region at the core-corona interface in the copolymer aggregates. To quantify the thickness of the interface, spin-diffusion experiments can be employed.[8]

The description of the ^{129}Xe NMR investigation of PS-*b*-PAA aggregates presented preliminary results, therefore future work in this area is substantial. The low sensitivity of ^{129}Xe NMR spectroscopy requires the preparation of samples with high copolymer concentrations. These limitations have given rise to complications in sample preparation, which will need to be addressed. The control of the aggregate morphologies posed a problem because of the high copolymer concentration of the aggregate solutions. In this study, vesicular and cylindrical PS-*b*-PAA copolymer aggregates were formed in dioxane/water solvent mixtures. The preparation of spheres from the PS-*b*-PAA copolymer may be possible using DMF as the co-solvent as previous studies have shown that spheres are formed when this solvent is used.[9] Unfortunately, to verify the aggregate morphologies, the DMF solvent must be removed by dialysis as TEM samples of the copolymer aggregates in DMF/water mixtures cannot be prepared. Simple spheres can also be prepared by increasing the PAA content of the copolymer used to form the micelles. By increasing the PAA content of the PS-*b*-PAA copolymer, spheres can be prepared in dioxane/water mixtures. Measuring the PS core T_g for micelles in dioxane/water mixtures will be more interesting than for aggregates in DMF/water mixtures since the DMF content in the PS core is expected to be negligible and will not plasticize the PS core to a large degree.

In addition to preparing PS-*b*-PAA copolymer spheres, precipitation of the copolymer during the degassing cycle must be avoided. To prevent this from occurring, two processes must be eliminated during the preparation of the samples: the freeze-thaw-pumping cycle and the flame sealing of the NMR tube, as both require immersing the NMR tube in liquid nitrogen. The removal of gaseous impurities from the copolymer solution can be performed without freezing the sample; however, it will be advantageous to cool a section of the NMR tube above the sample to prevent the evaporation of the solvent. To eliminate flame sealing the NMR tube, modified NMR tubes are available containing a valve, which can be reopened and sealed. Examples of such products are the J. Young NMR tube and the Pressure/Vacuum Valve Sample tube from the Wilmad Glass Company.

^{129}Xe NMR spectroscopy is not traditionally used to determine the glass transition temperature of polymers since simple alternative methods exist. For solid polymers, DSC provides a quick and simple determination of the T_g; however, for block copolymer aggregates suspended in solution, there are no alternative techniques. To our knowledge there are no systematic studies involving the determination of the glass transition temperature of PS using ^{129}Xe NMR spectroscopy, therefore, it will be necessary to undertake a detailed study of the influence of temperature on the ^{129}Xe NMR spectra of PS beads plasticized with various solvents. This will provide valuable information such as the slope of the chemical shift dependence on temperature, above and below the glass transition temperature. Another positive feature of this study is that the T_g values of the

PS beads can been verified by DSC analysis. The dioxane content in the PS core of the PS-*b*-PAA aggregates must be measured for solvent mixtures of high water contents to complement the data acquired by Yu *et al.*[10] This can be done by using PS beads, which will model the PS core of the copolymer aggregates. First, the PS beads will be immersed in dioxane. Once the PS beads are swollen with dioxane, they will be placed in different dioxane/water mixtures. The uptake or release of dioxane by the PS beads will be determined by measuring the degree of swelling of the PS beads before and after they are placed in the dioxane/water mixtures.

A question raised in Chapter 3 concerns the degree of xenon exchange between the PS and solvent phases. The presence of xenon exchange can be detected by two-dimensional exchange experiments, where the domain sizes determined by TEM can be employed to calculate the diffusion coefficient of xenon in the two components. One significant disadvantage to this method involves the excessive length of time, which will be required to acquire the 2-D exchange spectrum.

It would be advantageous to obtain ^{129}Xe NMR measurements of the remaining PS_{100}-*b*-PAA_{25} and PS_{218}-*b*-PAA_{20} copolymer aggregate solutions at different temperatures. Since the copolymer solutions contain varying amounts of dioxane, it would be interesting to determine the transition temperatures for the PS core as we would expect the transition temperature to decrease as the dioxane content in the copolymer solution is increased.

^{129}Xe NMR investigation of PS-*b*-PAA copolymer micelles shows promise as a unique and effective method to characterize these structures. Once the fundamental studies of PS beads have been completed, research of the PS-*b*-PAA copolymer aggregates will provide interesting challenges and invaluable structural information of these systems at the sub-micellar level.

4.3 References

1. Arsenieve, A. S.; Sobol, A. G.; Bystrov, V. F. *Journal of Magnetic Resonance* **1986**, 70, 427-435.
2. Kay, L. E.; Prestegard, J. H. *Journal of Magnetic Resonance* **1988**, 77, 599-605.
3. Kay, L. E.; Torchia, D. A.; Bax, A. *Biochemistry* **1989**, 28, 8972-8979.
4. Gao, Z.; Zhong, X.; Eisenberg, A. *Macromolecules* **1994**, 27, 794-802.
5. Landfester, K.; Boeffel, C.; Lambla, M.; Spiess, H. W. *Macromolecules* **1996**, 29, 5972-5980.
6. Blumich, B.; Spiess, H. W. *Angew. Chem. Int. Ed. Engl.* **1988**, 27, 1655-1672.
7. Spiess, H. W. *Chem. Rev.* **1991**, 91, 1321, 1338.
8. Blumich, B. *Advanced Materials* **1991**, 3, 237-244.
9. Yu, Y.; Eisenberg, A. *J. Am. Chem. Soc.* **1997**, 119, 8383-8384.
10. Yu, Y.; Zhang, L.; Eisenberg, A. *Macromolecules* **1998**, 31, 1144-1154.

Appendix

---

^{1}H NMR Measurements of the Polystyrene-*b*-poly(acrylic acid) Copolymer in Deuterated Dioxane /Deuterium Oxide Mixtures

---

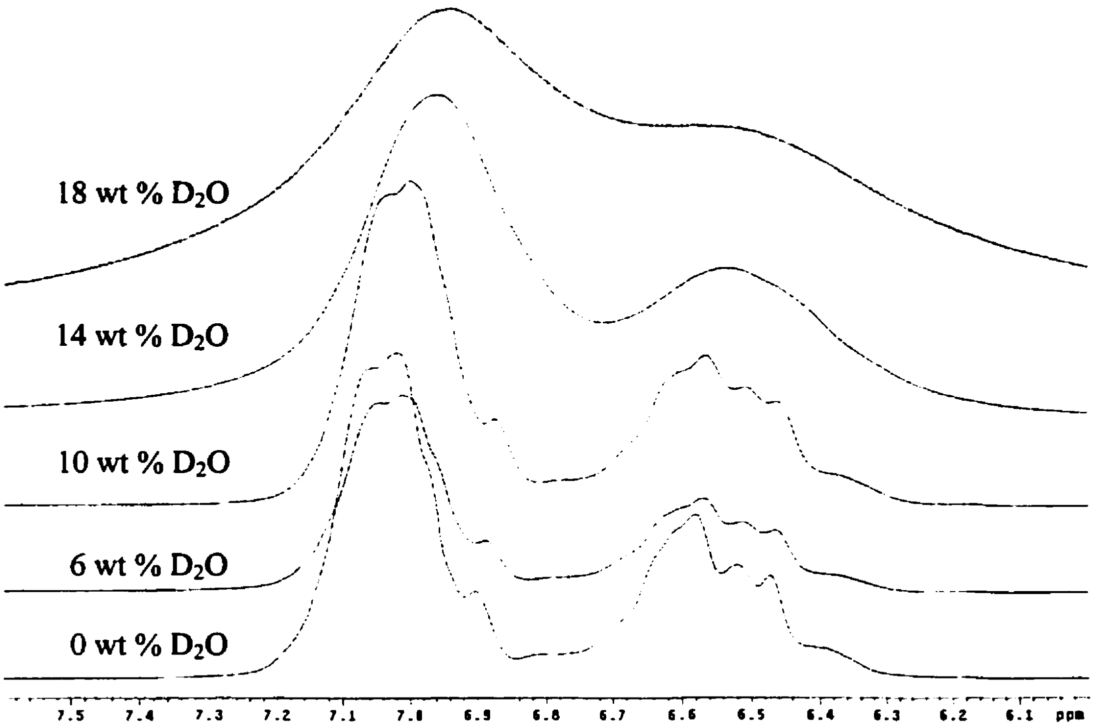

Figure A.1 Deuterium oxide dependence of the ^{1}H NMR line shapes of the 1 wt % PS$_{100}$-*b*-PAA$_{25}$ block copolymer in dioxane. The spectral region for the phenyl ring protons of the PS block is shown.

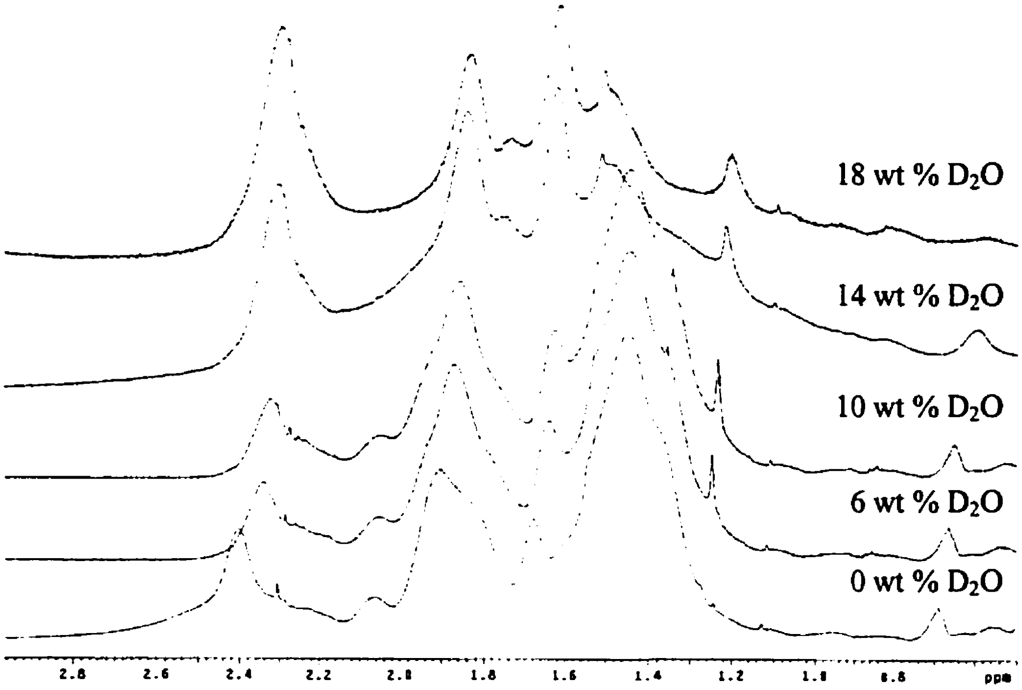

Figure A.2 Deuterium oxide dependence of the ^{1}H NMR line shapes of the 1 wt % PS$_{100}$-*b*-PAA$_{25}$ block copolymer in dioxane. The spectral region for the aliphatic protons of the PS$_{100}$-*b*-PAA$_{25}$ copolymer is shown.

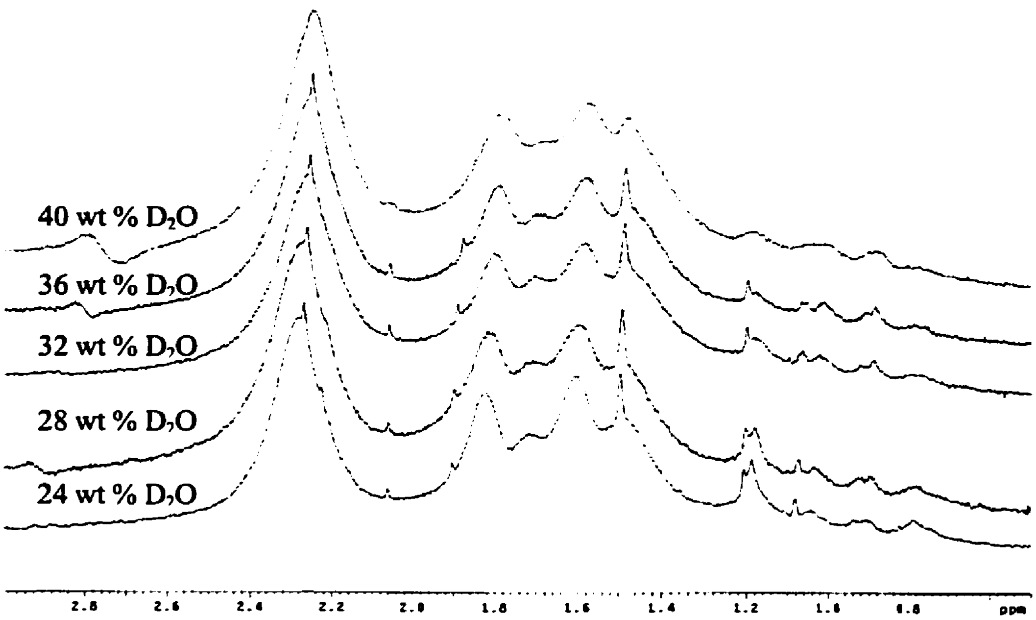

Figure A.3 Deuterium oxide dependence of the ^1H NMR line shapes of the 1 wt % PS_{100}-*b*-PAA_{25} block copolymer in dioxane at high deuterium oxide contents. The spectral region for the aliphatic protons of the PS_{100}-*b*-PAA_{25} copolymer is shown.

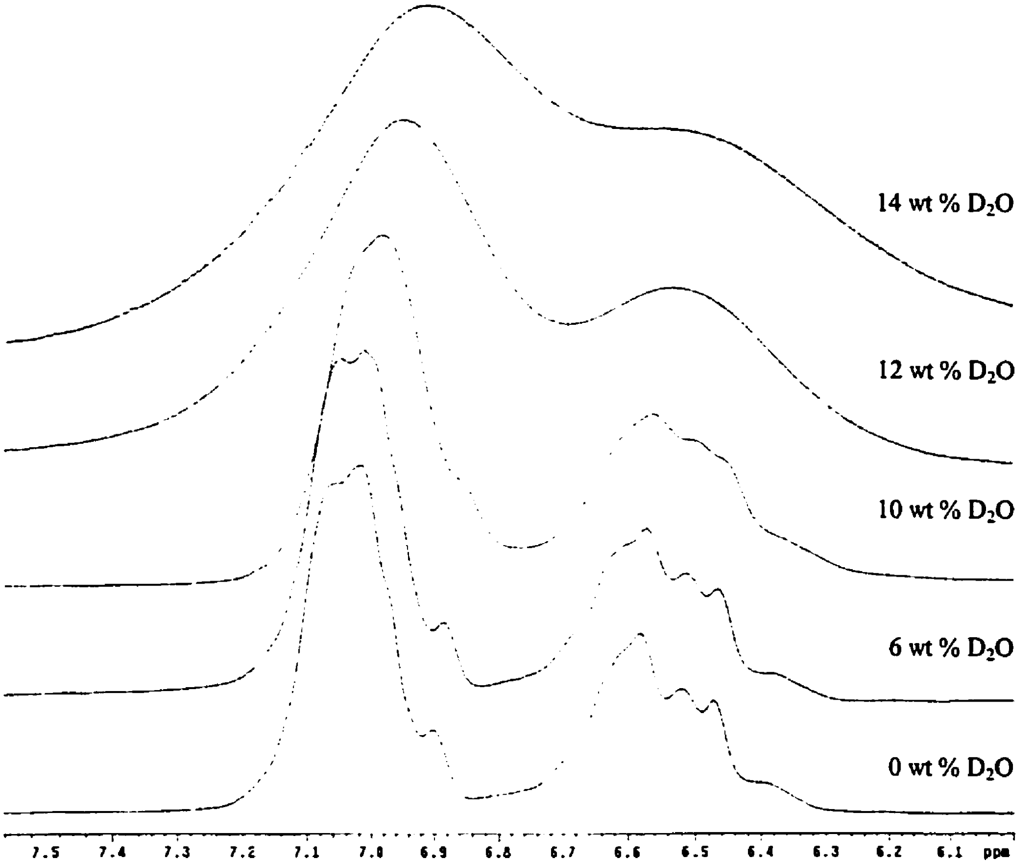

Figure A.4 Deuterium oxide dependence of the ^1H NMR line shapes of the 1 wt % PS_{218}-*b*-PAA_{20} block copolymer in dioxane. The spectral region for the phenyl ring protons of the PS block is shown.

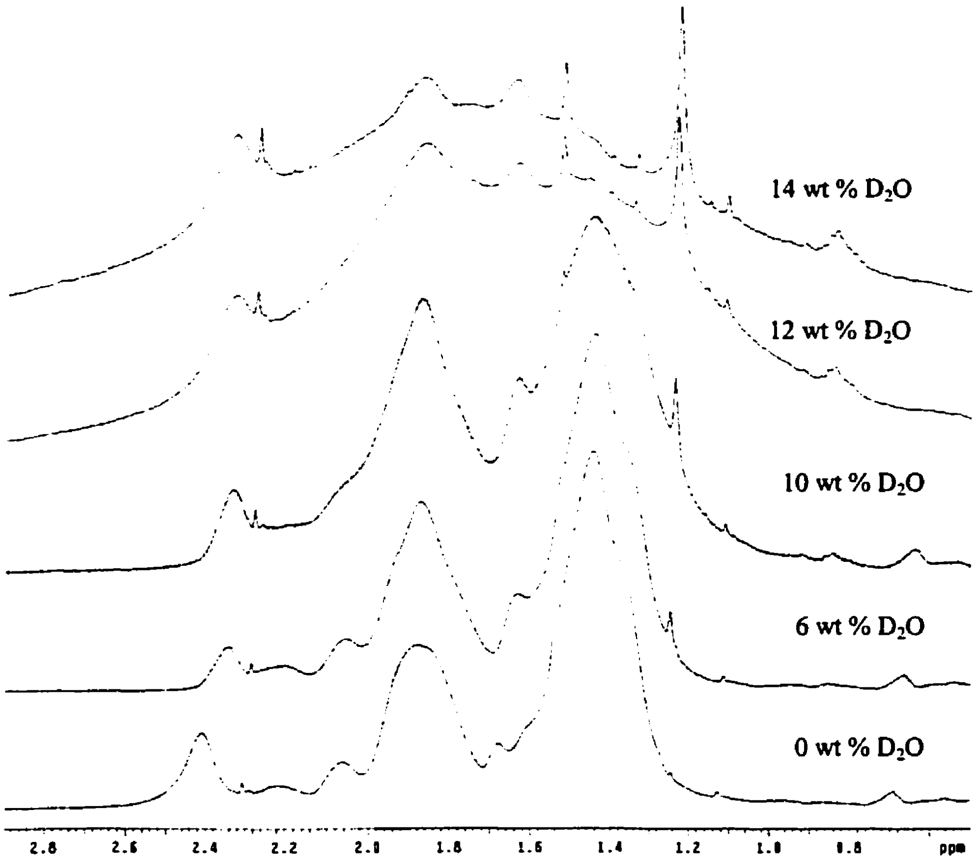

Figure A.5 Deuterium oxide dependence of the ^{1}H NMR line shapes of the 1 wt % PS_{218}-*b*-PAA_{20} block copolymer in dioxane. The spectral region for the aliphatic protons of the PS_{218}-*b*-PAA_{20} copolymer is shown.

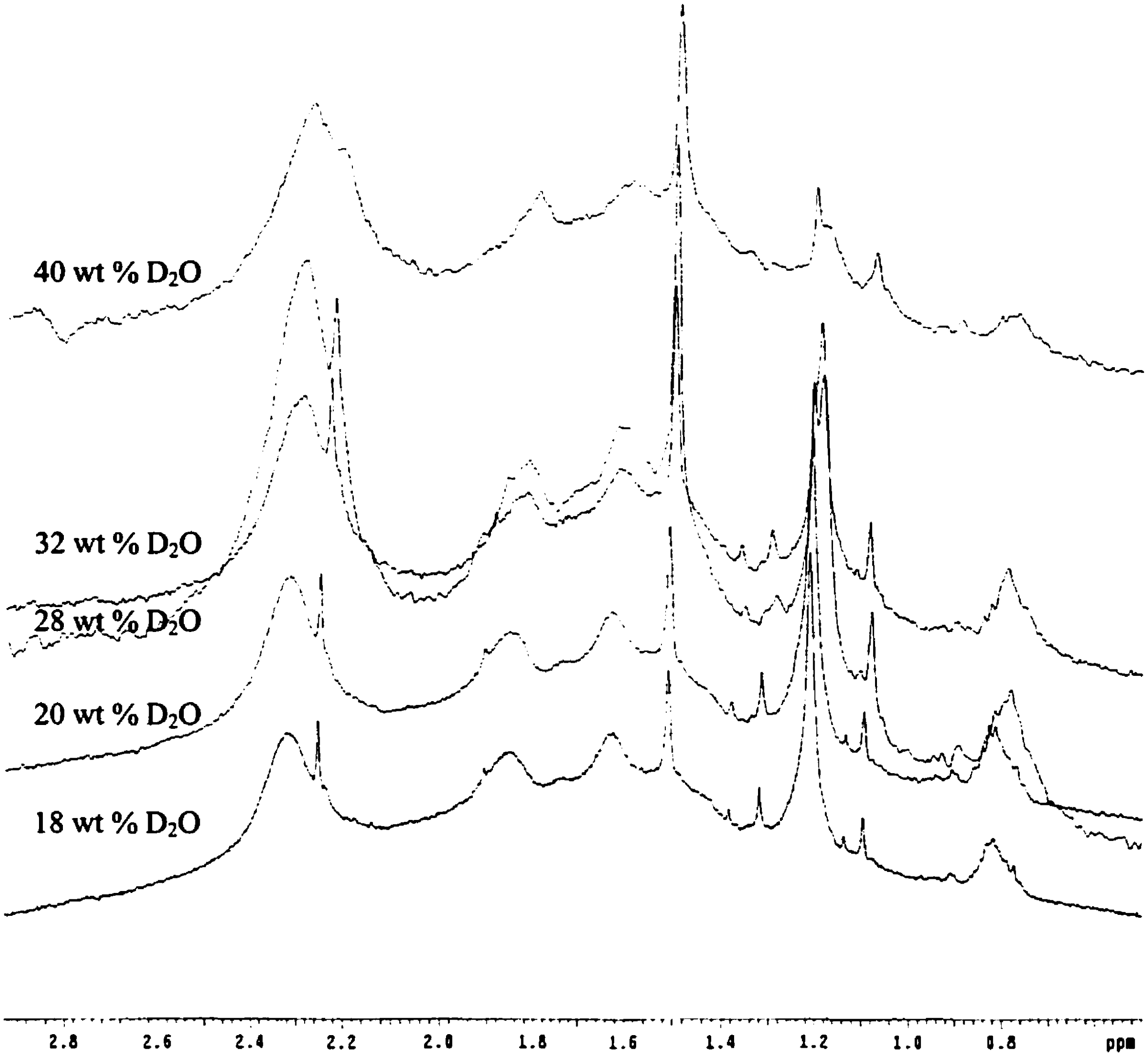

Figure A.6 Deuterium oxide dependence of the ^1H NMR line shapes of the 1 wt % PS_{218}-*b*-PAA_{20} block copolymer in dioxane at high deuterium oxide contents. The spectral region for the aliphatic protons of the PS_{218}-*b*-PAA_{20} copolymer is shown.

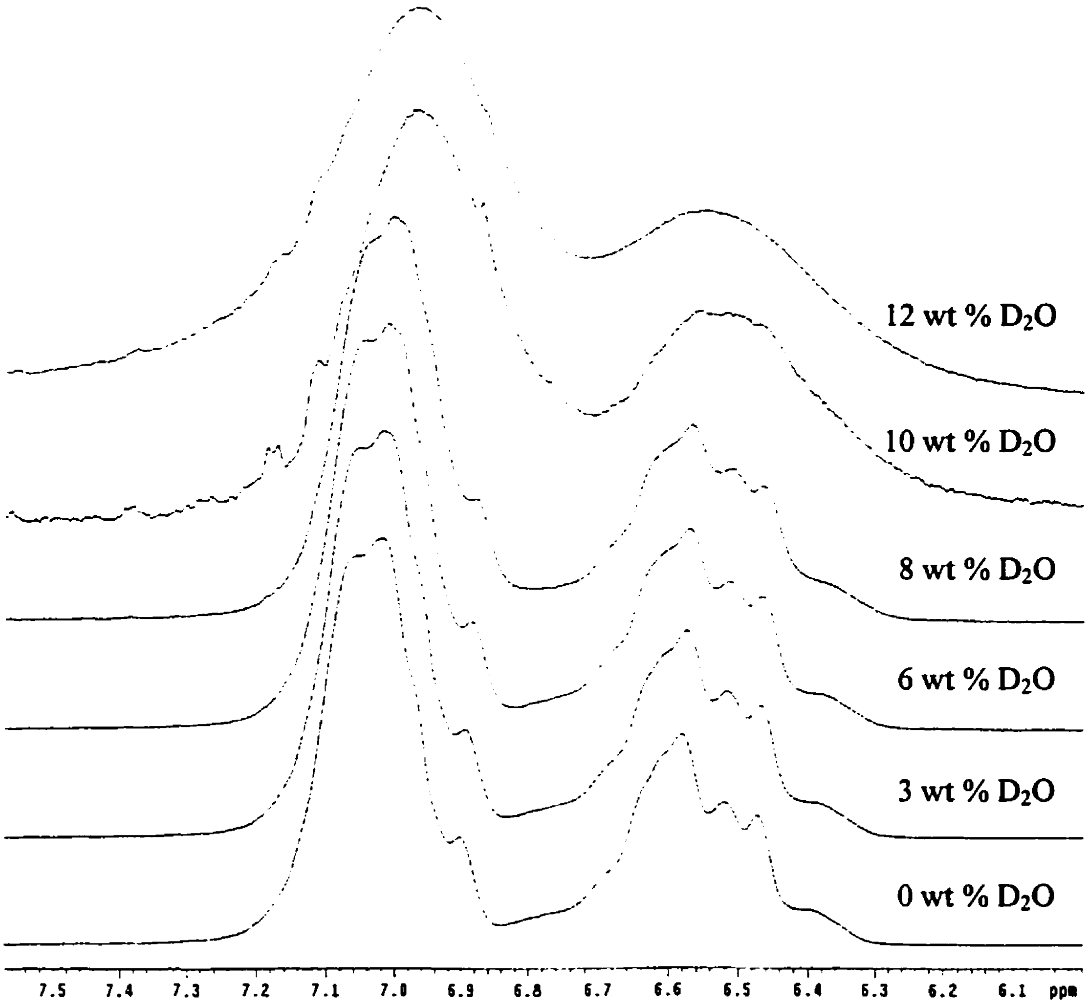

Figure A.7 Deuterium oxide dependence of the ^1H NMR line shapes of the 1 wt % PS_{208} homopolymer in dioxane. The spectral region for the phenyl ring protons of the PS block is shown.

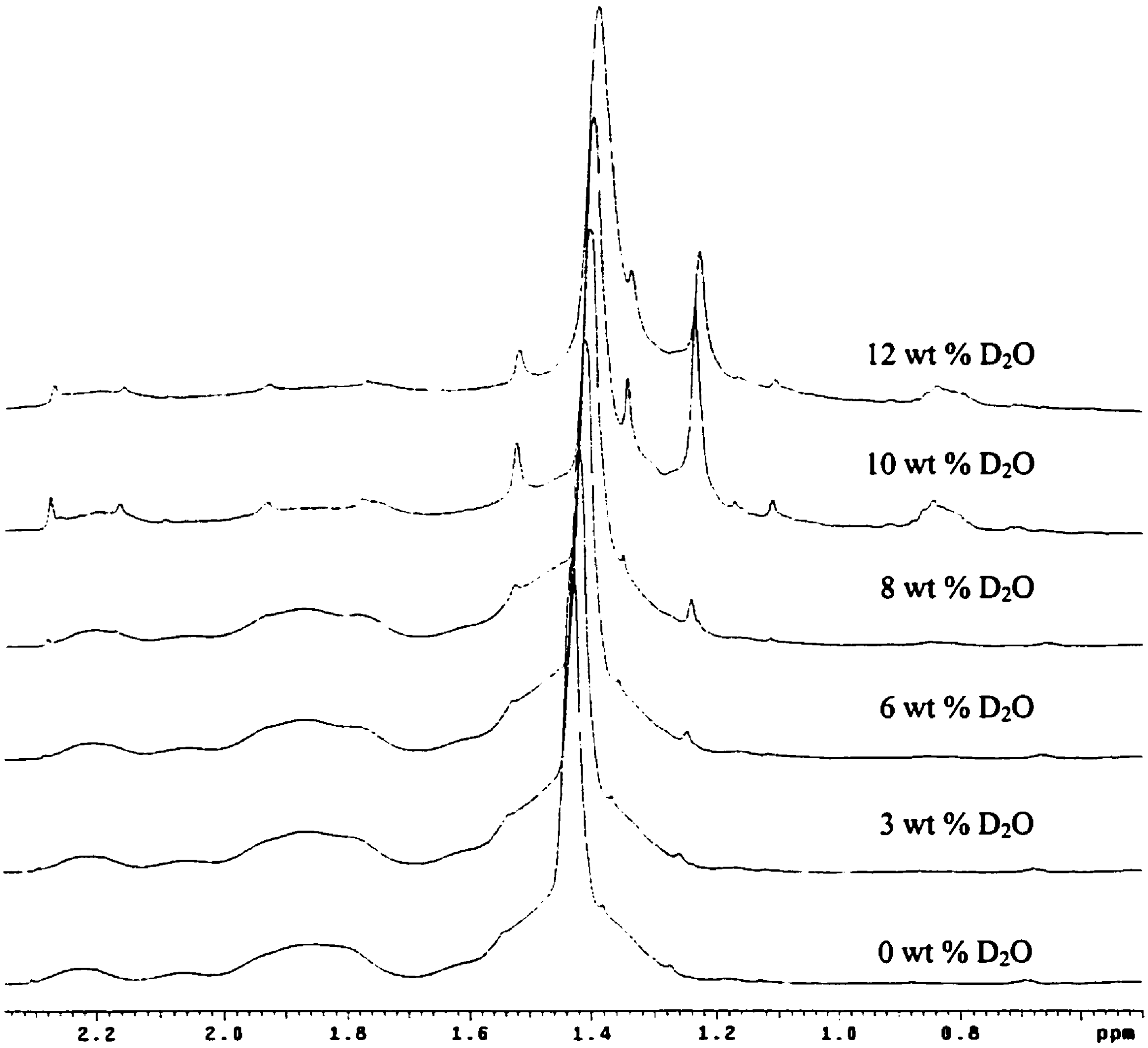

Figure A.8 Deuterium oxide dependence of the ^{1}H NMR line shapes of the 1 wt % PS_{208} homopolymer in dioxane. The spectral region for the aliphatic protons is shown.

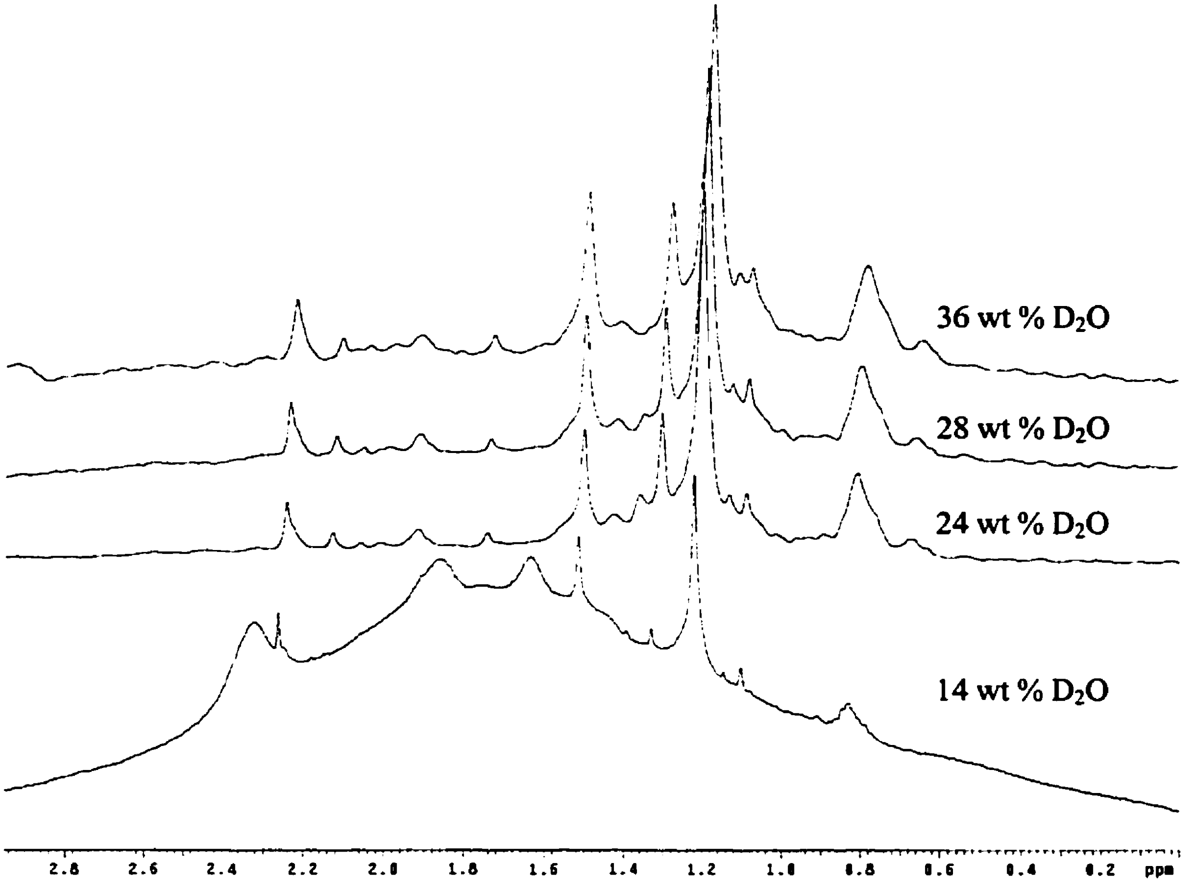

Figure A.9 Deuterium oxide dependence of the ^{1}H NMR line shapes of the 1 wt % PS_{208} homopolymer in dioxane at high deuterium oxide contents. The spectral region for the aliphatic protons is shown.

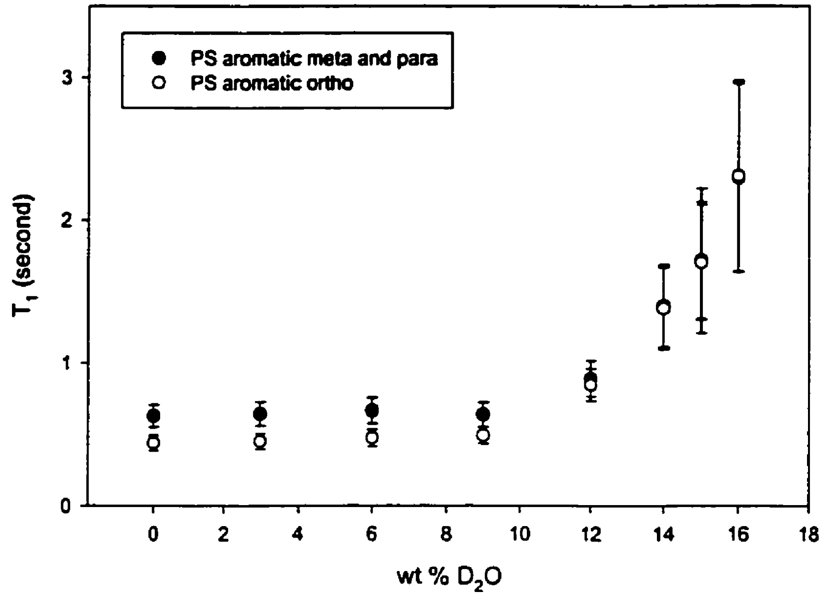

Figure A.10 Deuterium oxide dependence on the spin-lattice relaxation time for the PS phenyl ring protons of the 3 wt % PS_{100}-*b*-PAA_{25} copolymer in dioxane.

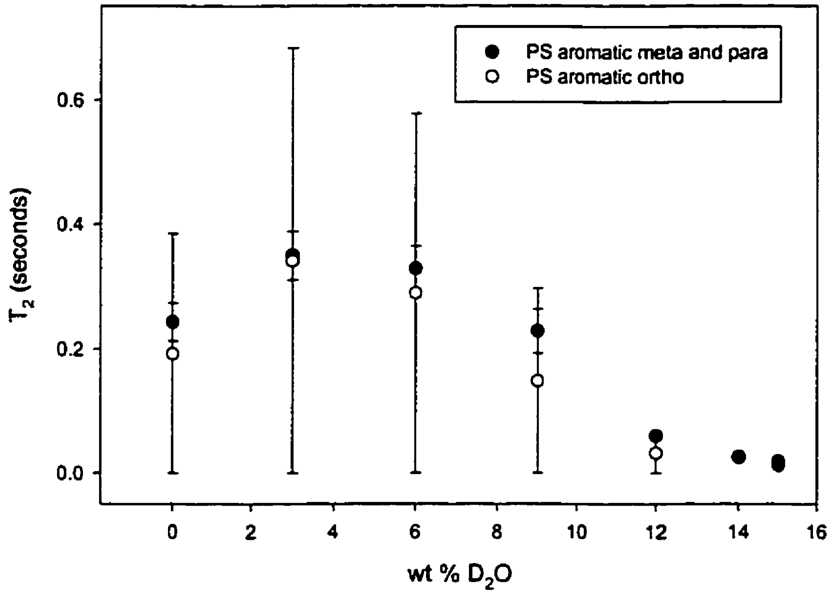

Figure A.11 Deuterium oxide dependence on the spin-spin relaxation time for the PS phenyl ring protons of the 3 wt % PS_{100}-*b*-PAA_{25} copolymer in dioxane.

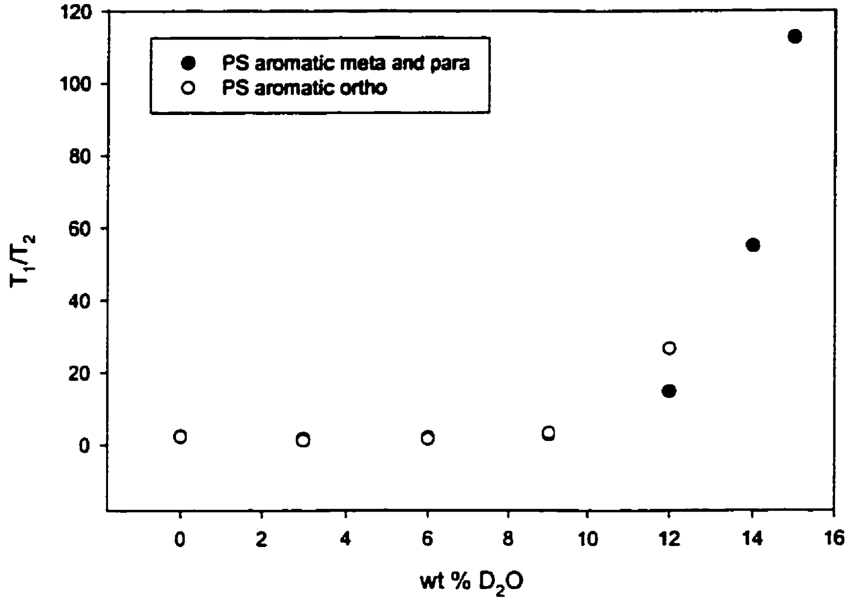

Figure A.12 T_1/T_2 values for the 3 wt % PS_{100}-*b*-PAA_{25} copolymer in dioxane as a function of deuterium oxide content. Data for the PS phenyl ring protons is shown.

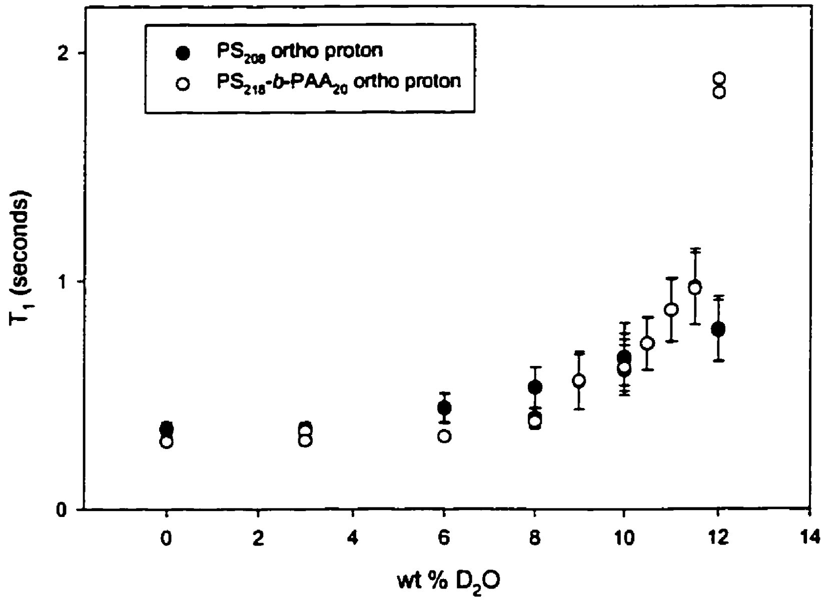

Figure A.13 Deuterium oxide dependence on the spin-lattice relaxation time for the PS phenyl ring protons of the 1 wt % PS_{218}-*b*-PAA_{20} copolymer and 1 wt % PS_{208} homopolymer in dioxane.

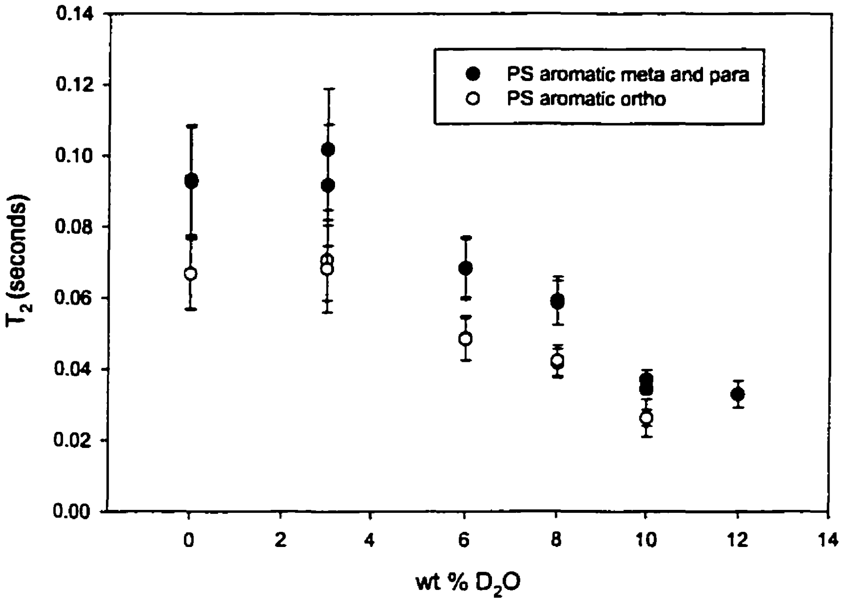

Figure A.14 Deuterium oxide dependence on the spin-spin relaxation time for the PS phenyl ring protons of the 1 wt % PS_{208} homopolymer in dioxane.

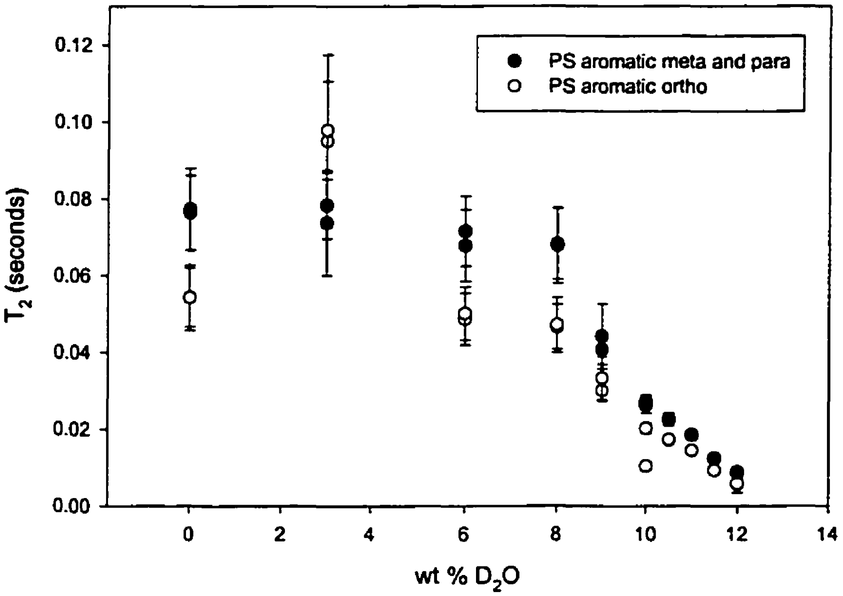

Figure A.15 Deuterium oxide dependence on the spin-spin relaxation time for the PS phenyl ring protons of the 1 wt % PS_{218}-*b*-PAA_{20} copolymer in dioxane.

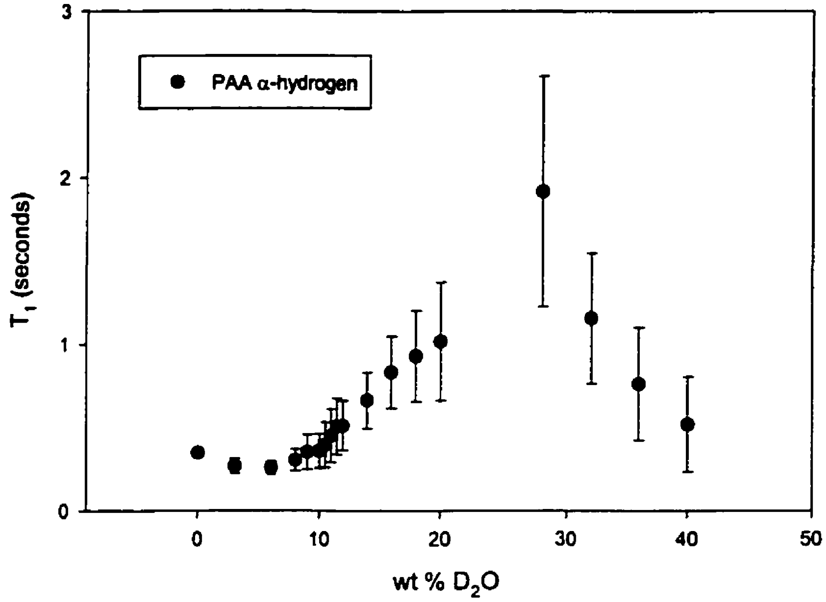

Figure A.16 Deuterium oxide dependence on the spin-lattice relaxation time for the PAA α proton of the 1 wt % PS_{218}-*b*-PAA_{20} copolymer in dioxane.

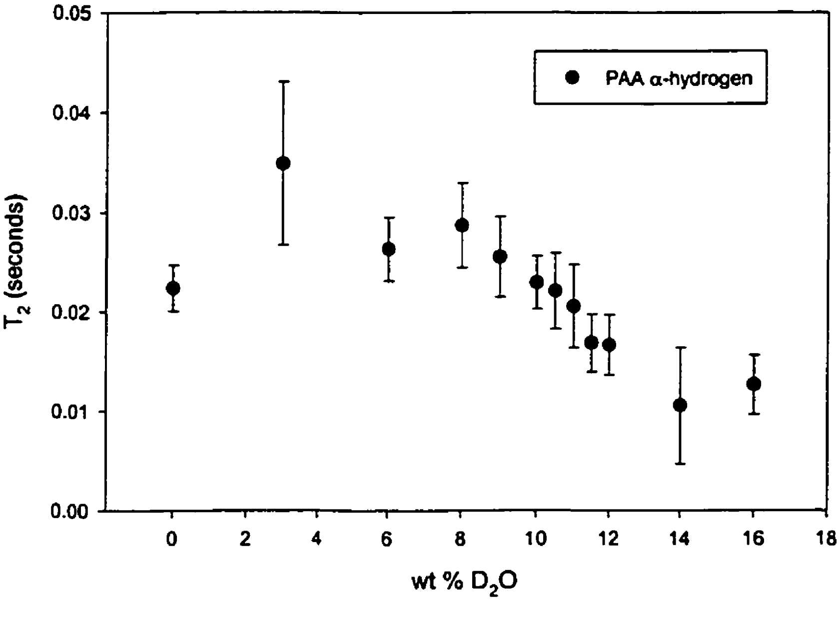

Figure A.17 Deuterium oxide dependence on the spin-spin relaxation time for the PAA α proton of the 1 wt % PS_{218}-*b*-PAA_{20} copolymer in dioxane.

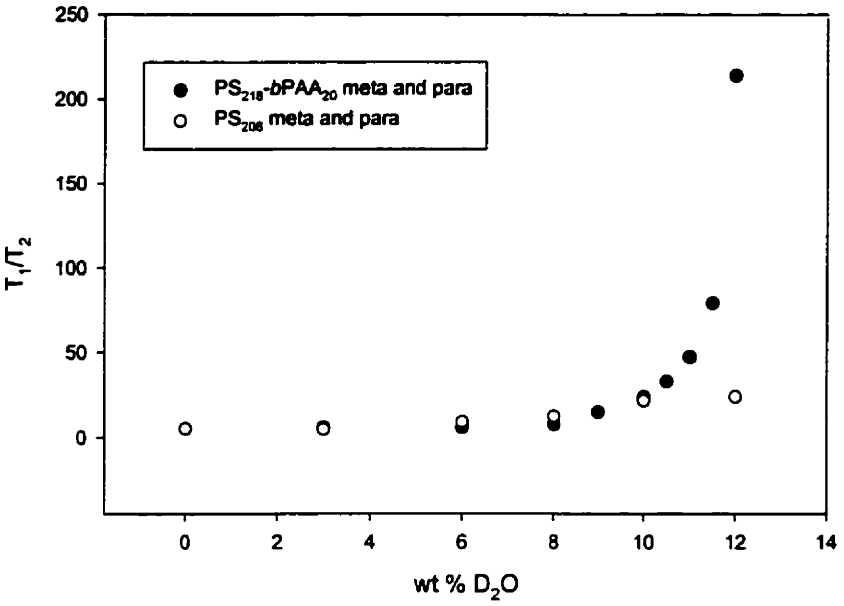

Figure A.18 T_1/T_2 values for the 1 wt % PS_{218}-*b*-PAA_{20} copolymer and 1 wt % PS_{208} homopolymer in dioxane as a function of deuterium oxide content. Data for the PS phenyl ring meta and para protons is shown.

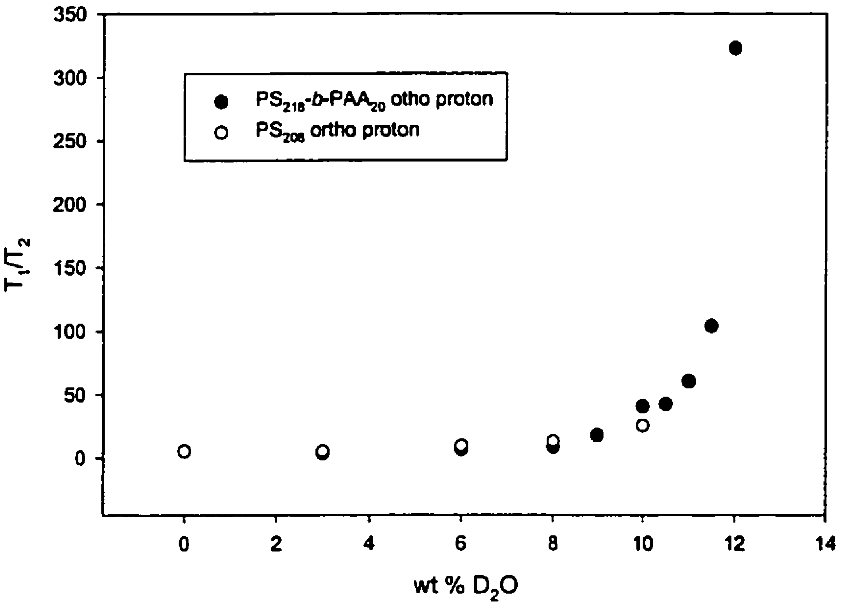

Figure A.19 T_1/T_2 values for the 1 wt % PS_{218}-*b*-PAA_{20} copolymer and 1 wt % PS_{208} homopolymer in dioxane as a function of deuterium oxide content. Data for the PS phenyl ring ortho proton is shown.

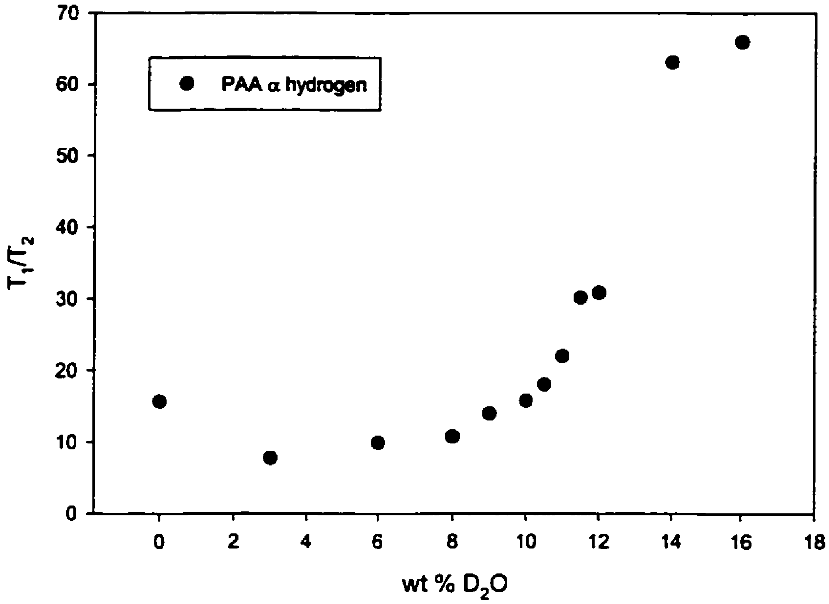

Figure A.20 T_1/T_2 values for the 1 wt % PS_{218}-*b*-PAA_{20} copolymer in dioxane as a function of deuterium oxide content. Data for the PAA α hydrogen is shown.